EXPERIMENTAL AND COMPUTATIONAL STUDY OF FLAME INHIBITION MECHANISMS OF HALOGENATED COMPOUNDS IN C_1-C_3 ALKANES FLAMES

A Dissertation

by

CARMEN HELENA OSORIO AMADO

Submitted to the Office of Graduate Studies of
Texas A&M University
in partial fulfillment of the requirements for the degree of

DOCTOR OF PHILOSOPHY

Chair of Committee,	M. Sam Mannan
Co-Chair of Committee,	Eric L. Petersen
Committee Members,	Perla Balbuena
	Miladin Radovic
Interdisciplinary Faculty Chair,	Ibrahim Karaman

August 2013

Major Subject: Materials Science and Engineering

ABSTRACT

After the restriction of different halogenated fire suppressants by the Montreal Protocol, there is an urgent need to identify environmentally friendlier alternatives. In particular, several efforts have been conducted to find substitutes of Halon 1301 (CF_3Br) which was considered the best in its class, not only because of its superior extinguishing performance, but also due to its relatively low toxicity. Different options have been proposed over the last decade. However, no single compound has been found to meet all of the exigent criteria. Further progress in this research requires fundamental combustion knowledge that can help us understand the unique performance of Halon 1301, to prevent this search from becoming a tedious trial-and-error process.

To this end, the present work aids in the search of fire suppressants alternatives by improving the flame inhibition mechanism understanding, starting with CF_3Br, which serves as a benchmark for new fire suppressants. Then, a case study of two of the most currently used fire suppressants, C_2HF_5 (HFC-125) and C_2HF_7 (HFC-227), is presented and compared with CF_3Br performance. For these analyses, a systematic analytical methodology was used to examine the effect of fire suppressants on ignition and laminar flame propagation of C_1-C_3 alkanes premixed mixtures, as good representatives of flammable gas fires (Class B fires). This methodology integrates model formulations and experimental designs in order to examine both chemical kinetics and thermal effects on fire suppressants at different stoichiometric conditions. Modeling predictions were based

on a detailed chemical kinetics mechanism which was assembled from a new, well-studied H_2, C_0–C_5 hydrocarbon mechanism from NUI Galway and recent CF_3Br and HFC fire suppressant chemistry from NIST. Experimental study involved the use of a shock tube (for ignition analysis) and a freely expanding flame speed bomb (for laminar flame speed analysis). Most of the experimental data provided in this work are the first measurements of their kind for the compounds and mixtures explored in this thesis. These measurements are extremely valuable since they can be used as a metric for model validation which represents one of the objectives of this work.

Current analyses indicate that the combustion properties of halogenated compounds cannot be generalized and depends on different factors. On one hand, the presented results showed that all the tested fire suppressants can decrease the laminar flame speed of the examined C_1-C_3 alkanes premixed flames; however, in some cases they can act as ignition promoters. In order to understand these behaviors, sensitivity analyses were conducted showing that halogenated species, resulting from the fire suppressants decomposition, can participate in both promoting and inhibiting reactions that compete to give a net effect. Identification of the key reaction responsible for such effects was conducted. Then, improvements on the fire suppressant chemistry can be done by modifying the corresponding Arrhenius parameters of such important reactions. This work not only provides fundamental knowledge of halogenated flame inhibition mechanisms, but also serves as the basis for more accurate chemical kinetics mechanisms that can be used for better predictions over a wide range of conditions.

DEDICATION

I want to dedicate this work to all the people who believed in me, including my grandparents Rosa and Julio Amado who have been always very proud of me; I want to tell them that I could not make it without them. My parents, Helena and Carlos; I want to thank them for giving me the life and the freedom to choose my own road, but still always willing to give me all their support at any time. Parents: this achievement is also yours. Also, I want to dedicate this to my sisters Silvia and Irmis, and my beautiful nephew. To my Mom Irma, I have not words to express all my gratitude. Thanks for wanting to be my second Mom and giving me all your love unconditionally. Finally, I want to dedicate this to my Uncle Alberto, who has giving me all his support and wise advice when I need it.

ACKNOWLEDGEMENTS

From my heart, I want to thank my advisors, Dr. Sam Mannan and Dr. Eric Petersen, who have been more than academic guidance for me during the course of this research. Thank you very much for believing in me and giving me all your support. I have been very lucky for having the opportunity to have both of you as my mentors. I have not words to express my gratitude. Thank you for all the passion and unconditional dedication to educate new generations. I have learned much from both of you. I also want to extend my gratitude to the members of my committee, Dr. Perla Balbuena, Dr. Miladin Radovic, and Dr. Tahir Cagin for their support. I especially want to thank Francisco Vides for their support in the last stage of this work.

TABLE OF CONTENTS

Page

LIST OF FIGURES

Page

LIST OF TABLES

Page

1 INTRODUCTION

1.1 History of Fire Suppressants

For many centuries, water was used as the main weapon against fires. However, the increases in population and standards of living have led to the necessity to develop scientific and technological advances in order to provide better capabilities to control fires. At the beginning of the 20th century, halogenated hydrocarbons, such as CCl_4 (Halon 104), began to be considered as fire extinguishers. Their acceptability was mainly due to their high efficiency, and unlike water, these suppressants leave no residue that could damage electrical equipment. Nonetheless, awareness arose about their toxicity. At the middle of the last century, more than 60 new candidates were evaluated by Purdue Research Foundation and the U.S. Army Corps of Engineers [1]. Four halogenated hydrocarbons, known as Halons, were considered for further study including Halon 1211 (CF_2ClBr), Halon 1301 (CF_3Br), Halon 1202 (CF_2Br_2), and Halon 2402 ($C_2F_4Br_2$). Results showed that Halon 1301 was the least toxic and the most effective after Halon 1211. Furthermore, it is well known that Halon 1301 also presents other unique properties such as a high speed of dispersion, non-corrosive, electrically non-conductive, and it is stable under long-term storage. Because of all these advantages, Halon 1301 had been considered as the ideal fire suppressant for many years, and it had been used in a wide range of applications in the manufacturing industry

and on aircraft, ships, and in electrical rooms as a total-flooding fire extinguisher and inerting agent.

1.2 Halons and the Ozone Layer

As mentioned above, halogenated compounds have been widely used in the field of fire protection. Nevertheless, many of these agents have been associated with the destruction of the ozone layer, as suggested in 1974 by Rowland and Molina [2]. Chlorofluorocarbons (CFCs) were among the first compounds identified as Ozone Depleting Substances (ODS), mainly because of their capability to reach the stratosphere and break down the O_3 molecules by the action of UV light [3, 4]. Halon 1301, like CFC, can also destroy stratospheric ozone; however, its effect is much higher than CFC since bromine species are considered stronger catalyzers of O_3 decomposition [3, 4]. Moreover, Halon 1301 is a very stable molecule with an atmospheric lifetime of 65 years, resulting in a relatively higher Ozone Depleting Potential (ODP). Table 1 shows the atmospheric properties of different chemical compounds [5]. Note that ODP is a relative measurement that relates the ozone layer degradation effect of a chemical compound compared to the effect caused by CCl_3F (CFC-11), which has a fixed ODP equal to 1.0.

Table 1. Atmospheric properties of different chemical compounds.[5]

Chemical	formula	Atmospheric lifetime (years)	(ODP)
Cholorofluorocarbons			
CFC-11	CCl_3F	50	1.0
CFC-12	CCl_2F_2	102	0.82
CFC-13	$CClF_3$	640	~1
CFC-113	CCl_2FCClF_2	85	0.90
CFC-114	$CClF_2CClF_2$	300	0.85
CFC-115	$CClF_2CF_3$	1700	0.40
Bromofluorochemicals			
Halon - 1301	CF_3Br	65	12
Halon - 1211	CF_2ClBr	20	5.1

In 1985, Joe Farman and his team revealed an alarming depletion of the Antarctic stratospheric ozone layer [6]. This evidence served as a warning of a major environmental hazard. These findings were confirmed by other scientists [7-11]. Some research also showed that this effect was mainly caused by man-made emissions of chlorine- and/or bromine-containing compounds [8, 11].

Based on this stark realization, the Vienna Convention and its Montreal Protocol were established as an international effort to protect the ozone layer and control the substances that can cause its depletion. The Montreal Protocol [12], originally agreed upon in 1987 and coordinated by the United Nations Environment Programme (UNEP), involves the participation of 197 parties including the United States. In compliance with this agreement, the U.S. Environmental Protection Agency (EPA), under the Clean Air Act (CAA), has banned the production and import of different fire suppressants including CF_3Br, CF_2ClBr, and $C_2Br_2F_4$ [13].

Undoubtedly, the Montreal Protocol has been one of the most successful environmental programs worldwide, resulting in a remarkable recovery of the ozone layer [14-18]. Nevertheless, Halons' restriction is currently faced with a practical downside due to their properties that make them ideal as fire suppressants. The following section provides a summary of different scientific efforts that have been conducted in the area of halon substitutes.

1.3 Previous Studies of Suitable Halon Alternatives and Research Gaps

Since the enactment of the Montreal Protocol, several international research programs have been created to search for suitable halon alternatives. In particular, finding substitutes for Halon 1301 is challenging at best because it is considered the gold standard of fire suppressants, especially in those inhabited, closed environments--such as aircrafts, ships, and oil platforms--where evacuation is almost impossible. This goal represents a significant challenge, since an ideal Halon 1301 replacement should meet with a number of requirements, not only related to its environmental impact, but also in terms of the desired operational properties. In summary, these requirements are [19]:

- Low Ozone Depleting Potential (ODP)
- Short atmospheric life-time
- Low Global Warming Potential (GWP)

- Low toxicity of the chemical
- Low toxicity of its decomposition and combustion products
- High fire suppression efficiency
- Effective in avoiding flame re-ignition
- Leave no/low residue (clean agent)
- Chemically stable under long storage conditions
- Low corrosivity
- Able to disperse at different atmospheric conditions
- Involve a feasible technology for high quantities production/supply
- Reasonably priced

In the United States, the Department of Defense (DoD) created the Alternative Technology Development Program (TDP) with the participation of several scientists from industry, government, and academia. Its main objective was to identify near-term, safe, and environmentally friendly halon alternatives that can be used in aircraft fire protection systems. From 1993 to 1998, several compounds were evaluated in laboratory- and real-scale tests. Based on these studies, different substitutes were found for applications other than fire protection.

Unfortunately, none of the tested chemicals met the criteria to be considered as an ideal CF_3Br substitute, with HFC-125 and HFC-227 identified as the best CF_3Br alternatives. The major limitation of these two compounds is their lower fire suppressant efficiency

compared to CF_3Br. Therefore, larger quantities of HFC are required to reach a performance similar to that of CF_3Br. This fact is particularly inconvenient in aircraft applications where space and weight are the main constraints. A third candidate, CF_3I (Halon 13001), was also examined due to its efficiency compared with CF_3Br; however, it was unlikely that CF_3I could be considered as a Halon 1301 "drop in" replacement due to its harmful, toxicological effects.

As an urgent need for better solutions surfaced, the U.S. DoD established the Next Generation Fire Suppression Technology Program (NGP). Over one decade (1997 to 2006), the NGP involved researchers nationwide including scientists and professionals in different areas from the National Institute of Standards and Technology (NIST), Air Force, Army, Naval Research Laboratory, New Mexico Engineering Research Institute, and the Environmental Protection Agency (EPA), among others. The NGP focused on the search of novel chemical compounds that can be used as Halon 1301 substitutes but also on technology developments that can be used to improve aircraft fire protection systems for long-term applications.

As part of this program, thousands of chemical compounds were examined using existing and novel screening methods. For instance, not a perfect CF_3Br replacement could be identified to meet the entire set of criteria. From this program, it was concluded that a more realistic approach was to search for a suitable chemical alternative

with better performance than HFC-125, and identify diverse agents that can be applied in different applications.

One outstanding trend involves the use of promising chemicals, such as phosphorous- and metal-containing compounds, which have shown relatively good flame inhibition performance [20-26]. In particular, iron pentacarbonyl ($Fe(CO)_5$) represents one of the strongest inhibitors. Nevertheless, some of them are considered toxic materials, and their efficiency may be affected by the formation of particles at flame conditions [27-31]. Therefore, a better understanding of their behavior is required to overcome such limitations.

Another interested group involves tropodegradable compounds that contain bromine. These substances can effectively suppress the flame by the action of the halogen (Br) and, at the same time, they can easily react with atmospheric constituents such as hydroxyl radicals and tropospheric ozone, leading to short atmospheric lifetimes. Therefore, they cannot reach the ozone layer in the stratosphere [20]. Unfortunately, successful application of these candidates is restricted by (1) the lack of mechanism understanding, (2) low dispersion capabilities (high boiling points), (3) high-quantity production limitations, and (4) toxic effects or absence of toxicological data.

On the other hand, combinations of different compounds have also been considered as promising Halon 1301 alternatives. Blends of iron-containing compounds and CO_2, for

example, were studied by Linteris et al. [32]. These blends can achieve inhibition efficiency close to CF_3Br, but as mentioned before, the observed particle formation limits their success.

Currently, many of the Halon 1301 alternatives approved by the EPA are blends, including the HCFC mixture *R-595* (NAF S-III), which is commercially available as a suitable replacement. Blends can offer a plentiful range of combinations, making it difficult to experimentally examine all of them [33]. For this task, researchers like Luo [34] have proposed the use of validated chemical kinetics mechanisms and analytical methodologies to predict and design optimal blend combinations.

The mentioned works are presented to show the need of a systematic methodology based on fire suppression mechanistic understanding, and the importance of validated chemical kinetics mechanisms that can be used to (1) identify the key roles on the inhibition process, (2) better predict fuel/oxidizer/suppressants systems at different conditions, and (3) help the design of fire suppressant blends.

These fundamental studies need to be carried out, not only to understand those novel alternatives, but also to obtain fundamental insight on the flame inhibition mechanism of CF_3Br to provide a comprehensive and accurate baseline that can be used as a reference. Thus, different alternatives can be compared to the Halon 1301 flame inhibition performance at similar conditions. This approach requires accurate experimental data on

CF_3Br as well as a validated chemical kinetics mechanism that can be used for a number of numerical analysis and predictions. However, after the Halon 1301 restriction, the research associated with it has been minimized, leaving only a partial understanding of its chemical performance, with limited experimental data available for comparison purposes and for chemical kinetic model validations.

In summary, despite the remarkable progress in the area of fire suppressants during the last few decades, advances have been limited by an incomplete understanding of the flame inhibition mechanism and the absence of a comprehensive knowledge of CF_3Br chemistry that can be used as a point of reference. To this end, the goal of this thesis is to fill these gaps as is described in the following section.

1.4 Scope of the Present Work

As mentioned before, further progress in the field of halon alternatives requires fundamental research on flame inhibition mechanisms, and as much of a complete understanding of CF_3Br properties as possible, which can be used as the baseline for future research.

Based on this main goal, the purpose of this dissertation is first to present a systematic methodology that serves as the filling gap related to the analysis of different fire

suppressant properties, of which incomplete understanding limits further advances. This methodology, explained in more detail in Section 3, is based on chemical kinetics analysis involving both experimental and numerical work. Considering the scarcity of experimental data required for model validation, the present methodology is also able to fill this gap by proving accurate measurements that can be directly compared with numerical predictions.

Starting with a fundamental flame inhibition analysis of CF_3Br, this work aims to provide a point of reference for further studies that attempt to identify novel candidates or to better understand the properties of current substitutes towards more efficient applications. Considering the last approach, this work also presents a case study by analyzing two of the currently most-accepted fire suppressant alternatives, including C_2HF_5 and C_3HF_7. This analysis aims to provide insight on their combustion behavior in CH_4 and C_3H_8 flames for safer and optimal applications.

1.5 Organization of Dissertation

The work presented herein is organized as follows:

Section 1 introduces the motivation of this dissertation related to the need of suitable halon alternatives. It presents different efforts conducted in this area, the challenges of

this search, and the necessity for further understanding of the flame inhibition mechanism for further advances in this area. It points out different research gaps, particularly the urgent need of a better understanding of CF_3Br and accurate experimental data needed for model validation. Based on this information, the scope of this dissertation is also presented.

Section 2 provides fundamental topics on fire theory, including types of fires, flame inhibition mechanisms, and fire suppressant classification based on their performance. A conceptual background on chemical kinetics is also provided in this section, since it constitutes the basis of this research.

Section 3 presents the methodology used for flame inhibition analysis, starting with an introduction defining the overall objectives of this systematic procedure. This section is divided in three parts: (i) the experimental techniques for ignition delay times, (ii) laminar flame speed, and (iii) the numerical analysis used. Each of these sections provides an introduction defining the importance of such determinations/analyses, as well as the basic concepts related to them. In the case of the experimental technique, the descriptions of the equipment are provided together with their corresponding uncertainty analyses. The numerical work section discusses the software and codes employed as well as the assembled chemical mechanism used. It also includes an overview of the different analyses performed using numerical approaches, including sensitivity analysis and assessment of flame inhibition effectiveness.

Section 4 contains the study of the CF_3Br flame inhibition mechanism. It starts by stating the importance of using CF_3Br as a baseline for research purposes. It also provides a summary of previous work where CF_3Br flame inhibition was the main subject and points out the scarcity of experimental data required for validated mechanisms. Then, it presents the detailed results and analyses obtained by applying the methodology described in Section 3.

Section 5 includes a case study where two halon alternatives (C_2HF_5 and C_3HF_7) are studied in detail by using the methodology described in Section 3, and then compares the results with the results obtained from the CF_3Br analysis (Section 2). This section first describes the reason why these two substitutes require a better understanding of their properties towards safer and more-efficient applications, and then, the results and analysis are presented. Finally, Section 5 provides the overall conclusions and recommendations of this dissertation, and discusses the potential future research work on this topic.

2 BACKGROUND

2.1 Fire Theory and Types of Fires

To understand how fire suppressants work, it is important to start with the basics of fire theory. Fire is the result of a rapid exothermic reaction between a fuel (i.e., methane) and an oxidizer (i.e., oxygen). For this process to take place, an ignition source should be present, thus the fuel can reach its ignition temperature and burn. For the flame to be sustainable, it is necessary to have a continuous chemical chain reaction, where enough fuel and oxygen produce the required active radicals responsible for the major heat release. This combustion process can be represented through the fire tetrahedron (Figure 1). Based on this concept, a fire can be extinguished by eliminating one of the four elements present in the process.

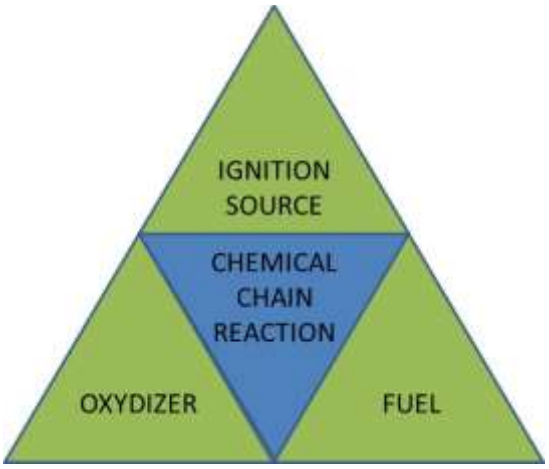

Figure 1. Fire tetrahedron.

This work focuses on understanding how fire suppressants can affect the chemical chain reaction and how inhibition efficiency can be measured. For this approach, it is important first to give a background related to fire chemistry.

2.2 Fundamentals of Fire Chemistry

Chemical processes are very dependent on highly reactive intermediates called free radicals such as H, O, OH, and HO_2. Unlike stable molecules (e.g., H_2O, O_2, H_2, H_2O_2), free radicals possess unpaired valence electrons which make them highly unstable. Due to the importance of this species class in combustion processes, elementary reactions can be categorized in four groups based on the production or consumption of the free radicals (Table 2).

Table 2. Classification of elementary reactions.

Initiation	One free radical is produced from stable molecules in the reactants
Propagation	One radical is consumed, and one radical-molecule is generated
Branching	Two free radicals are produced per single radical in the reactants
Termination	One radical-molecule is consumed to form stable species

This classification can help one to understand different phenomena. For example, generation and propagation of the flame can be attributed to branching reactions which are predominant over termination steps. A flame occurs when a large amount of radicals are produced due to a fast fuel decomposition.

Fire suppressants can break the chemical chain reaction by reducing the global reaction rate. One of the main ways to do this is by competing with the key branching reaction (R1), where two free radicals are produced. It can be approached by a thermal mechanism (decreasing the flame temperature), or by a kinetics mechanism (reducing the radical concentration through catalytic processes). In general, the global effect of a fire is the combination of these two mechanisms:

$$H + O_2 \rightleftarrows O + OH \qquad (R1)$$

CF_3Br, for example, behaves mainly by chemical action through catalytic cycles where the bromine atoms can effectively scavenge the H radical concentrations. However, the fluorine in the molecule can also contribute to its inhibition efficiency by scavenging radicals, but in a less effective way. The most efficient fire suppressants*, except water mist with drop size < 50 μm [35], are believed to behave mainly by a chemical mechanism. Analysis of these agents can be used to understand fundamental chemical and physical processes that can contribute to the overall suppression efficiency.

* Most efficient fire suppressants are considered those having similar or better efficiency than CF_3Br.

Overall, the chemical process of combustion depends on the entire web of reactions that interact between them. This entire system can be analyzed through the chemical kinetics mechanisms which contained all the information required for such a study. It includes all the elementary reactions along with their reaction rates (in terms of the kinetics parameters (A, n, Ea) as well as the thermodynamic properties of all the species involved. This database is known as the chemical kinetics mechanism, and it can be applied to different science and engineering applications. Section 3.4.1 contains more details about the use of kinetics mechanisms in combustion modeling. This analysis requires a fundamental background related to kinetic theory, which is reviewed in the following section.

2.3 Kinetics Theory

Reactions occur over a limited period of time which is defined by a specific rate (kinetics). In general, it depends mainly on the temperature, or sometimes pressure, concentration of reactants, and the presence of a catalyst or inhibitor. The kinetics of a global system depend on the individual reaction rates.

For a single reaction (i.e., C+D ⇄ E+G), its rate-of-progress (q) can be defined as the difference between its forward rate (K_f) and backward rate (K_b), as shown in Equation (1), where [ ] indicates the molar concentration of the species C, D, E, and G.

$$q = k_f[C][D] - k_b[E][G] \quad (1)$$

In general, this relationship can be written for any reaction (i) according to Equation (2), where Z^{th} represents the species involved in reaction, and (ν') and (ν'') are the coefficients of the reactants and the products, respectively.

$$q_i = k_{f,i} \prod_{z=1}^{Z} [Z]^{\nu'_{Z,i}} - k_{b,i} \prod_{z=1}^{J} [Z]^{\nu''_{Z,i}} \quad (2)$$

Reaction rates are considered very important because they can give information related to the total rate of production or decomposition (W_Z) of any species Z^{th}. Then, W_Z, can be found through Equation (3), by considering the rate-of-progress (q_i) of all the reactions where the Z^{th} is involved.

$$W_Z = \frac{d[Z]}{dt} = \sum_{i=1}^{I} (\nu'_{Z,i} - \nu''_{Z,i}) q_i \quad (3)$$

In order to solve this problem, it is necessary to provide the rate-of-progress (q_i) of all the reactions involved in the system, along with all their corresponding forward and back-forward rates constants (K_f, and K_b) characteristic of that reaction.

The forward rate constant can be defined using a modified version of the Arrhenius equation which, unlike the original Arrhenius, includes a temperature-dependent factor as follows:

$$k_{f,i} = A_i T^{n_i} \exp\left(\frac{-E_{a,i}}{TR_c}\right) \tag{4}$$

The solution of this equation requires three parameters for each of the reaction considered. These parameters are: *A* which represents the pre-exponential factor, *n* is the temperature exponent, and *Ea* is known as the activation energy. In Equation (4), T and R_c are the temperature and universal gas constant, respectively.

On the other hand, the backward constant (k_b) can be found using the equilibrium constant (K^0), which relates the ratio (k_f/k_b) with thermodynamic Gibbs functions as shown in Equations (5) to (8), where S_k and H_k are the species entropy and enthalpy, respectively.

$$K^0(T) = \left(\frac{k_f}{k_b}\right) \tag{5}$$

$$K_i^0(T) = exp\left[\frac{\Delta S_i^0}{R_c} - \frac{\Delta H_i^0}{R_c T}\right]\left(\frac{P_{atm}}{R_c T}\right)^{\sum_{z=1}^{z} \nu_{z,i}} \tag{6}$$

$$\frac{\Delta S_i^0}{R_c} = \sum_{z=1}^{Z} \left(\nu_{z,i} \frac{S_k^0}{R_c} \right) \tag{7}$$

$$\frac{\Delta \mathrm{H}_\mathrm{i}^0}{\mathrm{R_c T}} = \sum_{\mathrm{z=1}}^{\mathrm{Z}} \left(\nu_{\mathrm{z,i}} \frac{\mathrm{H}_\mathrm{k}^0}{\mathrm{R_c T}} \right) \tag{8}$$

Based on this review, we see that the solution of any chemical kinetics problem requires detailed information on all the elementary reactions involved in the system, as well as the thermodynamic parameters of each compound that participates in the process.

Usually, combustion systems involve hundreds of chemical reactions and species, leading to a high number of ordinary differential equations, making difficult its numerical solution without computational tools. Based on this fact, different software has been developed to solve different types of kinetics problems, with CHEMKIN being one of the most commonly used in this area. This program requires the input of a complete set of elementary reactions and their corresponding kinetics parameters, as well as specific thermodynamic data of all the species involved. Section 3.4 discusses the use of CHEMKIN for kinetics modeling, its input requirements, and describes the chemical kinetics mechanism used in this work.

3 FLAME INHIBITION MECHANISMS ANALYSIS METHODOLOGY*

3.1 Introduction

In this section, a methodology is proposed to investigate fundamental phenomena involved in the combustion inhibition mechanism of different flame inhibitors using CF_3Br as the baseline. As illustrated in Figure 2, this methodology integrates model formulations and experimental designs in order to examine the chemical kinetics and thermal effects of fire suppressants on different hydrocarbons, especially in low molecular weight alkanes (methane, ethane, and propane). In particular, ignition and flame speed experiments were conducted.

Experimental design involves the use of specialized equipment for combustion analysis including a shock tube (for ignition analysis), and a freely expanding flame speed bomb (for laminar flame speed analysis). These facilities provide highly repeatable test conditions and controllable experiments due to their unique designs. Modeling predictions are based on a detailed chemical kinetics mechanism which is processed using CHEMKIN. Comparison between numerical and experimental combustion parameters, such as ignition delay times, OH* time histories, and flame speed are used

*Part of this section has been reproduced from "C.H. Osorio, A.J. Vissotski, E.L. Petersen, M.S. Mannan. Effect of CF_3Br on C_1-C_3 Ignition and Laminar Flame Speed: Numerical and Experimental Evaluation. Combust. Flame, 160 (2013) 1044-1059". Copyright 2013, Elsevier.

as metrics for mechanism validation. In addition, identification of the key elementary reactions and pathways that most affect the inhibition mechanism(s) are determined through sensitivity analysis. This section also discusses the numerical assessment of potential blend performance by determining saturation concentration, synergistic effects, and global effectiveness based on laminar flame speed results. The following sections give more detail on the experimental and numerical techniques used for such purposes.

3.2 Shock-Tube Measurements

Shock tubes are considered valuable tools to obtain understanding of chemical kinetics mechanisms of different reacting systems, mainly due to their highly repeatable and controllable test conditions. In these experiments, fuel oxidation is reached behind reflected shock waves where near-zero-dimensional conditions are achieved. This approach allows the experimenter to focus on the chemistry involved in the process, since the complexity of the system is minimized. For the present study, reaction progress is analyzed based on chemiluminescence measurements. The following sections describe the shock-tube facility at the Texas &M University as well as the fundamental theory, and the techniques used for the experiments and data analysis.

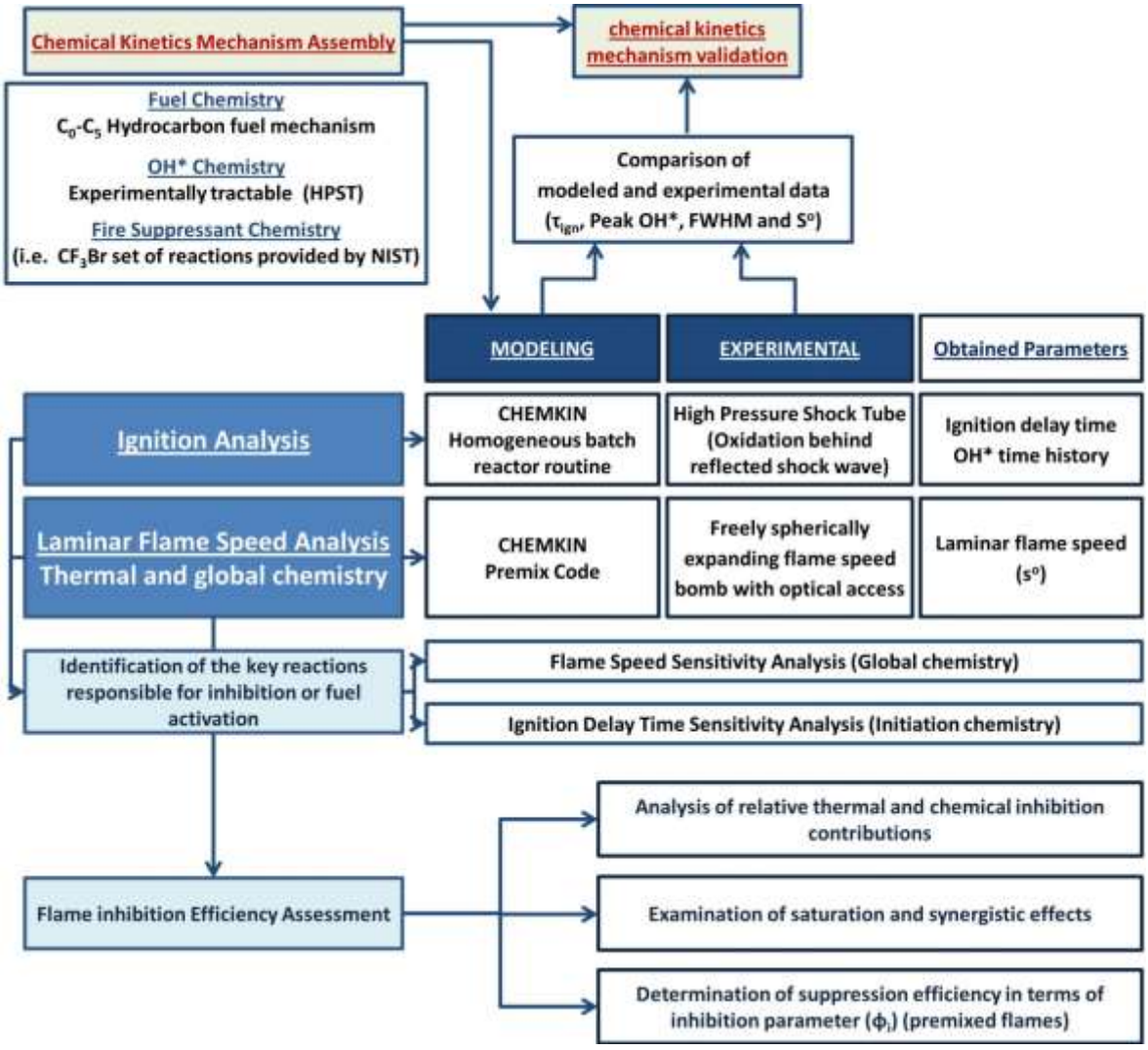

Figure 2. Methodology for flame inhibition study

3.2.1 Shock-Tube dynamics and facility description

The shock-tube facility at Texas A&M University, described in more detail by Aul [36], is provided with *driven* and *driver* sections that have ID's of 15.24 cm and 7.62 cm,

respectively, both with a 1.27-cm wall thickness, constructed entirely of stainless steel 304. The two sections are separated by a polycarbonate diaphragm that ruptures depending on its thickness and the pressure difference between the two sections (although the pressure difference is typically small compared to the bursting pressure of the diaphragm). The *driven* section contains the mixture to be tested at relatively low pressure (~20 torr, or 2.7 kPa), whereas the *driver* section is filled with an inert gas (Helium) up to a critical pressure (i.e., about 270 kPa) causing the diaphragm failure. Therefore, the created incident shock wave travels through the driven section comprising the test mixture, consequently increasing the pressure and temperature of the mixture. Figure 3 illustrates the dynamics of the shock tube and the different stages presented in the test. Incident shock wave velocity and then conditions behind the reflected shock wave are dependent on the pressure ratio between *driven* and *driver* sections which can be modified in every experiment to achieve the desired test conditions. Pressure is monitored through equally spaced pressure transducers located alongside the tube and one at the endwall. Incident-shock speed is calculated using the signal from the pressure transducers which give information of the time at which the shock wave travels from one transducer to the next. From the inferred shock speed, the temperature and pressure behind the reflected shock wave were determined by solving the standard 1-D normal shock relations with an uncertainty of about 10 K [37].

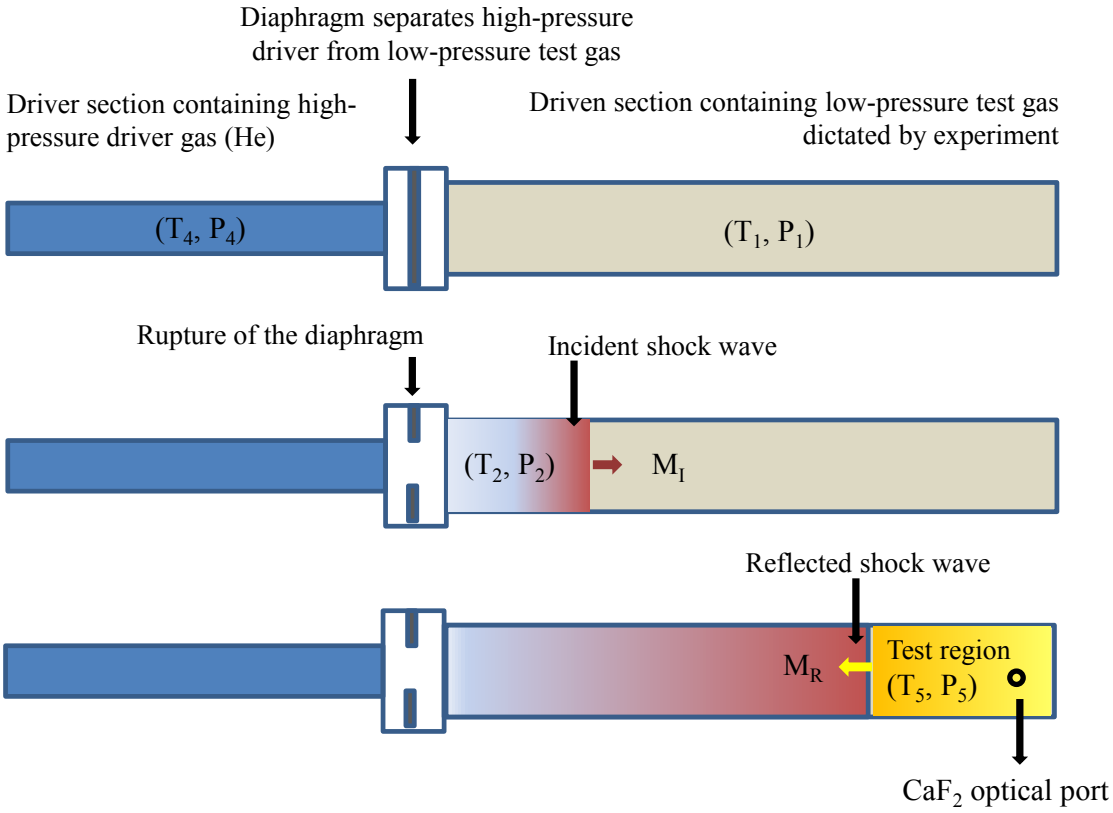

Figure 3. Shock-tube dynamics illustration (adapted from Rotavera [38])

3.2.2 Reaction progress monitoring definition of ignition delay time

Following the convention described by Petersen [39] for highly diluted mixtures, reaction progress was monitored using sidewall emission measurements of OH*. Chemiluminescence measurements were obtained near 310 nm through a window placed 1.6 cm from the end wall (Figure 4). The optical signal was amplified by a photomultiplier tube after passing through a narrowband (310±10 nm) filter and then

was captured using a computer-based data acquisition system from Gage Applied Sciences running GageScope software. OH* profiles and Ignition delay time can be determined by analyzing the pressure/OH* emission profiles obtained in each experiment.

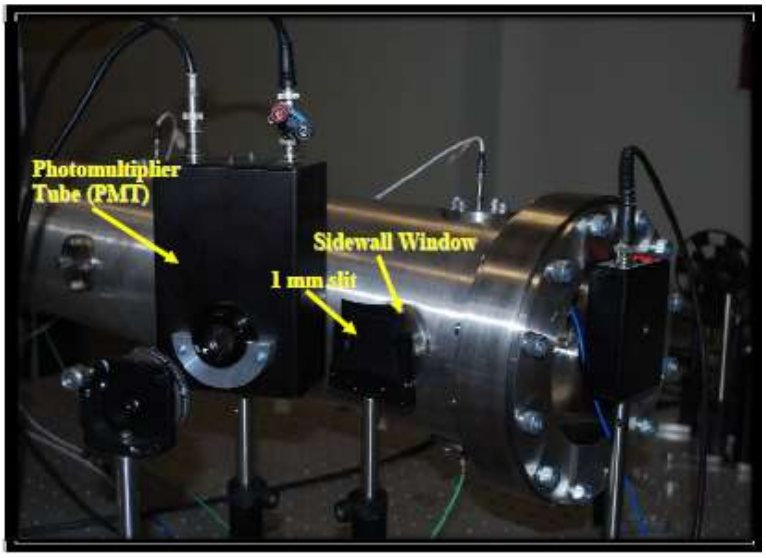

Figure 4. OH* Chemiluminescence diagnostics setup located at the endwall of the shock tube (Taken from Donato [40])

As shown in Figure 5, the ignition delay time (τ_{ign}) is defined as the time between the pressure rise due to the reflected shock wave (time zero) and the rapid increase of optical emission [39], which represents the buildup of radicals and hence OH* at the time of reaction. In other words, this technique uses the time of rapid formation of OH* as a marker of the onset of the ignition process. This methodology has been widely used in previous works [41-47], and it was chosen because it shows an accurate agreement with the historical ignition delay times obtained by pressure and emission diagnostics [39].

Further discussion of this technique can be found in Petersen [39]. Note that the choice of such definition can vary amongst different investigators [48]; therefore it is necessary to be consistent when comparing the results from different sources. In the same way, comparison between modeled and experimental data requires the use of the same definition. From here, it is suggested that subsequent use of the ignition delay time data herein be done using OH* time histories.

From the typical pressure trace (Figure 5), the dP/dt during the test intervals was small (~ 1-2%/ms), implying that facility effects due to boundary layers did not impact the results provided herein. This conclusion is typical for shock tubes with the relatively large inner diameter for the driven section used herein (15.24 cm) and for ignition delay times that are typically less than 2 ms and mostly less than 1 ms. In addition, the mixtures utilized for shock tube measurements are highly diluted in Argon, so additional gas dynamic effects that might occur due to energy release as the result of chemical reactions were not present in these experiments.

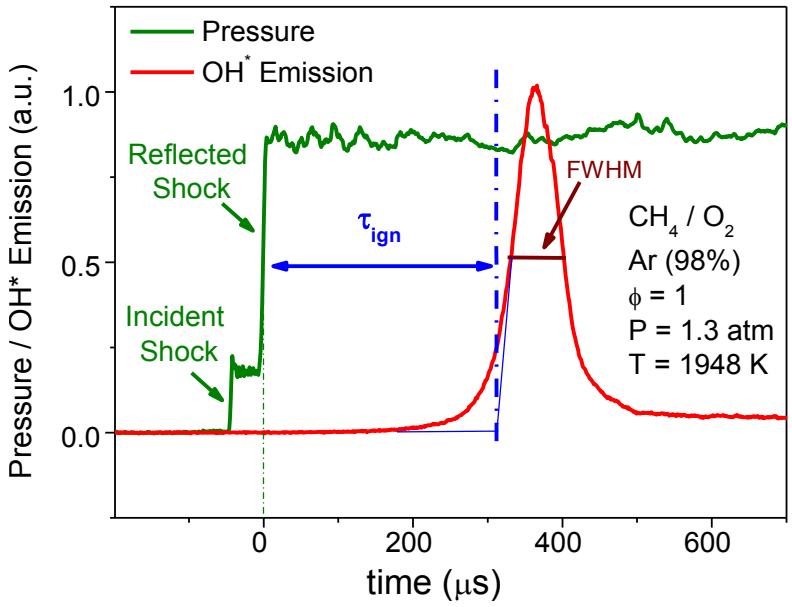

Figure 5. Pressure - OH* emission oscillogram and definition of ignition delay time (τ_{ign}).

The most common information obtained from this method is the ignition behavior, however this study also examines other parameters such as peak OH* and Full Width at Half Maximum (FWHM) of the OH* time history. Determination and comparison of these parameters require special caution to keep identical optical settings in all tests.

3.2.3 Ignition delay time adjustments based on pressure dependency

Ignition delay time measurements are adjusted for small variations in pressure to the average pressure of a particular set of experiments. As suggested by Krishnan and Ravikumar [49], Equation (9) was used to adjust measured ignition delay times based on

their pressure dependence. In Equation (9), the pressure exponent (b) represents the negative sum of the exponents x, y and z, of Equation (10). A is the pre-exponential factor, ignition delay time (τ_{ign}) is given in seconds, concentration ([ ]) in mol/cm^3, activation energy (Ea) in kcal/mol, and Temperature (T) in K.

$$\tau_{adj} = \tau_{meas}\left(\frac{P_{meas}}{P_{avg}}\right)^{b} \tag{9}$$

$$\tau_{ign} = Aexp\left(\frac{E_a}{RT}\right)[fuel]^x[O_2]^y[Ar]^z \tag{10}$$

For this work, the pressure dependent exponents (b) were obtained from correlations in earlier studies involving fuel/O_2 mixtures highly diluted in Argon [50-52]. Such information is summarized in Table 3. The complete set of measured ignition delay times as well as the adjusted data is provided in Appendix A.

Table 3. Summary of correlation parameters for ignition delay time adjustment for fuel/O_2/Ar highly diluted mixtures, based on pressure dependency.

Fuel	***A***	***Ea***	***x***	***y***	***z***	***b***	**Ref.**
CH_4	4.05×10^{-15}	51.8	0.33	-1.05	0	0.72	[50]
C_2H_6	7.15×10^{-9}	39.6	0.79	-1.21	-0.42	0.84	[51]
C_3H_8	5.06×10^{-15}	56.5	0.85	-1.3	0	0.45	[52]

3.2.4 Uncertainty analysis

Uncertainties for ignition delay time measurements come from the observed steepest rate of change from the OH* profile (definition of τ_{ign}), and the determination of the test temperature. However, there is special emphasis made on the "measured" temperature since the monitoring of OH* time histories provides a relatively smaller uncertainty. Further discussion of the accuracy of using OH* profiles as the marker for ignition delay times is provided by Petersen [39].

Test conditions (T_5, P_5,) can be determined using the 1-D simplification of the Rankine-Hugoniot relationships (Equations (11) and (12)). For the determination of the test conditions, propagation of a planar shock wave through an ideal gas is assumed [53, 54]. An adiabatic condition is also considered since there is insufficient time and area for significant heat losses. These calculations required the measured initial conditions (T_1, P_1), specific heat ratio ($\gamma = Cp/Cv$), and the Mach number (M_1). Therefore, the main source of uncertainty comes from the reliance on the numerical solution to yield experimental conditions, particularly on the accuracy of the velocity and pressure measurements which serve as inputs in the conservation equations. Petersen et al. [37] carried out a detailed uncertainty analysis of a shock tube facility of similar details to that used in this work, taking into account the different aspects that can affect the pressure and incident shock wave measurements, and their effect on the calculated test conditions. Petersen et al. concluded that the uncertainty in the determination of the test

temperatures (T_5) is lower than 10 K for those atmospheric pressure tests (P_5~1 atm), and temperature around 1800 K, which are equivalent to the conditions achieved in this thesis.

$$\frac{P_5}{P_1} = \left\{\frac{2\gamma M_1^2 - (\gamma - 1)}{\gamma + 1}\right\}\left\{\frac{(3\gamma - 1)M_1^2 - 2(\gamma - 1)}{(\gamma - 1)M_1^2 + 2}\right\} \tag{11}$$

$$\frac{T_5}{T_1} = \frac{\{2\gamma(\gamma - 1)M_1^2 + (3 - \gamma)\}\{(3\gamma - 1)M_1^2 - 2(\gamma - 1)\}}{(\gamma + 1)^2 M_1^2} \tag{12}$$

3.3 Laminar Flame Speed Measurements

3.3.1 Importance

Premixed laminar flame speed (S_L) represents one of the most fundamental and practical parameters that can be used to understand and predict combustible mixture behavior. A study of the laminar flame speed can be used to understand different phenomena including flame propagation, quenching, stabilization, and inhibition. Laminar flame speed is considered as an intrinsic property that combines the characteristic thermodynamic, diffusive and reactive properties of a specific mixture. Then, it can be used to characterize different systems, especially in terms of its reactivity. Since the fundamental chemical information can be extracted from laminar flame speed, it has also

been widely used as metric for chemical kinetic mechanism validation. Despite the fact that this parameter is only characteristic of laminar systems, it is a fundamental property of premixed chemical systems and serves as a prerequisite for future studies involving more realistic, but more complex systems such as premixed - turbulent flames. Due to all these properties, this parameter has been the subject of many studies for different applications in power generation, propulsion, environmental, and fire and explosion fields.

In terms of fire suppressant fundamental research, laminar flame speed is used to rank different agents in terms of their efficiency to reduce laminar flame speed (inhibition parameter), and to determine the relative thermal and chemical flame inhibition contributions of a specific inhibitor (see Section 3.4.7) . Moreover, numerical analysis is carried out to predict inhibition properties, and to determine the key reactions that most affect the combustion process in those systems in the presence of an inhibitor. It is worth noting that the confidence in such predictions depends on the experimental technique used for model validation. Then, experimental data using accurate techniques, such as freely propagating flames, are extremely important in this field.

After detailing the importance of laminar flame speed measurements, this section provides a general background of premixed flame theory, followed by a description of the current facility and the data analysis employed for this study. Special emphasis is

made on the advantages of using a freely propagating flame and encourages its use to examine the inhibition effect of different fire suppressants.

3.3.2 Premixed laminar flame theory

Premixed mixtures refer to those systems where the fuel has been mixed with the oxidizer before ignition. However, combustion will only take place if the system is within its flammability limits, and reaches a minimum ignition temperature. It can be done by compressing the mixture (auto-ignition) or by applying an ignition source. After combustion takes place, a rise of active radical concentration is observed, forming a highly explosive reaction zone.

By definition, a premixed flame is "a rapid, self-sustaining chemical reaction occurring in a discrete reaction zone" [55]. If the combustion of a premixed flame supports a wave that travels at subsonic velocity (deflagration), it is called a laminar premixed flame [56]. Thus, the laminar flame speed, also known as laminar burning velocity or deflagration velocity, is defined as the characteristic one dimensional- steady velocity at which a planar, adiabatic, subsonic wave freely propagates through a uniform (unburned) premixed mixture at rest [57].

As shown in Figure 6, laminar flames can be analyzed either assuming an unsteady flame, where the wave moves towards the unburned gases ($V_o = 0$), or by fixing the flame as the reference frame, thus the unburned gases approach the wave flame. Note that the static properties are the same in the both systems; therefore the laminar flame speed equals the laminar burning velocity of the unburned gases. For the analysis of laminar premixed flame, the following assumptions apply [56]:

- Steady State
- 1-D (x-direction)
- Adiabatic
- Planar (un-stretched), thin wave
- No friction (no momentum)
- Constant / Average heat capacity (Cp)
- Ideal gas
- Constant pressure ($P_o = P_\infty$)
- Shear work neglected
- Subsonic wave speed (deflagration)

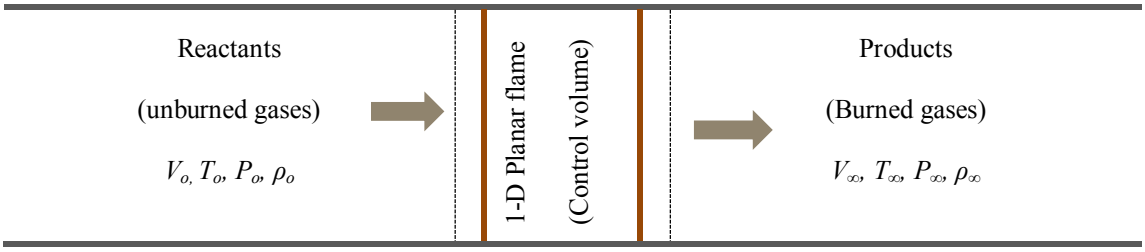

Figure 6. Steady, 1-D, planar premixed flame representation using the flame as the fixed reference frame.

These assumptions reduce the complexity of the governing equations (Table 4) solution of which led to the laminar flame speed. These calculations require detailed information on the reacting mixture contained in a detailed chemical kinetics mechanism, as well as the thermodynamic and transport properties of the species involved. Different computational tools can be used to solve such systems. In this work, the CHEMKIN-PREMIX code is used for such purposes. Section 3.4 provides more detail about this work's numerical methodology. A more-fundamental discussion of flame theory can be found in references [55, 56, 58-60].

In Table 4, $\dot{m}$ is the mass burning rate per unit area; $\dot{\omega}_i$ is the volumetric species production rate; M_w is the molecular weight of the mixture; v_o is the burned velocity; v_∞ is the unburned velocity; and ρ_o and ρ_∞ are the burned and unburned gas densities, respectively. Υ_i is the mass fraction of species i; $v_{i,diff}$ is the diffusion velocity of species i; C_p and $C_{p,i}$ are the specific heat of the mixture and the species i; k is the thermal conductivity of the mixture; and h_i represents the enthalpy of species i.

Table 4. Equations governing the propagation of premixed laminar flames

Conservation of Mass:

$$\left(\frac{d\dot{m}''}{dt}\right) = 0 \rightarrow \nu_o \rho_o = \nu_\infty \rho_\infty \tag{13}$$

Conservation of Species:

$$\dot{m}'' \left(\frac{d\Upsilon_i}{dx}\right) + \frac{d\left(\Upsilon_i \rho v_{i,diff}\right)}{dx} = \dot{\omega}_i M_w \tag{14}$$

Conservation of Energy:

$$\dot{m}'' C_p \left(\frac{dT}{dx}\right) + \frac{d}{dx}\left(-k\frac{dT}{dx}\right) + \sum_{i=1}^{N} \Upsilon_i \rho v_{i,diff} C_{p,i} \left(\frac{dT}{dx}\right) = -\sum_{i=1}^{N} h_i \dot{\omega}_i M_w \tag{15}$$

One of the objectives of laminar flame speed evaluation is the validation of a chemical kinetics mechanism. This application requires that the experiments can resemble the laminar flame speed definition and its assumptions, thus measurements can be directly compared with calculated data.

Methods for flame speed determination include those based on stationary flames, such as Bunsen burner flames, flat flames, and the heat flux method. These methods had been widely used in the past; however, some of their disadvantages are caused by flame curvature, non-uniform upstream flow, and heat transfer effects [61]. Thus, these conventional techniques provide measurements that move away from the laminar flame speed definition. New techniques have been developed allowing the flame to freely expand at adiabatic conditions and constant pressure avoiding complexity. This

technique also allows for examination, and exclusion of the effects of flame stretch on laminar flame speed. This approach provides useful information regarding stretch and instability effects that can affect the rate of flame surface distortion by turbulence; therefore, the obtained results can also be used in future research to simulate turbulent flames [62].

In this study, the freely propagating flames technique was used for laminar flame speed measurements. The following section describes the facility and shows interesting advantages of this technique as a tool for chemical kinetics mechanism.

3.3.3 Facility description and data analysis

Laminar, premixed flame speed measurements were conducted using a freely expanding, spherical flame facility, described in more detail in [61]. It consists of a constant-volume cylindrical vessel constructed from aircraft-grade aluminum, with inside and outside diameters of 30.5 cm and 38.1 cm, respectively, and an internal length of 35.6 cm. The window aperture has a 12.7-cm diameter, so the maximum observable flame diameter is also 12.7 cm. Non-ideal effects from the cylindrical vessel shape distorting the spherical flame growth should be less than 5% for this maximum flame diameter, per the analysis presented by Burke et al. [63]. Direct observation of the flame is possible through two fused quartz windows located at the end-walls of the vessel. It allows the

examination of flame-shape deformation, cellular instabilities, buoyancy effects, and stretch intensity. Therefore, it is possible to determine whether or not the flame becomes wrinkled, and to distinguish at which conditions and time intervals a laminar flame can be assumed. Measurements were made using a high frame rate camera (up to 20,000 frames per second) and applying a Z-type schlieren optical diagnostic technique which magnifies density gradients across the flame within its line of sight. Figure 7 shows sequential images from a typical flame speed experiment in this work.

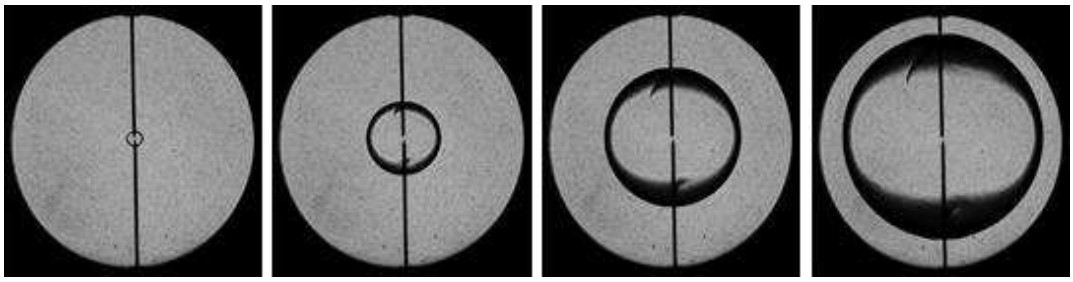

Figure 7. Example of a spherically expanding flame from this work (CH_4-Air, ϕ = 1.0, 0.5% CF_3Br, 1 atm, 298 K)

The imaging technique defines the flame radius as a function of time. Data reduction was conducted by fitting a circle to the flame in each image via a six-point method described by de Vries et al. [64], yielding the flame radius as a function of time. The stretched flame speed in relation to the burned gases, $S_{L,b}$, can be obtained by differentiating the flame radius, R_f, with respect to time, as shown in Equation (16).

$$S_{L,b} = \frac{dR_f}{dt} \tag{16}$$

The measured spherical flames undergo some stretch; therefore the experimental data are corrected for stretch. For this correction, the Markstein flame-stretch relationship was used, Equation (17) [61]; where α and $L_{m,b}$ represent the flame stretch and burned Markstein length, respectively.

$$S^o_{L,b} = S_{L,b} + L_{m,b}\alpha \tag{17}$$

$$S^o_{L,u} = \left(\frac{\rho_b}{\rho_u}\right) S^o_{L,b} \tag{18}$$

Unburned, un-stretched laminar flame speed $\left(S^o_{L,u}\right)$ is obtained by applying conservation of mass at the boundary of the flame using Equation (18); where ρ_u and ρ_b denote the unburned and burned gas densities, respectively. For simplicity, in this thesis the term S_L refers to the unburned, unstretched laminar flame speed and is therefore identical to $S^0_{L,u}$.

3.3.4 Uncertainty analysis

As suggested by Moffat [65], the global experimental uncertainty (U_{SL}) is determined by considering both precision (P_{SL}) and the systematic errors (B_{SL}) through the root sum square (RSS) method as represented in Equation (19).

$$U_{SL} = \sqrt{B_{SL}^2 + P_{SL}^2} \tag{19}$$

The precision error is related with the repeatability of the measurements. It can be obtained by repeating the tests at fixed conditions, but also by considering the random uncertainties coming from different instruments used in the experiments such as thermocouples, pressure transducers, and the camera with a finite resolution. Different studies carried out in the current facility show that the last method is adequate to determine the precision error [64, 66, 67]; therefore, it was employed in this work with no reason of repeating the tests. Equations (20) and (21) serve to predict the precision error (P_{SL}), where $t_{v,095}$ is the student t-distribution with 0.95 confidence, S_{yx} is the standard deviation as a function of the experimental value (y_i), the predicted value ($y_{c,i}$) and the degrees of freedom (v). N represents the total number of data points.

$$P_{SL} = \pm t_{v,0.95} S_{yx} \tag{20}$$

$$S_{yx} = \sqrt{\frac{\sum_{i=1}^{N} \left(y_i - y_{c,i}\right)^2}{v}} \tag{21}$$

On the other hand, the systematic error (B_{SL}), related to the accuracy of the measurements, is determined using Equation (22). For this analysis, each sensitivity coefficient $\left(\frac{\partial S_L(x_i)}{\partial x_i}\right)$, which relates the laminar flame speed with respect to a specific independent variable (x_i), is required, as well as the fixed error (Bi) of each x_i. N is the number of independent variables.

$$B_{SL} = \sqrt{\sum_{i=1}^{N} \left(\frac{\partial S_L(x_i)}{\partial x_i} B_i\right)^2} \tag{22}$$

De Vries, Lowry, and colleagues have conducted an extensive analysis to find each of the elemental errors that contribute to the precision and/or systematic uncertainties in our facility. In their works, these researchers also provide the functions that relate the

measured laminar flame speed with the initial pressure, temperature, and equivalence ratio [61, 64, 66, 67]. In this thesis, current measurements present a total uncertainty less than 1.6 cm/s.

3.4 Numerical Approach

3.4.1 Chemical reaction mechanism: Concepts and applications

Chemical reaction mechanisms are used to describe a global chemical process through a set of individual steps called elementary reactions. This analysis requires detailed information of the reaction rates of each individual reaction as well as the thermodynamic and transport properties of all the species involved in the process. Reaction rates are described in terms of the three kinetic parameters (A, n, Ea), as discussed in Section 2.3. Then, the veracity of a chemical mechanism is highly dependent on the accuracy of such parameters.

There are a number of sources from where this information can be extracted. Thermodynamic and transport data, for example, can be found in Burcat's CHEMKIN thermodynamic database, the NIST-JANNAF (Joint-Army-Navy-NASA-Air Force) thermodynamic tables, the NIST Chemistry Webbook, and the Sandia National Laboratories thermodynamic data. In terms of chemical kinetics data, one of the most

famous sources is the NIST chemical Kinetics Database [68] which includes the kinetics parameters of more than 38,000 gas-phase chemical reactions resulting from over 12,000 experimental and numerical studies. Commonly, more than one set of data is reported for a single reaction by different researchers. Then, the selection of the correct parameters depends on the pressure and temperature ranges at which these values apply.

Development and validation of detailed chemical mechanisms represents a complex task, which can take several years of work, involving the collaboration of many research groups with diverse fields of expertise. Even the kinetic mechanism of a "simple" CH_4/O_2 system, can include hundreds of reactions requiring the accurate selection of the species properties, and kinetic data for all the reactions. But also, the performance of the global mechanism needs to be validated against different types of measurements that confirm its veracity at a wide range of conditions. Here is where research groups, experts in experimental measurements, play a crucial role in the development of chemical mechanisms.

Considerable advances have been done on the development of low molecular weight fuels such H_2, CH_4, and C_2H_4. Most of these chemical kinetics mechanisms are easily found from the internet and provided by recognized research centers including:

i. Gas Research Institute (GRI)
ii. Lawrence Livermore National Laboratory

iii. California Institute of Technology

iv. National Centre for Atmospheric Science – University of Leeds

v. National Institute of Standards and Technology (NIST)

vi. Combustion Chemistry Center – Galway University

Accurate chemical kinetics mechanisms are considered very important since they can be used to predict combustion properties of different systems (fuel/oxidizer/inhibitor) at different conditions. Important combustion properties include ignition delay times, laminar premixed flame speed, and flammability limits, among others. In the area of flame inhibition, modeling of chemical mechanisms can be used to design fire suppressants mixtures by predicting the best combination performance; also, they can be used to rank the inhibition performance of different chemicals (or blends) in a specified system. They also are considered an important tool to study environmental effects of the combustion process, and to understand atmospheric chemistry and changes related to ozone depleting potential and global warming. The following section provides a description of the numerical techniques and computational tools used for the current modeling work.

3.4.2 Chemical kinetics mechanism used

In general, the mechanisms used in this work for the different analyses were assembled from different sets of reactions. These are:

i. Hydrocarbon oxidation mechanism: It represents a detailed set of reactions where several C_0-C_5 hydrocarbons and related species are included. It was provided by researchers from the Combustion Chemistry Center at Galway University (Ireland), who have worked together with the Texas A&M - Petersen combustion group for the development of such mechanisms [69-71]. These mechanisms are available online at http://c3.nuigalway.ie/mechanisms.html.

ii. OH* chemistry: the set of OH* reactions was incorporated for accurate predictions of ignition delay time (τ_{ign}). Note that the rapid formation of OH* is used as the marker for ignition process, and represents the primary diagnostic used in the experiments, as discussed previously in Section 3.2.2. These data have been the result of different studies conducted by Hall, Petersen, and colleagues [69, 70].

iii. Fire suppressant chemistry: CF_3Br kinetics data have been provided by researchers at the National Institute of Standards and Technology (NIST), from the works of Babushok et al. [72, 73] which contain the Br chemistry together

with a large set of elementary reactions involving C_1-C_2 fluorinated species. On the other hand, two different sets of data for C_2HF_5, and C_3HF_7 HFC-125/HFC-227 were provided by Luo et al. [34, 74-76], and Babushok et al. [73]. In essence, these sources have the same basis. However, they included few isolated modifications.

Information on the detailed chemistry used in the different analyses is specified in Sections 4.3 and 5.3. Thermodynamic and transport data were taken from the Burcat [77], NIST [78] and NUI-Galway [71] databases.

3.4.3 Computational tools

In this work, modeling is performed to predict parameters such as ignition delay time, laminar flame speed and OH* time histories, to conduct sensitivity analysis, and to assess the flame inhibition performance based on laminar flame speed calculations. For this calculation, CHEMKIN, a Fortran-based chemical kinetics package for gas-phase reaction analysis [79], is used. CHEMKIN is able to solve the hundreds of ordinary differential equations (ODEs) coming from the kinetics analysis discussed in Section 2.3, in conjunction with the conservation of energy equation characteristic of a particular scenario. For this, CHEMKIN includes a collection of codes that are integrated to provide the solution and interpretation of different kinetics problems involved in gas-

phase systems. As mentioned in previous sections, kinetics analysis requires a detailed reaction mechanism that should be provided together with thermodynamic, and in some cases, transport data. This information is processed and associated into a linking file required for other specific routines, such as Senkin [80] and Premix codes [81], used for sensitivity analysis and laminar flame speed calculations, respectively. Figure 8 shows a general structure of CHEMKIN.

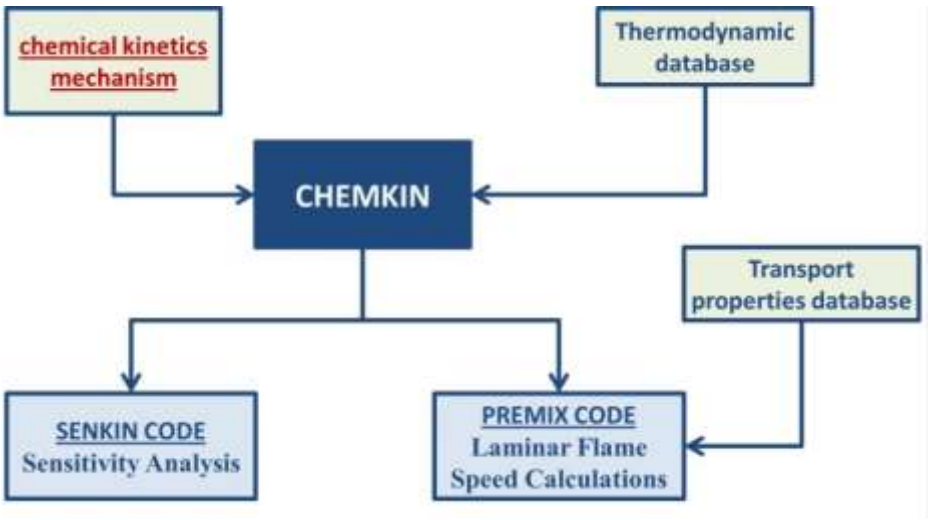

Figure 8. General CHEMKIN's structure (Adapted from reference [80])

CHEMKIN requires the input of kinetics and thermodynamic data in a specific format [82]. Figure 9 shows a simple example of a set of reactions written in the CHEMKIN format, where the kinetics parameters are specified for each reaction. This information is a requirement to calculate the reaction rates (see Section 2.3 for kinetics theory).

```
!COMMENTS: VERSION, AUTHORS
!-------------------------------------------------------------

ELEMENTS
H       N       O
END
!-------------------------------------------------------------

SPECIES
H         O         OH        H2      O2      OH    HO2       H2O
END
!-------------------------------------------------------------

!                                 A           n         Ea
REACTIONS
H+O2<=>O+OH                    1.040E+014     0.000   15286.0
O+H2<=>H+OH                    5.080E+004     2.670    6292.0
OH+H2<=>H+H2O                  2.247E+008     1.520    3450.0
O+H2O<=>OH+OH                  3.445E+006     2.020   13400.0
H2+M<=>H+H+M                   4.577E+019    -1.400  104400.0
HO2+H<=>OH+OH                  7.079E+013     0.000     295.0
H2+O2<=>H+HO2                  5.176E+005     2.433   53502.0
HO2+O<=>OH+O2                  3.250E+013     0.000       0.0
HO2+OH<=>H2O+O2                2.456E+013     0.000    -497.0
END
!-------------------------------------------------------------
```

Figure 9. Example of a chemical kinetics mechanism in CHEMKIN format. Taken from the AramcoMech1.0 [69-71]

CHEMKIN is also able to calculate different thermodynamic properties such enthalpy (H^0), entropy (S^0), and specific heat capacity (Cp), by solving the polynomials represented in Equations (23) to (25). For this calculation, it is necessary to provide the corresponding set of coefficients (α_1- α_7) for each of the species involved in the process. Figure 10 shows a typical thermo-database which includes a total of fourteen coefficients for two ranges of temperature.

$$\frac{H^0}{RT} = a_1 + \frac{a_2}{2}T + \frac{a_3}{3}T^2 + \frac{a_4}{4}T^3 + \frac{a_5}{5}T^4 + \frac{a_6}{T} \tag{23}$$

$$\frac{S^0}{R} = a_1 lnT + a_2 T + \frac{a_3}{2}T^2 + \frac{a_4}{4}T^3 + \frac{a_5}{5}T^4 + a_7 \tag{24}$$

$$\frac{Cp}{R} = a_1 + a_2 T + a_3 T^2 + a_4 T^3 + a_5 T^4 \tag{25}$$

```
THERMO
H                               1               G   300     5000     1000          1
0.02500000E+02 0.00000000E+00 0.00000000E+00 0.00000000E+00 0.00000000E+00    2
0.02547163E+06-0.04601176E+01 0.02500000E+02 0.00000000E+00 0.00000000E+00    3
0.00000000E+00 0.00000000E+00 0.02547163E+06-0.04601176E+01                   4

H2                              2               G   300     5000     1000          1
 0.02991423E+02 0.07000644E-02-0.05633829E-06-0.09231578E-10 0.01582752E-13    2
-0.08350340E+04-0.01355110E+02 0.03298124E+02 0.08249442E-02-0.08143015E-05    3
-0.09475434E-09 0.04134872E-11-0.01012521E+05-0.03294094E+02                   4

 O                              1               G   300     5000     1000          1
 0.02542060E+02-0.02755062E-03-0.03102803E-07 0.04551067E-10-0.04368052E-14    2
 0.02923080E+06 0.04920308E+02 0.02946429E+02-0.01638166E-01 0.02421032E-04    3
-0.01602843E-07 0.03890696E-11 0.02914764E+06 0.02963995E+02                   4

 O2                             2               G   300     5000     1000          1
 0.03697578E+02 0.06135197E-02-0.01258842E-05 0.01775281E-09-0.01136435E-13    2
-0.01233930E+05 0.03189166E+02 0.03212936E+02 0.01127486E-01-0.05756150E-05    3
 0.01313877E-07-0.08768554E-11-0.01005249E+05 0.06034738E+02                   4
```

Figure 10. Typical thermodynamic input file containing the fourteen coefficients required to calculate the thermodynamic properties of different species. Taken from the AramcoTherm 1.0 [69-71]

Some CHEMKIN applications, including laminar flame speed calculations, require the input of some transport properties of the species involved. Therefore, it is necessary to include a file with some molecular parameters such as the Lennard-Jones potential well depth and collision diameter, dipole moment, polarizability, and the rotational relaxation collision number, from where the conductivity, diffusivity, and viscosity are calculated based on the collision theory.

3.4.4 Ignition delay time predictions

Following the same definition of ignition delay time discussed in Section 3.2.2, the OH* profiles were used as a marker of the ignition process. OH* profiles, and therefore the ignition delay times, were predicted by modeling the conditions behind a reflected shock wave. For this scenario, a zero-dimensional, homogeneous batch reactor routine was assumed with volume and internal energy as constants. For the mixtures used herein, which were highly diluted in argon, there was minimal pressure rise due to energy release so that constant-enthalpy and -pressure calculations would yield the same result.

3.4.5 Laminar flame speed calculations

The CHEMKIN-PREMIX code was used to model the unstretched, laminar flame speeds using the Steady Laminar 1-D Premixed Flames module [81]. All flame speed runs were conducted at initial ambient and atmospheric conditions (298 K, 1 atm), using more than 250 grid points, through 10 continuations. GRAD and CURV parameters at the last continuation were set at.01 each. Fundamental theory related to laminar flame speed can be found in Section 3.3.2.

3.4.6 Sensitivity analysis

Sensitivity analysis is conducted to identify the most significant reactions that are responsible for the ignition and flame speed when a fire suppressant is present in the system. In other words, sensitivity analysis tell us which reactions we can change the rate in order to modify a specific output (i.e. OH* time history). Therefore, this analysis not only helps us to better understand the effect of flame inhibitors on ignition and flame propagation processes, but it can also be used to identify those reactions for which modifications in their reaction rates may provide betters predictions. For this type of calculation, Senkin was used.

SENKIN, developed by Lutz et al. [80], is a famous Fortran-based program that can be used through the CHEMKIN interface. It is mainly used to conduct kinetic sensitivity analysis with respect to the reaction rate (in terms of the Arrhenius A-factor). In this study, two different cases are analyzed: (1) flame speed sensitivity analysis, and (2) Ignition sensitivity analysis. For the first case, the flame speed analysis considers the changes of its equivalent parameter the flow rate with respect to the A-factor, while the ignition analysis involves the determination of sensitivity coefficients based on OH* related to A-factor. (Appendix D provides all the plots obtained using Senkin for those sensitivity analyses related to CF_3Br study). This last analysis takes into account the strong relationship between the rapid formation of OH* and the onset of the ignition process. This assumption can be verified by conducting a second brute force analysis, where the sensitivity coefficient is obtained by considering the changes on the ignition delay times when doubled and halved the pre-exponential factor (Equation (26)). Section 4.5.2 presents the results of this validation when systems with and without CF_3Br were analyzed.

$$SC_{\tau_{ign}} = \frac{\tau_{A/2} - \tau_{2A}}{\tau_A} \tag{26}$$

3.4.7 Flame inhibition efficiency assessment

The present methodology also includes the assessment of the flame inhibition of single inhibitor or a fire suppressants blend. For this assessment, laminar flame speed is used to characterize the performance of an inhibitor in terms of an inhibition parameter (Φ) as suggested by Rosser et al. [83] and by Fristrom and Sawyer [84]. Later on, Noto et al. [78] modified this parameter by considering the exponential reduction of the laminar flame speed ($S_L / S_{L,o}$) as a function of the inhibitor mole fraction (X_i), and using the oxygen mole fraction (X_{O_2}) as a normalizing parameter (Equation (27)). Then, the inhibition parameter can be obtained through Equation (28). This definition serves as the basis for further analyses which are discussed in the following sections.

$$\frac{S_L}{S_{L,o}} = \left(\frac{1}{X_{O_2}}\right) \exp(-\Phi X_i) \tag{27}$$

$$\Phi = \left(\frac{X_{O_2}}{X_i}\right) ln\left(\frac{S_{L,o}}{S_L}\right) \tag{28}$$

3.4.7.1 Fire suppressant thermal inhibition contribution

Analysis of thermal inhibition contribution is examined numerically by isolating the chemistry of the fire suppressant from the chemical kinetics mechanism, and calculating the laminar flame speed. Thus, the resulting relative reduction of the flame speed will be caused solely by the physical effect of the fire suppressant (Equation (29)). In the case of a fire suppressant blend (components 1 and 2), the final thermal effect will be the sum of the thermal effect on the individual agents, following the Equation (30) [34, 78]

$$\frac{S_L}{S_{Lo}} = e^{-(\Phi_{th} X_i)} \tag{29}$$

$$\frac{S_L}{S_{Lo}} = e^{-(\Phi_{th1} X_1 + \Phi_{th2} X_2)} \tag{30}$$

Where (S_L) and (S_{Lo}) are the uninhibited and inhibited laminar flame speed; X_1 and X_2 denote the molar concentrations of the two components of the fire suppressant blend; and *p* corresponds to the physical inhibition index. [34, 78]

3.4.7.2 Chemical inhibition contribution

Chemical inhibition contribution (Φ_{chem}) of a mixture can be obtained by isolating the thermal effect from the global inhibition effect (Φ_{global}), as represented in Equation (31) [34, 78]

$$\Phi_{chem} = \Phi_{global} - \Phi_{thermal} \tag{31}$$

3.4.7.3 Examination of synergistic effect

Chemical interaction between two or more agents can cause a synergistic effect. In this case, the resulting flame speed reduction $\frac{S_L}{S_{Lo}}$ would differ from that obtained using the Equation (30) [34, 78]

$$(\Phi_{chem})_{mixture} > (\Phi_{chem})_1 + (\Phi_{chem})_2 \tag{32}$$

4 STUDY OF CF_3Br FLAME INHIBITION MECHANISM*

4.1 Introduction: Importance of CF_3Br for Research Purposes

Halon 1301 (CF_3Br) had been widely used as a fire suppressant for many years, mainly due to its high efficiency and relatively low toxicity, among other properties [85]. Even though CF_3Br together with other halogenated fire suppressants have been phased out by the Montreal Protocol due to their high ozone-depleting potential [12], further study on the chemical kinetics of CF_3Br is required and continues to be a topic of current research [73, 86-93] for many reasons. Two important reasons include the fact that CF_3Br serves as a useful baseline to which alternative substances can be compared, and detailed knowledge of its chemical kinetics can be used to guide the design or identification of future fire suppressants.

After the Montreal Protocol restriction, several replacements are currently being designed and coordinated as cleaner alternatives but with capabilities similar to Halon 1301. Despite all previous efforts, no single Halon 1301 substitute has been found that meets all the required criteria. A more likely approach is then to identify diverse agents for specific applications. Assessment of such alternatives includes the evaluation of different combustion properties such as ignition, extinction, and flame speed, so the

*This section has been reproduced from "C.H. Osorio, A.J. Vissotski, E.L. Petersen, M.S. Mannan. Effect of CF_3Br on C_1-C_3 Ignition and Laminar Flame Speed: Numerical and Experimental Evaluation. Combust. Flame, 160 (2013) 1044-1059". Copyright 2013, Elsevier.

alternatives can be compared to the Halon 1301 flame inhibition performance at similar conditions. However, such an approach would be possible only if the flame inhibition mechanism of CF_3Br were well understood and there were adequate and plentiful chemical kinetics data on CF_3Br, to set an accurate baseline and to offer a guideline for this search.

An accurate CF_3Br-fuel chemical kinetics mechanism can be used to predict different kinetics parameters commonly used in the field such as ignition delay time, flame speed, and species time-history profiles; it can also be employed to determine the relative contributions in terms of the thermal and chemical flame inhibition mechanisms. Furthermore, such a mechanism can be used to identify the most significant pathways and reactions that affect the inhibition process.

The need for an accurate chemical kinetics mechanism is certainly not new, making Halon 1301 the subject of several studies over the past decades. Most of them focused on numerical analyses, and in most of the cases they were restricted to determining the effects of CF_3Br on relatively simple hydrogen and methane flames. These limitations have mainly been due to the surprising lack of experimental data and validated fuel chemistry not only for H_2 and CH_4 but for other fuels, as well as the high computational requirements for more-complex calculations. Experimental methods commonly utilized in chemical kinetics studies that allow for precise measurements of oxidation behavior coupled with the recent availability of validated kinetic mechanisms for different fuels

can be used to better understand the performance of CF_3Br over a wider range of conditions and fuels.

To this end, the present work provides new experimental data of ignition delay times, species time histories, and laminar flame speeds for three hydrocarbon fuels. These data serve as both a baseline for novel fire suppressants studies and as a metric for model validation. Herein, results from shock-tube measurements and laminar flame speeds of freely propagating flames are compared against a modern chemical kinetics model. A detailed C_0-C_5 hydrocarbon-CF_3Br chemical kinetics mechanism was assembled and used herein. These data and calculations provide insight regarding the effect of CF_3Br on the initiation stage and the overall reaction rate of different fuels over varying conditions, and they also show where improvements are needed. Sensitivity analyses using the kinetics model are presented and compared with established inhibition theories. Considering the laminar flame speed as an intrinsic property of the reacting mixture, it is used as a tool for inhibitor characterization in terms of inhibition parameter. It also allows us to determine the relative thermal and chemical flame inhibition contributions, and calculations of the relative contributions are provided. Dependence of the CF_3Br effectiveness on the fuel type is also discussed.

4.2 Previous Works on CF_3Br Kinetics Mechanism

Halon 1301 has shown unique properties, the understanding of which could certainly provide direction to the current search for a suitable fire suppressant. The specific Halon 1301 inhibition mechanism is complex and depends on several factors including the type of fuel and the initial conditions (temperature and pressure).

Fundamental studies suggest that Halon 1301 has the strong ability to compete with the chain branching reaction R1: $H + O_2 \rightleftarrows O + OH$, considered as one of the most limiting reactions in any hydrocarbon combustion process [94-97]. It can be approached through catalytic reactions leading to a reduction in radical concentration within the reaction zone (chemically active, or kinetic, mechanism) or by reducing the flame temperature (chemically passive, or thermal, mechanism).

Sheinson et al. [98] predicted the physical and chemical suppression contribution of specific chemical species on pool fires (cup burner flames) by using a linear, additive model. For CF_3Br, they found that 20% of the total suppression action is by a physical mechanism, while 80% corresponds to chemical means (55% due to Br and 25% due to CF_3).

An initial, detailed chemical kinetic mechanism that describes the effect of CF_3Br on hydrocarbon fuels was proposed by Westbrook [94] and was based in part on the Rosser

et al. [83], Butlin and Simmons [99], and Dixon-Lewis and Simpson [100] studies. Westbrook [94] demonstrated the importance of H-radical ($H^{\bullet}$) recombination by the action of HBr acting as a catalyst through the catalytic cycles I and II (Table 5). Considering that the C-Br bond is weaker than the C-F bond, Halon 1301 can be seen as a carrier of bromine that combines with hydrogen to form HBr. The net effect of these cycles is therefore to consume the H-radicals and produce less-reactive hydrogen (H_2) molecules.

Table 5. Catalytic cycles involving Bromine species.

Cycle I [94]	**Cycle II [94]**	**Cycle III [4, 97]**	**Cycle IV [101]**
$H+HBr \rightleftarrows H_2+Br$	$H+HBr \rightleftarrows H_2+Br$	$H+CF_3Br \rightleftarrows CF_3+HBr$	$CH_3+HBr \rightleftarrows CH_4+Br$
$H+Br_2 \rightleftarrows HBr+Br$	$H+CH_3Br \rightleftarrows HBr+CH_3$	$H+HBr \rightleftarrows H_2+Br$	$CH_3+Br \rightleftarrows CH_3Br$
$Br+Br+M \rightleftarrows Br_2+M$	$CH_3+Br_2 \rightleftarrows CH_3Br+Br$	$CF_3+Br_2 \rightleftarrows CF_3Br+Br$	$CH_3Br+H \rightleftarrows HBr+CH_3$
	$Br+Br+M \rightleftarrows Br_2+M$	$Br+Br+M \rightleftarrows Br_2+M$	
Net: $H+H=H_2$	Net: $H+H=H_2$	Net: $H+H=H_2$	Net: $CH_3+H=CH_4$

In this sense, the inhibition efficiency of CF_3Br may be very similar to any other inhibitor containing one Bromine atom, such as HBr and CH_3Br. However, some results showed that CF_3Br is somewhat more efficient than HBr and CH_3Br [94]. Westbrook explained this additional effectiveness by the Fluorine contained in the CF_3Br molecule which can also contribute to the permanent removal of hydrogen atoms from the radical pool [94]. This work has served as a basis for further studies in which the laminar flame

speed was used as one of the main tools for flame inhibition understanding. Noto et al. [95] determined the influence of different inhibitors including CF_3Br on the C_1-C_2 laminar flame speed, as well as their individual thermal and kinetic inhibition contributions. For this estimate, the chemical action of the inhibitor is isolated; therefore the observed reduction of flame speed is purely due to thermal effects. They also point out that scavenging of radicals can be made with and without restoration of the scavengers and that fluorinated species belong in the latter category. In parallel to their work, Casias and McKinnon described the ways in which CF_3Br molecules and the fragments CF_3 and Br can contribute to the flame inhibition of C_2H_4 flames through the catalytic cycle III (Table 5) [4, 97]. Casias and McKinnon found that the CF_3Br chemical action represented 74% of the total inhibition effect in terms of laminar flame speed reduction.

Saso et al. classified the scavengers as catalytic, non-catalytic, and thermal inhibitors. They investigated numerically the effect of many inhibitors on the global kinetics of methane flames by relating their influence on the flame speed with the changes in the Arrhenius parameters (pre-exponential factor A and activation energy Ea) [102]. Therefore, catalytic scavengers, such as CF_3Br, can change Ea in a significant way, while non-catalytic scavengers are those that reduce the pre-exponential factor, A without altering the Ea. Thermal inhibitors cause insignificant effects on A and Ea [102].

Determination of relative thermal and chemical inhibition effects can also be done through laminar flame speed analysis. Rosser et al. [83],and Fristrom and Sawyer [84] proposed a parameter, known as inhibition parameter (Φ), which was later modified by Noto et al.[78]. As mentioned in Section 3.4.7, this parameter considers the exponential behavior of the laminar flame speed reduction as a function of the additive concentration. Then, thermal (or chemical) effects can be obtained by calculating the Φ when the inhibitor is restricted (or allowed) to react. Following this approach, Noto et al. [78] found that CF_3Br can reduce the laminar flame speed on CH_4-Air stoichiometric flames by a factor of 0.5 acting 22% and 78% through physical and chemical means.

On the other hand, Tucker et al. [103] studied the performance of fire suppressant mixtures composed of CF_3Br and inert gases. They inferred that chemical inhibition effects decrease when the agent concentration exceeds a critical value known as the concentration of saturation. This value may play a significant role in the design of fire suppressant blends and can be calculated considering the laminar flame speed data as reported by Luo [34]. Inhibition properties may also vary according to the type of fuel and the temperature. Babushok and Tsang conducted flame speed sensitivity analysis on (C_1-C_3) mixtures with and without CF_3Br to examine the variation of the inhibition effect in relation to the fuel type. Their results indicate that alkane fuel flame speeds are practically governed by the same reactions [104].

Inhibitor performance can also be affected by the temperature. Walravens et al. [101] used a well-stirred reactor to study the effect of CF_3Br on CH_4/O_2/He mixtures over a range of 800 - 1300^oC and found a maximum inhibition efficiency at around 1073 K due to the catalytic cycle IV (Table 5), where two radicals (H and CH_3) are consumed. On the other hand, high-temperature chemistry is studied through shock-tube measurements. By using this technique, Suzuki et al. [105] showed that the addition of CF_3Br can promote ignition on methane, but the opposite effects were observed for ethane mixtures. These observations suggested that during the induction times, the decomposition of fuel versus decomposition of fire suppressant plays an important role on inhibition performance. Similar results were obtained from numerical analyses made by Babushok et al. [72, 96].

Walravens et al. [101] suggested that the promoting effect observed in shock tubes may be explained by the decomposition reaction, $CH_3Br \rightarrow Br + CH_3$, that starts taking place at temperatures above 1273 K. Further understanding of the effect of CF_3Br on the ignition process requires updated chemical model mechanisms that can be used for different fuels and conditions, as well as more and varied experimental data that confirm such predictions, such as radical concentration measurements during the chemical induction time.

Halon 1301 is not the only halogenated fire suppressant that can enhance hydrocarbon-air combustion [72, 78, 87, 88, 95, 106, 107]. Recently, Babushok et al. [73] explored

the currently available experimental data regarding the combustion enhancement by different fire suppressants. Numerical analyses of different properties, including flammability limits, flame speeds, and ignition delay times, showed that some fluorinated compounds present enough energy to contribute and support combustion with flame speeds that can be measured at slightly elevated temperatures.

These studies show the importance of a reliable chemical kinetics mechanism that can help in understanding different phenomena related to flame inhibition. Validation of these models requires accurate experimental data that can be compared to predicted values. As discussed before, laminar flame speed represents a very useful tool not only for validation purposes but also for estimation of different inhibition properties. However, most of the previous studies are based on laminar flame speeds obtained from experimental techniques where the heat losses and stretch effects are significant, creating greater uncertainties in the measurement. In response to this concern, the technique used by the authors allows the flame to freely expand throughout the test period and has negligible heat losses. Un-stretched flame conditions can also be easily determined using the Markstein relationship.

Currently, accurate measurements of un-stretched flame speed involving CF_3Br are scarce. Kim et al. [108] employed a freely propagating flame technique on CF_3Br-H_2-air flames. Results show that Halon 1301 can also induce instabilities on the flame surface, enhancing the reaction area and therefore promoting flame propagation velocities [108],

nevertheless its net effect is to decrease the H_2 flame speed due to its strong chemical mechanisms. The present study shows interesting advantages of freely propagating flame experiments and encourages the use of this technique to examine the inhibition effect on different hydrocarbon flames at different conditions.

The broader scope of our effort beyond the present study was to gain a more comprehensive understanding of flame inhibition mechanisms for a larger range of fuels and fundamental data than heretofore studied by evaluating the effect of CF_3Br on the ignition kinetics and flame speeds of different alkanes as a baseline, model suppressant. This goal can be approached by using a complete chemical kinetic mechanism for examination of important C_0-C_5 hydrocarbon combustion parameters. Such predictions are compared against stretch-free laminar flame speed measurements and high-temperature oxidation data for different reacting mixtures. Detailed information about the numerical and experimental methods used in this study can be found in the section 3.

4.3 Mechanism Used

For the analysis of CF_3Br, the mechanism used has been assembled from three existing sets of chemical reactions: (1) a C_0-C_5 hydrocarbon mechanism from NUI-Galway [71]; (2) Br and F chemistry reactions [78]; and, (3) the Hall and Petersen OH* sub-mechanism [69, 70]. The fuel mechanism is based on the hierarchical nature of

hydrocarbon oxidation including H_2-O_2, CO-CH_4, C_2-C_3, and C_4–C_5 sets of reactions [69-71]. Halon chemistry, provided by Noto et al. [78], contains the Br chemistry together with a large set of elementary reactions involving C_1-C_2 fluorinated species. Moreover, the OH* chemistry was incorporated for accurate predictions of ignition delay time (τ_{ign}) as this was the primary diagnostic used in the experiments described in more detail below. The complete mechanism includes 333 species and 1980 reactions.

4.4 Experimental Specifications

Table 6 presents the different mixtures of fuel (CH_4, C_2H_6, or C_3H_8), O_2, and CF_3Br highly diluted in Ar (~98% v/v) that were tested using the shock tube. Measurements were made covering temperatures from 1250 to 2250 K, at different equivalence ratios. The concentration of CF_3Br was selected based on the fuel:CF_3Br ratio. Since real fires mostly occur at atmospheric pressure, this study was carried out at pressures close to 1 atm.

Table 6. Summary of the mixtures (highly diluted in Argon) analyzed using the HPST. Percentages are in volume percent, with the balance in each mixture being Argon, about 98%.

Fuel	ϕ	Mixture	CF_3Br/Fuel	CF_3Br (%)	Fuel (%)	Oxygen (%)	Argon (%)
Methane	0.50	1	-	0.00	0.40	1.60	98.00
		2	1/10	0.04	0.40	1.60	97.96
	1.00	3	-	0.00	0.67	1.33	98.00
		4	1/50	0.01	0.67	1.33	97.99
		5	1/20	0.03	0.67	1.33	97.97
		6	1/10	0.07	0.67	1.33	97.93
	2.00	7	-	0.00	1.00	1.00	98.00
		8	1/10	0.10	1.00	1.00	97.90
Ethane	0.50	9	-	0.00	0.25	1.75	98.00
		10	1/10	0.02	0.25	1.75	97.98
	1.00	11	-	0.00	0.44	1.56	98.00
		12	1/20	0.02	0.44	1.56	97.98
		13	1/10	0.04	0.44	1.56	97.96
	2.00	14	-	0.00	0.73	1.27	98.00
		15	1/10	0.07	0.73	1.27	97.93
Propane	0.50	16	-	0.00	0.18	1.82	98.00
		17	1/10	0.02	0.18	1.82	97.98
	1.00	18	-	0.00	0.33	1.67	98.00
		19	1/10	0.03	0.33	1.67	97.97
	2.00	20	-	0.00	0.57	1.43	98.00
		21	1/10	0.06	0.57	1.43	97.94

4.5 Results and Discussion

In this work, two different aspects were examined: (1) the effect of CF_3Br on the methane, ethane, and propane combustion, and (2) the accuracy of the numerical predictions by comparing the experimental with the modeled data. As mentioned,

important combustion parameters such as ignition delay times, peak OH*, Full Width at Half Maximum (FWHM) as well as laminar flame speed have been considered as tools for fire inhibition analysis but also as metrics for mechanism validation. This section describes the ignition and flame speed results including the sensitivity results for each case.

4.5.1 Fuel-CF_3Br oxidation behind reflected shock wave

4.5.1.1 Ignition delay time

Figures 11 to 14 show the effect of CF_3Br on ignition delay time, peak OH*, and FWHM, respectively. The complete set of measured ignition delay times, as well as the adjusted data is provided in the Appendix A. Experimental adjustments were based on the pressure dependence of the ignition delay time ($\tau_{adj} = \tau_{meas}(P_{meas}/P_{avg})^b$) as suggested by Krishnan and Ravikumar [49] (see Section 3.2.3). The exponents (*b)* were obtained from correlations in earlier studies, (0.72 for CH_4 [50], 0.84 for C_2H_6 [51], and 0.45 for C_3H_8 [52]).

Results show that CF_3Br speeds up ignition in all methane mixtures tested, with a relatively smaller effect at fuel-rich conditions (Figure 11a-c). On the other hand, as shown in Figure 11(d-e), CF_3Br acts by retarding the ignition in those mixtures

containing ethane and propane. As mentioned above, similar results were also seen in the shock-tube experiments of Suzuki et al. [105] for methane and ethane. In addition to providing a new, comprehensive set of ignition delay time data that can be used for baseline comparisons of future suppressants to Halon 1301, the present work also provides a snapshot of the current state of the art in the chemical kinetics modeling of the effect of CF_3Br on hydrocarbon fuel ignition. In general, the mechanism assembled herein for this purpose agrees with the pure-fuel results reasonably well. This good agreement, however, is not unexpected given the comprehensive nature by which the baseline mechanism from NUI Galway has been updated and validated in recent years for lower-order hydrocarbons [70, 109, 110].

Of more immediate significance is how well the halon chemistry is predicted for the mixtures containing CF_3Br (Figure 11). In most of these cases, the model does predict the experimental behavior in terms of the effect of CF_3Br (enhancing or inhibiting), but in terms of the absolute magnitude of the effect, the compiled mechanism in most cases, rather surprisingly, performs quite poorly. Starting with the methane-based results (Figure 11a-c), the CF_3Br mechanism does fairly well at predicting the reduction in ignition delay time with the addition of CF_3Br, particularly for the lean case and for the rich case (which shows a minimal impact for both the model and the data). At higher temperatures for $\phi = 1.0$, the mechanism under-predicts the effect of the halon addition to CH_4-based mixtures. On the other hand, for both ethane and propane, the model predicts that the effect of the CF_3Br addition at the levels used in the experiments should

produce a minimal effect, or only about a 10% increase in ignition delay time. However, the actual experiments indicate that the effect of the CF_3Br is to increase the ignition delay times by about 100% over the entire range of equivalence ratios and temperatures studied. In other words, the model misses the effect of the halon addition on ignition delay times by an order of magnitude. Some improvements in the halon chemistry are probably in order if CF_3Br is to be used as a model fuel for the identification of future suppressants.

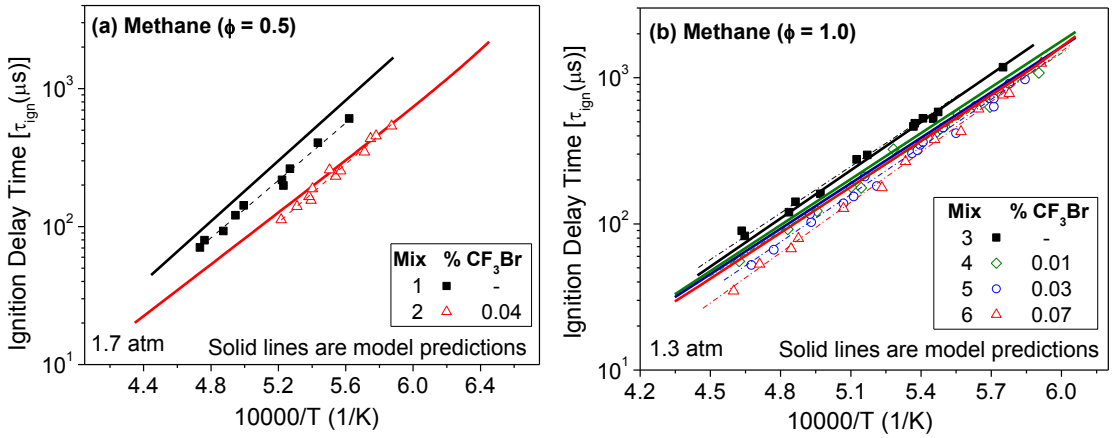

Figure 11. Ignition delay times at atmospheric pressure. ; (a) Methane ϕ = 0.5, (b) Methane ϕ = 1.0, (c) Methane ϕ = 2.0, (d) Ethane ϕ = 0.5, (e) Ethane ϕ = 1.0, (f) Ethane ϕ=2.0, (g) Propane ϕ = 0.5, (h) Propane ϕ = 1.0, (i) Propane ϕ = 2.0. Solid lines are model calculations, while dashed lines are best fits to the data, for convenience.

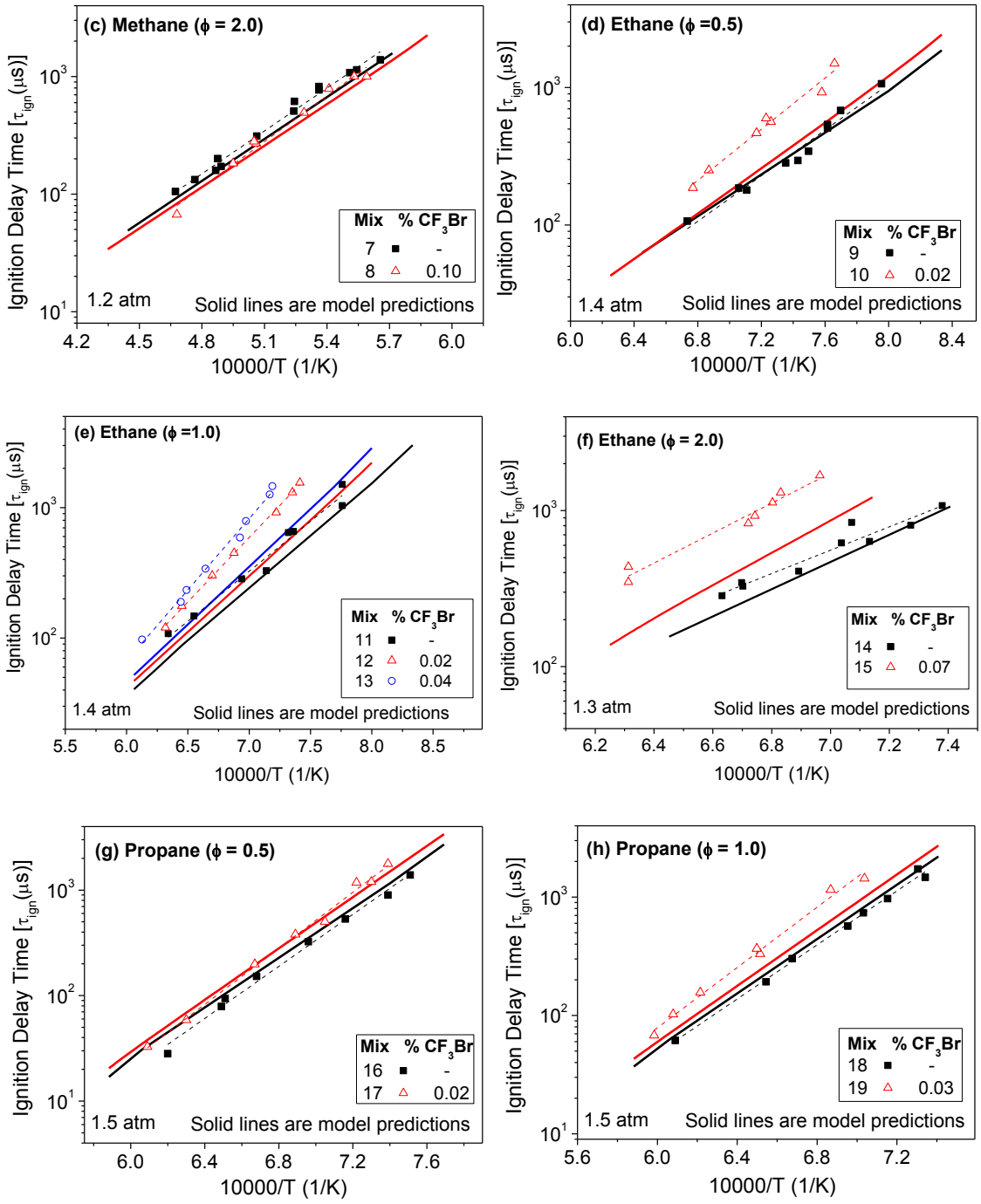

Figure 11. (Continued)

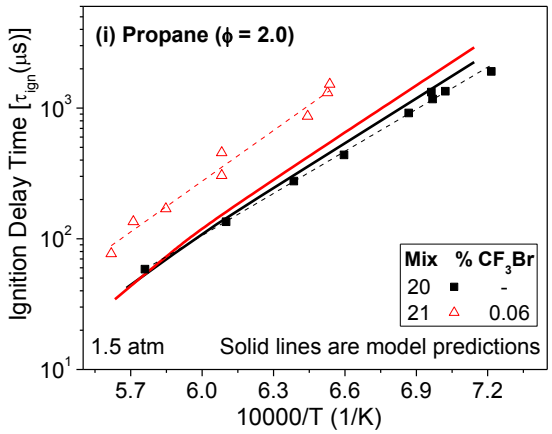

Figure 11. (Continued)

4.5.1.2 OH* time histories and peak OH* concentration

Measurements of OH* time histories were performed, keeping the optical settings identical in all the experiments so that the results in terms of concentrations could be directly comparable to each other. Since a calibration of absolute OH* concentration is difficult to obtain, the OH* data were normalized by taking as a reference one arbitrary condition; in these cases, the test that registered the highest temperature within a set of measurements. Experimental results do not show any significant effect from Halon 1301 on lean and stoichiometric methane data in terms of peak OH* concentration (Figure 12a, b). For the rich methane case, the addition of CF_3Br has a tendency to decrease the peak OH* concentration by about 30-40%. In contrast, the addition of Halon 1301 noticeably decreases this parameter on all ethane and propane systems, more so for the

ethane mixtures (Figure 12.d, b). Since the height of the peak is dictated by the main OH* formation reaction $CH+O_2 \rightleftarrows OH^*+CO$ [111], then it is likely that in those cases where the peak OH* is reduced, the Halon leads to fewer CH molecules.

For the model predictions of peak OH* concentration, there is fair agreement, with at times an over-prediction and at other times an under-prediction of the effects of CF_3Br. The baseline hydrocarbon model (with added OH* kinetics) performs well for the cases with pure fuels; it does particularly well in predicting the temperature dependence of the OH* peak concentration. In the cases with CH_4, the model over-predicts the impact of CF_3Br for the lean case but under-predicts the effect for the rich ($\phi = 2.0$) case. For the other two fuels, the model performs the best for C_3H_8, where there is only a small effect on the maximum OH* concentration from CF_3Br addition. The impact of CF_3Br on OH* concentration for the C_2H_6 cases is under-predicted by the mechanism (Figure 12d and f), where the data show up to a 100% decrease in peak OH*.

4.5.1.3 Full Width at Half Maximum (FWHM)

FWHM provides information on how fast the OH* molecules are produced and consumed. In other words, larger FWHM values imply that the production or consumption (or both) of OH^* is slower. For the analysis of FWHM for the OH* time histories, each experiment and its respective modeled data were normalized to 1, with the peak OH* concentration being unity. Also, the calculated time histories were

adjusted in time to coincide with the experiment, to remove any differences in ignition delay time from the analysis of the OH* time history shape, as illustrated in Figure 13.

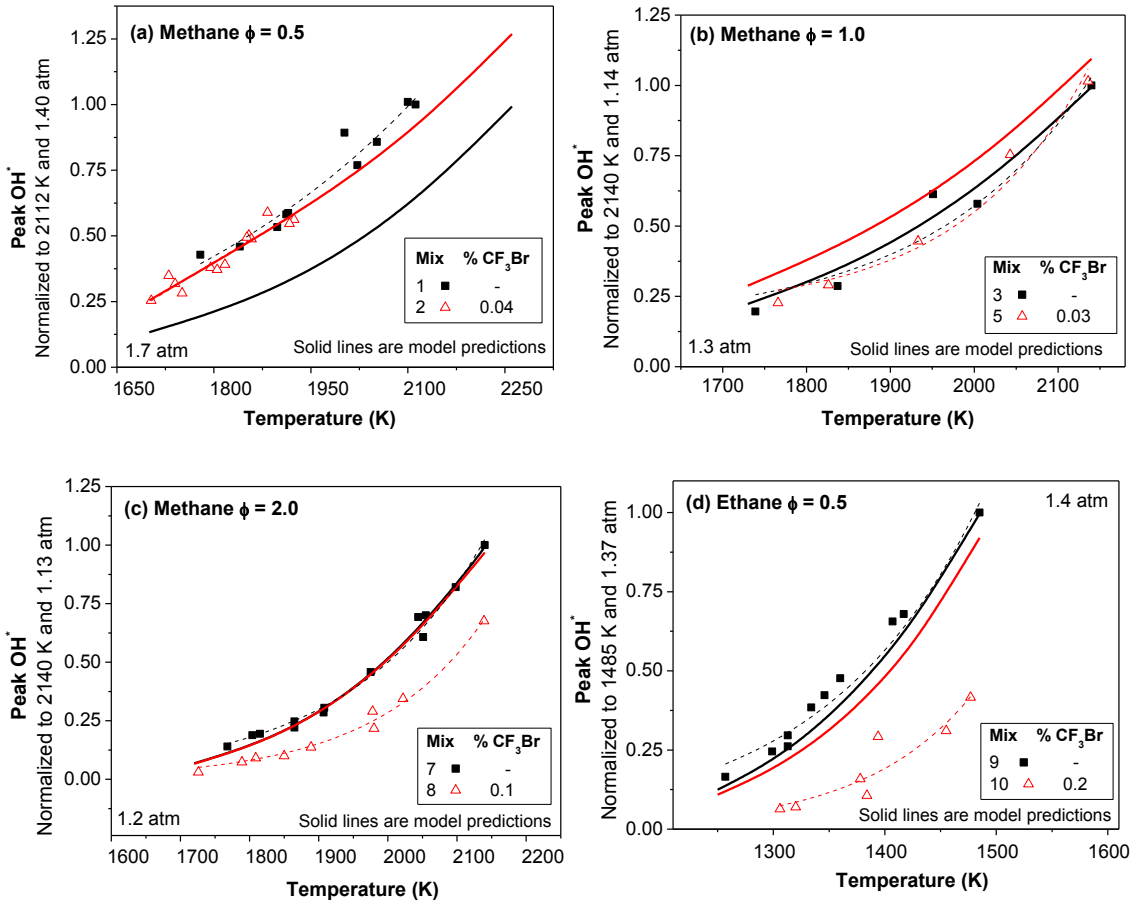

Figure 12. Normalized, peak OH* at near-atmospheric pressure; (a) Methane ϕ=0.5, (b) Methane ϕ = 1.0, (c) Methane ϕ = 2.0, (d) Ethane ϕ = 0.5, (e) Ethane ϕ = 1.0, (f) Ethane ϕ=2.0, (g) Propane ϕ = 0.5, (h) Propane ϕ = 1.0, (i) Propane ϕ = 2.0. Solid lines are model calculations, while dashed lines are best fits to the data, for convenience.

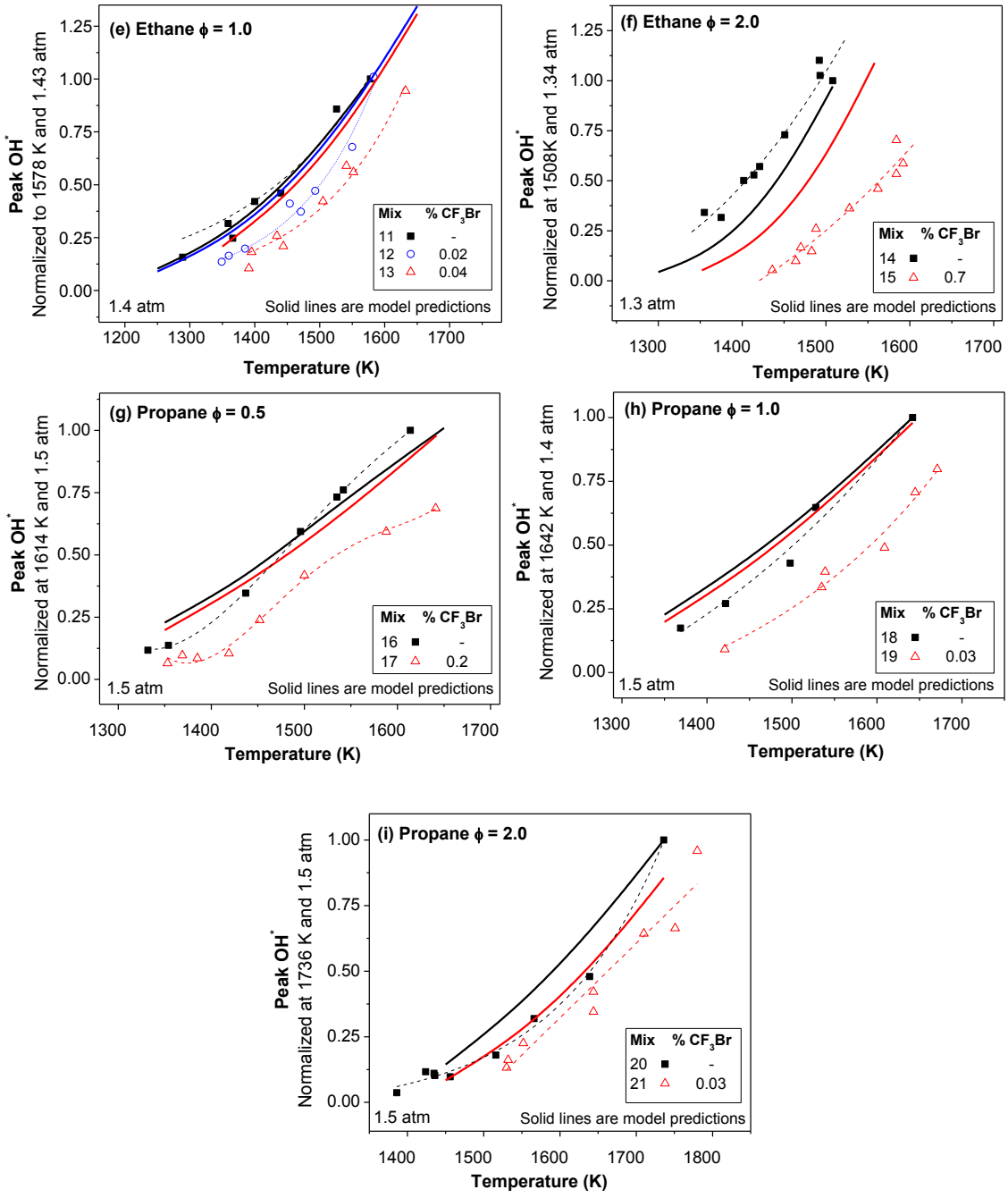

Figure 12. (Continued)

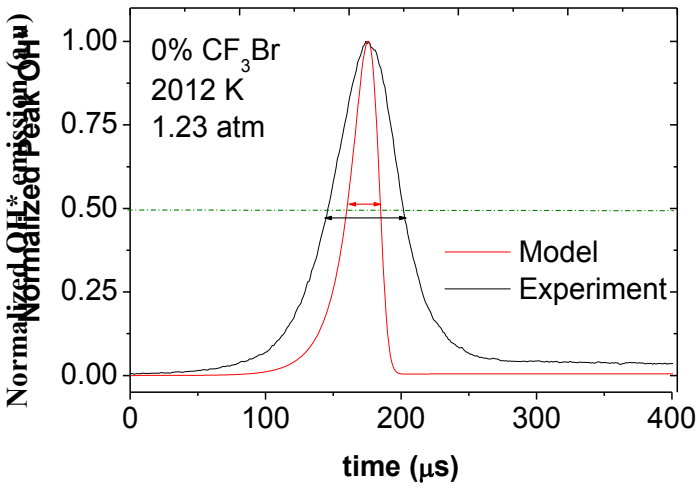

Figure 13. Normalized experimental and modeled OH* emission profiles for a 0.67% CH_4; 1.33% O_2; and 98% Ar mixture at 2012K and 1.23 atm for determination of FWHM.

In general, the results show an increase of FWHM by the action of Halon 1301 in all the systems except in stoichiometric and lean methane mixtures (Figure 14). This behavior parallels the trends seen in the ignition delay times, with the leaner mixtures showing more of a promotion due to halon addition compared to the richer mixtures.

Although the additive had a strong effect on the OH* time history profiles, the model considerably under-predicts this phenomenon, although it does predict the correct trend. This result may be partly attributed to the general under-prediction of the profile width by the baseline hydrocarbon mechanism. As seen in Figure 14, the widths are predicted to be much thinner than the measured profiles, even for the cases with the pure fuels. This under-prediction of the OH* FWHM has been seen in similar chemiluminescence

measurements in the authors' laboratory and is the basis of ongoing study. Recent, detailed measurements indicate that the effect is a deficiency in the kinetics model and not due to any broadening effects in the experimental optics setup [112]. As mentioned above, the width of chemiluminescence time histories in shock-tube experiments is dominated by the ground state chemistry and not the chemistry of the excited species. Further comparisons of the FWHM with and without CF_3Br are pending resolution of the baseline discrepancy with the hydrocarbon mechanism.

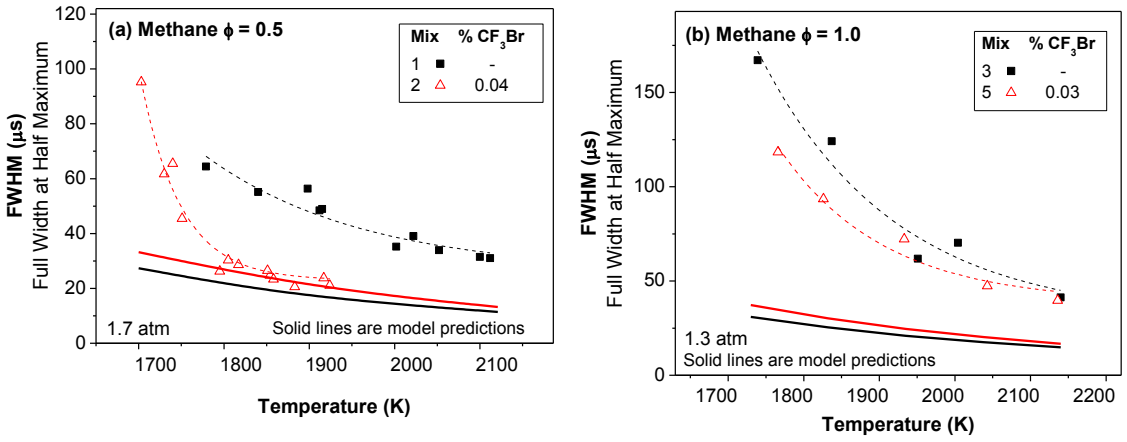

Figure 14. Full Width at Half Maximum dependence on the temperature at near-atmospheric pressure; (a) Methane ϕ=0.5, (b) Methane ϕ = 1.0, (c) Methane ϕ = 2.0, (d) Ethane ϕ = 0.5, (e) Ethane ϕ = 1.0, (f) Ethane ϕ=2.0, (g) Propane ϕ = 0.5, (h) Propane ϕ = 1.0, (i) Propane ϕ = 2.0. Solid lines are model predictions, and dashed lines are fits to the data trends.

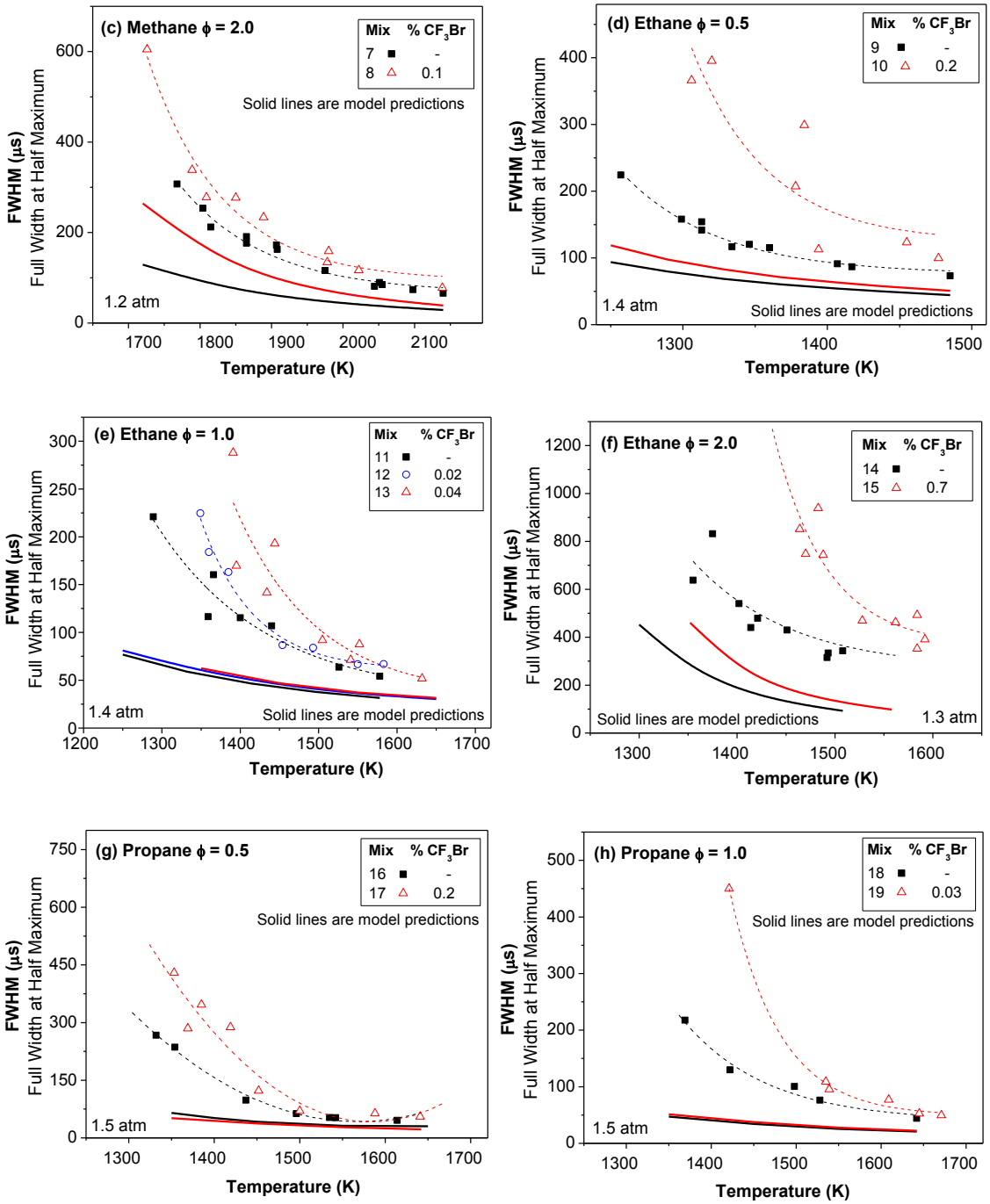

Figure 14. (Continued)

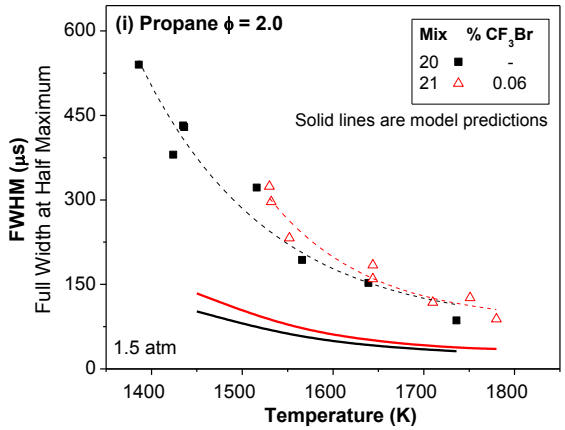

Figure 14. (Continued)

4.5.2 OH* and ignition sensitivity analysis

The ignition process is driven by the formation of active radicals such H, O, and OH. As shown in past studies, the formation of OH* (the diagnostic used in the experiments) tends to be a good marker for the ignition since its concentration is directly linked to the radicals near the time of ignition [71, 113]. Hence, the identification of the key reactions responsible for the formation of OH* should be the same as those responsible for the main ignition process. Considering this connection between OH* and ignition, sensitivity coefficients with respect to OH* were determined and normalized at the ignition delay time, as illustrated in Figure 15. This procedure was conducted for all the systems with and without CF_3Br using the SENKIN code [80]. Appendix C provides all the plots resulting from the OH* sensitivity analysis related to CF_3Br study.

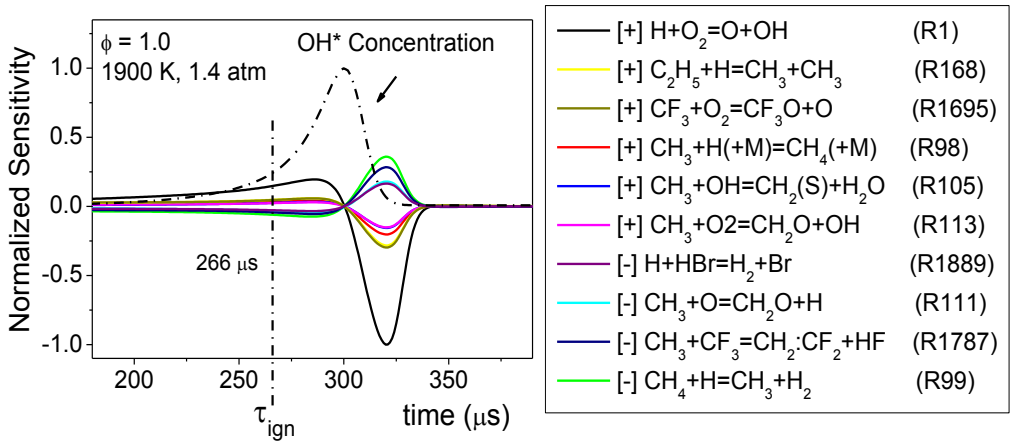

Figure 15. Local sensitivity analysis with respect to OH*, and ranking of the most significant reactions observed at the time of ignition for stoichiometric CH_4-air (0.07% CF_3Br) at 1900 K.

To verify the relative OH* sensitivity coefficients with the ignition delay time sensitivity coefficients; a second, brute-force analysis was carried out. The sensitivity coefficients ($SC\tau_{ign}$) were determined using Equation (26), where τ_A, $\tau_{A/2}$ and τ_{2A} are the ignition delay times obtained when the pre-exponential factor (A) is modified ($A/2$ and $2A$) for each elementary reaction analyzed. Similar results were obtained from the OH* and ignition analysis. It confirms the strong dependency between these two parameters.

$$SC_{Tign} = \frac{\tau_{A/2} - \tau_{2A}}{\tau_A} \tag{26}$$

Comparison between the sensitivity coefficients of different stoichiometric mixtures, with and without CF_3Br, is shown in Figures 16-18, for methane, ethane, and propane,

respectively. The reaction numbers in these figures correspond to the actual numeration in the assembled mechanism. Positive and negative coefficients represent promotion and inhibition of the ignition, respectively. In all the mixtures studied, the branching reaction (R1: $H + O_2 \rightleftarrows O + OH$) is the most influential one. The relative sensitivity of the remaining reactions can be interpreted (i.e., normalized) as their contribution to the H-atoms supplied from this branching reaction (R1). Thus, the sensitivity coefficient of reaction (R1) was considered as a reference equal to 1. Results show that the addition of CF_3Br can affect the ignition process by promoting or inhibiting key reactions which compete simultaneously with each other, leading to a net positive of negative effect. Table 7 summarizes these observations.

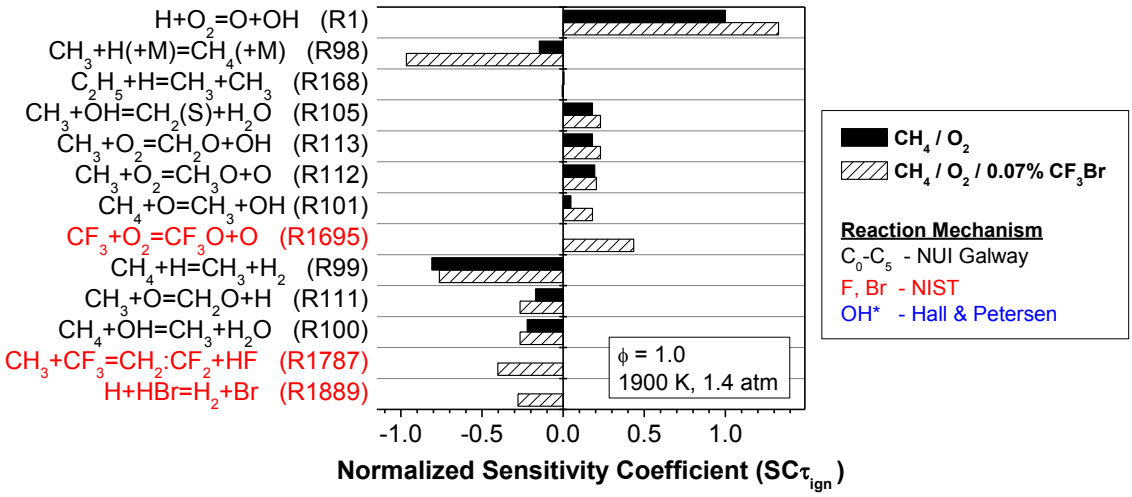

Figure 16. Comparison of the normalized sensitivity coefficients ($SC\tau_{ign}$) of the most significant reactions for methane (ϕ =1.0) with and without CF_3Br (Mixtures 3 and 6).

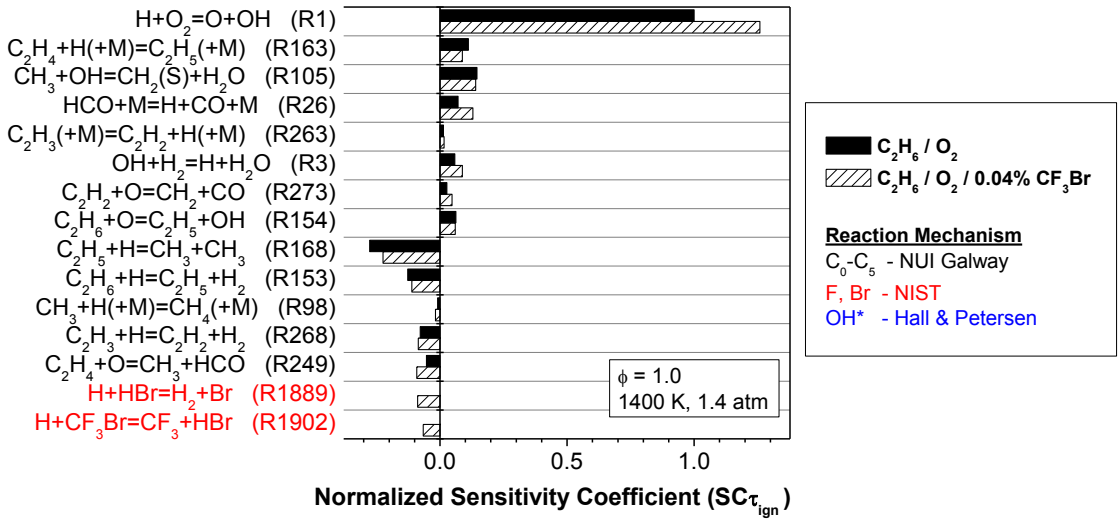

Figure 17. Comparison of the normalized sensitivity coefficients ($SC\tau_{ign}$) of the most significant reactions for ethane (ϕ=1.0) with and without CF_3Br (Mixtures 11 and 13).

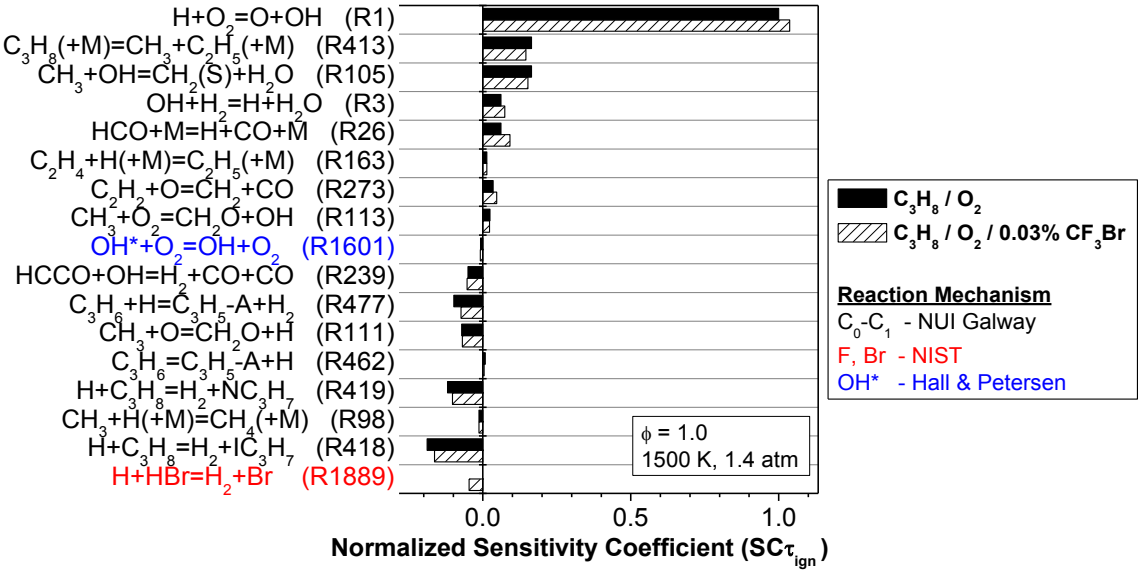

Figure 18. Comparison of the normalized sensitivity coefficients ($SC\tau_{ign}$) of the most significant reactions for propane (ϕ=1.0) with and without CF_3Br (Mixtures 18 and 19).

In all the cases, the branching reaction (R1: $H + O_2 \rightleftarrows O + OH$) is the most influential for ignition. The relative sensitivity of the remaining reactions can be interpreted as their contribution to or scavenging of the H-atoms for this branching reaction (R1). In the case of methane, CF_3Br addition can increase the sensitivity magnitude of (R1), contributing to the faster ignition seen in the experiments.

$$H + HBr \rightleftarrows H_2 + Br \quad \text{(R1889)}$$

From the results, it can be seen that the reaction R1889 represents the strongest inhibition reaction activated by Halon 1301. This observation is in agreement with Westbrook [94], who proposed that the main inhibition capabilities of Halon 1301 are due to the catalytic cycles, mentioned in Table 5. Similarly, the fluorine part of the Halon 1301 molecule can contribute to the inhibition effect through the reactions R1787 and R1902 for methane and ethane systems.

$$CH_3 + CF_3 \rightleftarrows CH_2{:}CF_2 + HF \quad \text{(R1787)}$$

$$H + CF_3Br \rightleftarrows CF_3 + HBr \quad \text{(R1902)}$$

However, this analysis shows that CF_3 can also accelerate the ignition of methane by activating the reaction R1695.

$$CF_3 + O_2 \rightleftarrows CF_3O + O \quad \text{(R1695)}$$

To date, these observations can help us to understand the different Halon 1301 effects on the methane, ethane, and propane ignition processes. More importantly, since the mechanism does a poor job at predicting the effect of CF_3Br on the ignition delay times of ethane and propane, the sensitivity analysis can lead to the identification of reactions for which the estimated or calculated rate coefficients need to be improved. The sensitivity analysis above is only as good as the mechanism that was used to produce it, so future changes in the mechanism can in turn alter the picture of the ignition process summarized in Figures 16-18, and Table 7. Another area for improvement lies in the fact that the Br-F chemistry used herein does not account for possible reactions between hydrocarbons and the halogenated species. Of course, the global effect of Halon 1301 on the combustion mechanism is very complex and cannot be attributed to a single phenomenon.

The following section presents the flame speed results which arguably prove more useful than ignition delay time regarding the effect of flame inhibitor on a global basis, considering the effects not only in the kinetics but also in the thermodynamics.

Table 7. Summary of the CF_3Br effect by the activation or reduction of the most significant reactions found in the sensitivity analysis at stoichiometric conditions (ϕ=1.0).

EFFECT	NET PROMOTION Sensitivity enhanced by CF_3Br toward promoting ignition	NET INHIBITION Sensitivity enhanced by CF_3Br toward inhibiting ignition	NET EFFECT
CH_4	$CF_3+O_2 \rightleftarrows CF_3O+O$ (R1695) $H+O_2 \rightleftarrows O+OH$ (R1) $CH_4+O \rightleftarrows CH_3+OH$ (R101)	$CH_3+CF_3 \rightleftarrows CH_2{:}CF_2+HF$ (R1787) $H+HBr \rightleftarrows H_2+Br$ (R1889) $CH_3+H(+M) \rightleftarrows CH_4(+M)$ (R98)	Speed Up Ignition
C_2H_6	$H+O_2 \rightleftarrows O+OH$ (R1) $HCO+M \rightleftarrows H+CO+M$ (R26) $C_2H_5+H \rightleftarrows CH_3+CH_3$ (R168)	$H+CF_3Br \rightleftarrows CF_3+HBr$ (R1902) $H+HBr \rightleftarrows H_2+Br$ (R1889)	Slow Down Ignition
C_3H_8	$HCO+M \rightleftarrows H+CO+M$ (R26)	$H+HBr \rightleftarrows H_2+Br$ (R1889)	Slow Down Ignition

Note: Reactions in black represent the baseline-mechanism reactions whose influences are significantly altered by the presence of CF_3Br, while the reactions in red are the Br- and F-containing reactions.

4.5.3 Flame speed results

The effect of CF_3Br on different alkane laminar flames was examined numerically and experimentally. For this determination, different concentrations of CF_3Br were added to fuel/air mixtures, covering equivalence ratios from 0.7 to 1.3, at atmospheric pressure and temperature (298 K, 1 atm). The details of the experimental procedure are described in Section 3.3. A complete listing of the new flame speed data is provided in Appendix B. As expected, CF_3Br causes a decrease in the laminar flame speed in all the fuels and all the equivalence ratios examined (Figure 19). Current experimental data are also compared with previous measurements for the neat fuels from Bosschart and DeGoey [114], Vagelopoulos and Egolfopoulos [115], Park et al. [116], Egolfopoulos et al. [117], Hassan et al. [118], Jomaas et al. [119], Rozenchan et al. [120], Gu et al. [121], and Halter et al. [122] in Figure 19; and from Sanogo et al. [123], Linteris et al. [32], and Parks [124] in Figure 20. Experimental data for the pure fuels were previously measured in the same facility and are treated in a previous study [67, 125]. Experimental uncertainty was evaluated, leading to values from 2.5% to 10.5%, with the largest uncertainties being at the lean conditions.

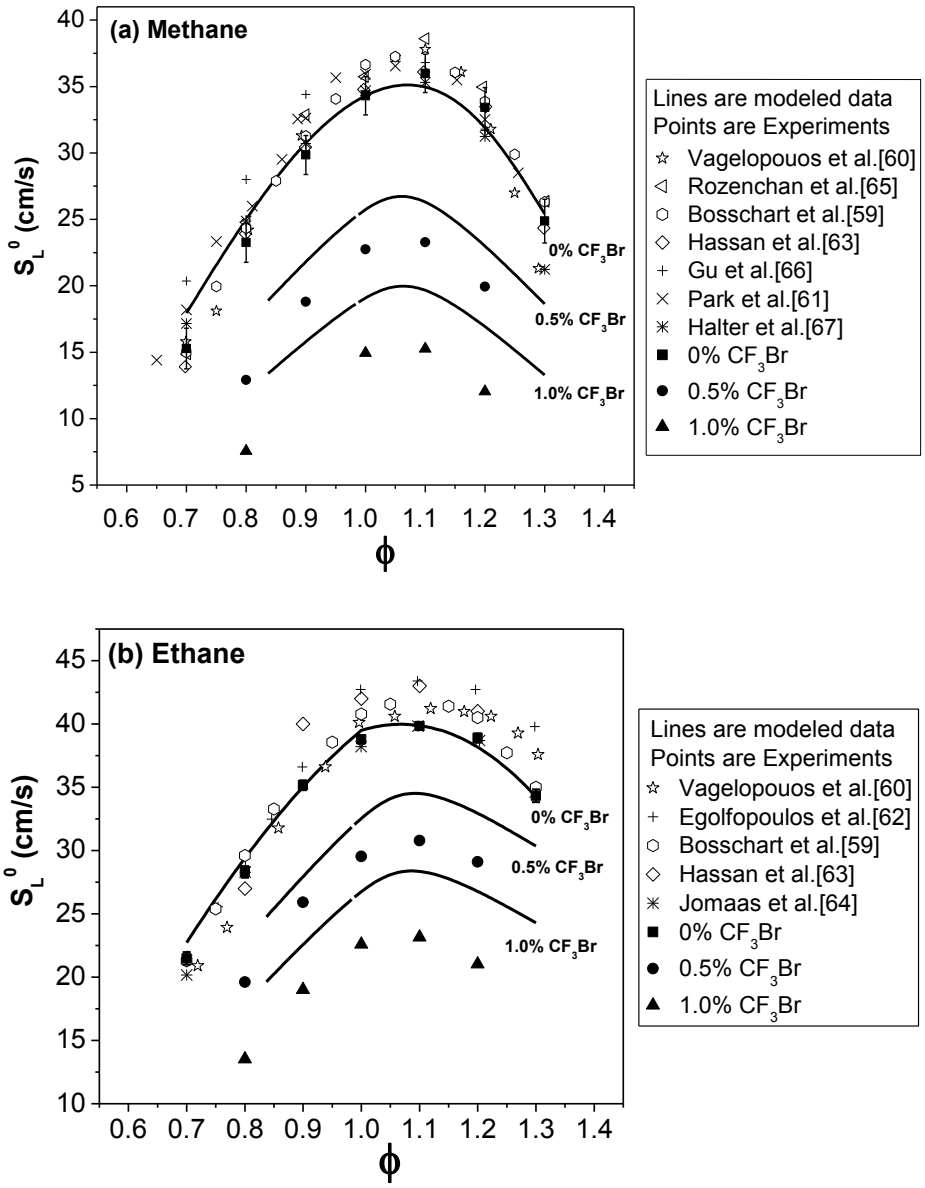

Figure 19. Laminar Flame Speed of different fuel-air mixtures (a) methane; (b) ethane; and (c) propane as a function of the equivalence ratio (1 atm, 298 K), and comparison between this study and previous data [114-122]. The data are also compared to the model predictions.

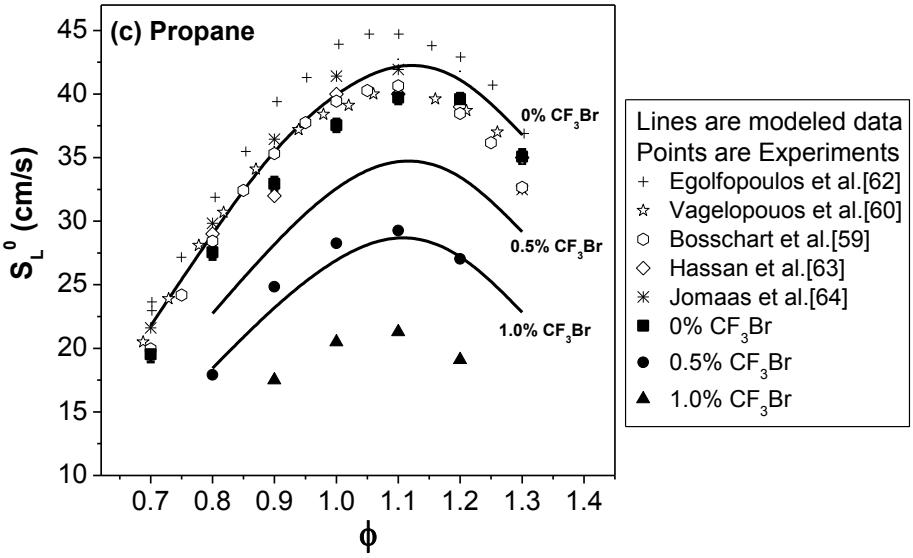

Figure 19. (Continued)

Figure 20 shows that there is good agreement between the results of the present experiments for methane and the only other data available in the literature for CH_4-air-CF_3Br experiments [32, 123, 124]. Comparison between experiment and model shows that the model can predict the same experimental trends; that is, the presence of CF_3Br decreases the laminar flame speed. However, absolute numerical disagreements are present in both Figure 19 and Figure 20. Despite the small differences between the model and measurements of the pure fuels (before CF_3Br addition) for ethane and to some extent for propane, what is most important in the present study overall is the relative effect when adding the CF_3Br. Specifically, the model including the Halon chemistry consistently over-predicts the laminar flame speeds, hence under-predicting the inhibiting effect of the Halon 1301. The under-prediction of the effect of CF_3Br is

seen in both Figure 19 and Figure 20. For example, Figure 20 shows that the over-prediction of the laminar flame speed increases with increasing levels of CF_3Br. These discrepancies suggest that the CF_3Br mechanism can be improved, and the experimental laminar flame speed data of this thesis can be used as the target criteria for guiding future work in this area. Using the present model as a starting point, a sensitivity analysis was conducted and described as follows.

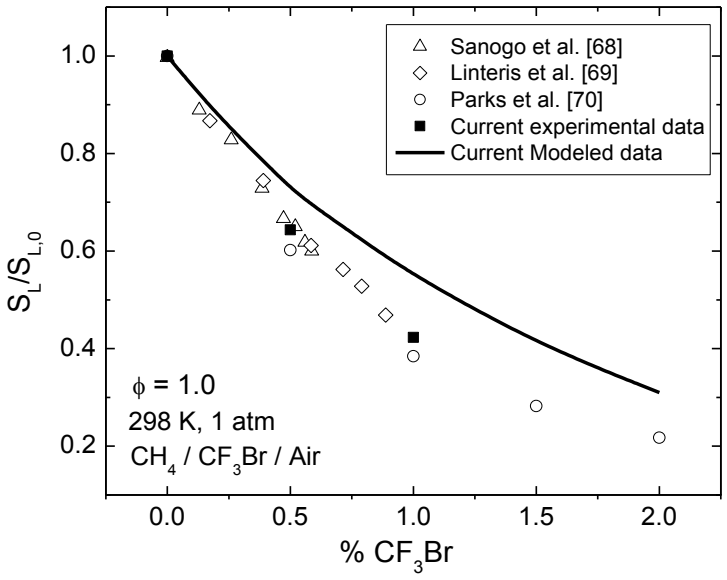

Figure 20. Variation of laminar flame speed with CF_3Br concentration for the methane-air mixture at ϕ=1.0 Comparison between current and previous experimental data are shown, along with the assembled mechanism. (CH_4/air mixtures at 298 K and 1 atm). [32, 123, 124]

4.5.4 Flame speed sensitivity analysis

This analysis aims to identify the most significant reactions that affect laminar flame speed of a given reactant mixture. These results can be used to better understand the flame inhibition mechanism and as a baseline for future improvements of the CF_3Br kinetics effect. Calculations were based on the flow rate sensitivity analysis, which is equivalent to the flame speed. Figure 21 compares using bar plots the relative sensitivities obtained for methane and propane at a stoichiometric equivalence ratio, with and without CF_3Br. Positive and negative coefficients represent promotion and inhibition effects on the flame speed, respectively, and the branching reaction (R1) was considered as the reference. In general, the similitude of the CF_3Br effect on different alkane flames can be seen, in agreement with Babushok and Tsang [104].

As discussed above, improvements in the sub-mechanism involving Br and F chemistry can lead to better laminar flame speed predictions. This thesis focuses only in the Halon effect, giving special attention to those reactions that are activated by the presence of CF_3Br. The reactions R1902, R1889, and R1955 present the highest sensitivity coefficients. As expected, they indeed contribute to the flame inhibition effect, since all of them present negative coefficients.

$$H + CF_3Br \rightleftarrows CF_3 + HBr \quad (R1902)$$

$$H + HBr \rightleftarrows H_2 + Br \quad (R1889)$$

$$Br + HCO \rightleftarrows HBr + CO \quad (R1955)$$

Note that the reaction R1955 shows a particularly strong effect compared with the other reactions activated by CF_3Br. These same three key reactions were reported by Babushok and Tsang [104] and Noto et al. [78, 95], but are absent in the initial mechanism proposed by Westbrook [94]. Based on the strong effect of these reactions on the flame speed prediction, particularly for R1955, it is possible to conclude that more-accurate rate coefficient values can lead to better estimates of the laminar flame speed. Unfortunately, there currently are limited data available regarding measurements for the very important reaction R1955. The NIST Chemical Kinetics Database [126], for example, reports only one measurement for this reaction, conducted by Poulet et al. [127]. Further study is required to get the rate coefficient (experimentally and theoretically) of the Br + HCO reaction and other key reactions (such as R1902 and R1889) to ultimately obtain a better halon mechanism.

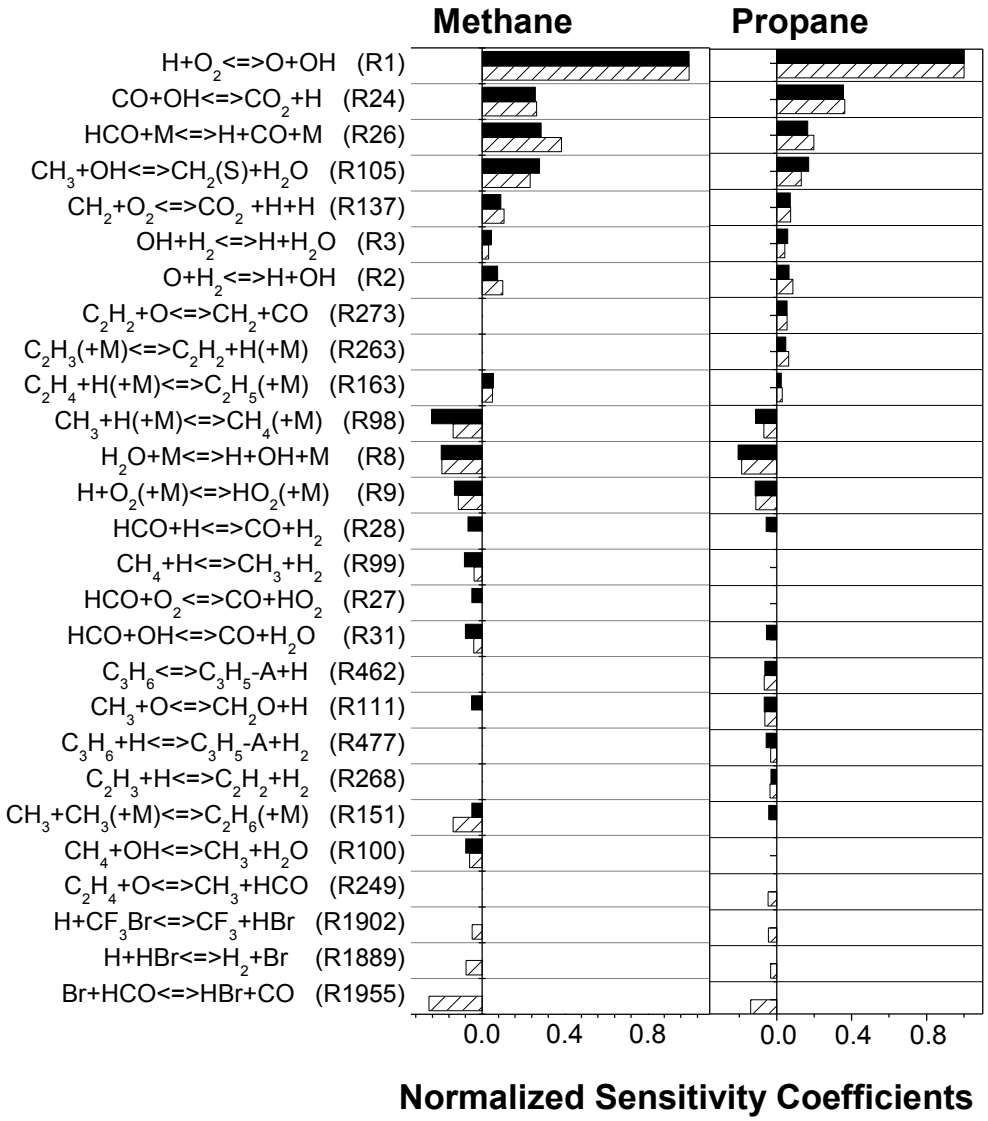

Figure 21. Comparison of the top sensitivity coefficients for stoichiometric methane and propane flames at 298 and 1 atm. (black: 0% CF_3Br, hashed: 1% CF_3Br). Note that reaction numbers in this figure correspond to the actual numeration in the mechanism.

4.5.5 Modification of chemical kinetics mechanism

This section gives an appraisal of how the flame speed predictions can be improved by changing the Arrhenius parameters of the most significant reaction. It is important to point out that the intent of this modification is not to offer a final, validated mechanism, but rather a tool to gauge the extent to which the rate coefficients of the important reaction(s) would have change to get better agreement with the data.

For this excursion, the focus is on the reaction R1955, considering its relatively strong effect (Figure 21). The model used in this study includes the R1955 kinetics parameters ($A = 1.69\times10^{14}$, n = 0 and Ea = 0 in cm, g, s, mol, K and cal units) and agrees with the values reported by Poulet et al. [127]. To show to what extent a modification of the pre-exponential factor (A) can lead to better predictions, it was modified, by trial and error, to five times larger than the original A ($A_{\text{R1995modified}} = 9.3\times10^{14}$). Figure 22 compares the experimental laminar flame speeds with the predictions using the original mechanism and the mechanism containing the modified R1955 rate on mixtures containing methane and propane with 0.5% CF_3Br. Results show an improvement when the modified rate for R1955 is used, especially on those mixtures with CF_3Br concentrations higher than 0.5%. Again, these results are not aimed to be directly transposed to the current mechanism, but they do demonstrate the order of change that may be needed to the rate of this important reaction in a final, comprehensive CF_3Br mechanism. Of course, R1955

and other reactions found to be important for CF_3Br herein can also be important for studies involving other compounds containing Br and F atoms.

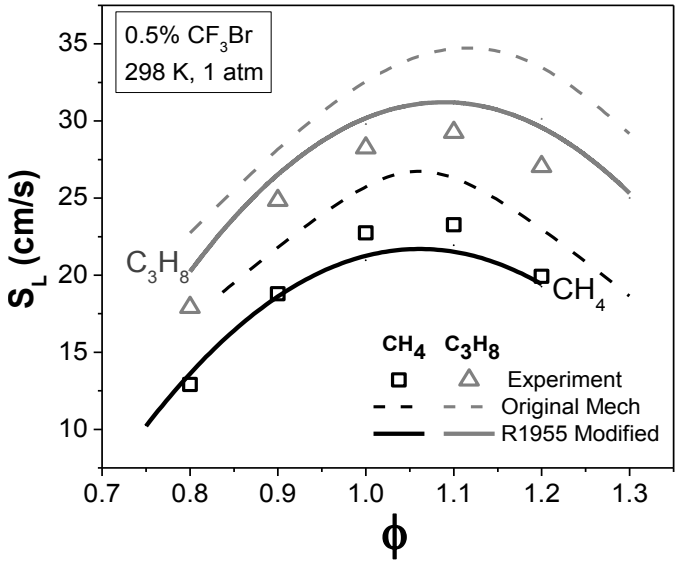

Figure 22. Comparison of the experimental and predicted laminar flame speeds using the original mechanism and the mechanism with the modified rate for R1955, Br+HCO⇄HBr+CO, for methane and propane mixtures with 0.5% CF_3Br at 298 K and 1 atm.

4.5.6 Inhibition efficiency: Thermal and chemical effects

Quantification of the global, thermal, and chemical inhibition contributions were determined in terms of the inhibition parameters Φ_g, Φ_{th}, and Φ_{ch}, respectively. The thermal effect was examined numerically by excluding the F and Br chemistry from the mechanism but otherwise retaining their presence as non-reacting species, following the

methodology employed by Noto et al.[95]. Modeled and experimental results were fitted to the exponential expression presented before (Equation (27)).

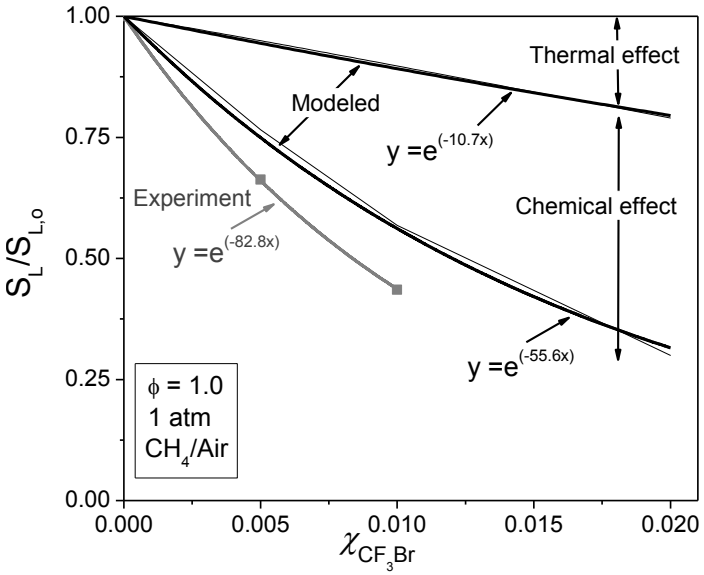

Figure 23. Thermal and chemical effects of Halon 1301 on stoichiometric methane-air flames at 298 K and 1 atm, as suggested by Noto et al. [78].

Figure 23 shows the global and thermal reduction of the flame speed as a function of the CF_3Br concentration for the methane-air test case at ϕ = 1.0. A summary of the inhibition parameters obtained for all three fuels methane, ethane, and propane is presented in Table 8. All modeled and experimental results show that CF_3Br is more effective on methane flames when compared with the other fuels studied herein. This difference is mainly due to the chemical effect, which is stronger at these conditions. Propane and ethane flames present responses similar to each other with regard to the addition of CF_3Br. Sensitivity analysis shows that the CH_4 and C_3H_8 chemistry is very

similar in the presence of CF_3Br (Fig. 12). Nevertheless, the higher efficiency of CF_3Br on methane flames can be explained by noting the sensitivity coefficients of the reactions (R1889) and (R1955) in the same figure, whose negative values are around twice as large in methane compared with those for propane (and hence ethane) flames.

Table 8. Global, thermal and chemical effect expressed as a function of calculated and experimental inhibition parameters (Φ_g, Φ_{th}, and Φ_{ch}), and percentage (%)

	Global		**Thermal**		**Chemical (global − thermal)**	
	$(\Phi_g)_{Calc.}$	$(\Phi_g)_{Exp.}$	$(\Phi_{th})_{Calc.}$	$(\%)_{Calc.}$	$(\%)_{Calc.}$	$(\%)_{Exp*.}$
CH_4	10.6	15.7	2.0	18.9	81.1	87.3
C_2H_6	7.1	10.7	2.0	28.2	71.8	81.3
C_3H_8	7.9	11.9	1.6	20.3	79.7	86.6

* Chemical effect was obtained from the experimental global effect minus the calculated thermal effect.

4.6 Summary and Conclusions

New experimental data were obtained, and the effect of Halon 1301 on different fuel mixtures was studied using a chemical kinetics mechanism. Such research continues to be important because CF_3Br is arguably the standard to which future fire suppressants will be compared, designed, and chosen, so an accurate picture of its kinetic scheme and benchmark kinetics data are needed. High-temperature oxidation and freely propagating

flames were examined by numerical and experimental means, covering three fuels (CH_4, C_2H_6, and C_3H_8) over a range of stoichiometric conditions. Experiments were conducted using a shock tube and a cylindrical vessel provided with optical access, wherein the freely expanding spherical laminar flames were observed. Modeling was performed using a detailed chemical kinetics mechanism containing the CF_3Br chemistry from Noto et al [78], and recent C_0-C_5 chemistry from NUI Galway. Comparisons between modeled and experimental data show that predicted values follow the general experimental trends with regard to the effect of the halon addition; however, disagreements in the actual values—in some cases quite large—suggest that the model containing the Br and F chemistry should be improved. A particular area for improvement lies in the fact that the Br-F chemistry used herein does not consider reactions between bromine containing species and large hydrocarbons. Sensitivity analyses were conducted to identify the most significant reactions that affect the ignition process as well as the flame speed when CF_3Br is present.

Analysis of the Halon 1301 effect on high-temperature chemistry shows that the reaction $H+HBr\rightleftarrows H_2+Br$ (R1889) presents the strongest effect on delaying the ignition process. Fluorine species can further contribute to the inhibition effect on ignition through the reactions $CH_3+CF_3\rightleftarrows CH_2{:}CF_2+HF$ (R1787) and $H+CF_3Br\rightleftarrows CF_3+HBr$ (R1902) for methane and ethane systems. However, for methane mixtures, CF_3 can also accelerate the ignition by activating the promoting reaction $CF_3+O_2\rightleftarrows CF_3O+O$ (R1965).

The reaction Br+HCO⇄HBr+CO (R1955) presents the strongest effect on flame speed compared with the other reactions activated by CF_3Br, but there is a large uncertainty in its rate since there are limited direct measurements. For instance, this work gives an appraisal of how the sensitivity analysis can be applied to demonstrate the level of change needed in the R1955 rate coefficient to improve the agreement between the chemical kinetics mechanism and the data, which in the present case was a factor of five.

Global Inhibition efficiency as well as the relative thermal and chemical contributions were examined in terms of inhibition parameter. Results show that the chemical effect is significantly higher than the thermal inhibition mechanism for Halon 1301. Furthermore, the CF_3Br effect is stronger on methane than either ethane or propane premixed flames, since the inhibiting reactions Br+HCO⇄HBr+CO and H+HBr⇄H+Br show stronger effects on methane.

5 ANALYSIS OF FIRE SUPPRESSANTS ALTERNATIVES: A CASE STUDY OF HFC-125 AND HFC-227 FLAME INHIBITION MECHANISM

5.1 Introduction

C_2HF_5 (HFC-125) and C_3HF_7 (HFC-227) represent two of the most-used Halon 1301 (CF_3Br) substitutes in the field of fire protection. Their wide acceptance is due to their low ozone-depleting potential, relatively low toxicity, low flammability, and good dispersion capabilities [128]. In terms of Minimum Extinguishing Concentration (MEC), HFC-125 and HFC-227 have shown to be more efficient than other clean alternatives in the market [34, 129]. Furthermore, some of their properties are similar to CF_3Br leading to an easy re-use or adaptation of those installations from which Halon 1301 is removed.

At the time of the end of this work, the Significant New Alternatives Policy (SNAP) program by the Environmental Protection Agency (EPA) includes HFC-227 and HFC-125 in the list of substitutes for Halon 1301 as a total flooding agent [130]. There have been some concerns related to the high global warming potential (GWP) associated to HFCs molecules, however the use of HFC-125 and HFC-227 for fire protection applications is minimal, and their impact on climate change represents less than .01% of the impact of all Green House Gases (GHG) emissions [128]. Thus, HFC-125 and HFC-227 are expected to remain as environmentally friendly Halon 1301 substitutes into the foreseeable future [128].

Based on this realization, the use of HFC-125 and HFC-227 has been suggested by several programs that search for potential alternatives, including the Halon Alternative Technology Development Program (TDP) by the U.S Department of Defense (DoD). Under the TDP, HFC-227 was identified as the best fire suppressant alternative applied in manned spaces of ships, critical command and control facilities, while HFC-125 represented the optimal compound used to suppress fires in engines. Consequently, the Next Generation Program (NGP) by the National Institute of Standards and Technology (NIST) found HFC-125 as the best single fire suppressant in airplane cabins and cargo bays; this finding shows that it is unlikely that a superior fluid that can be used for such purposes will be discovered [131]. Currently, several industries use HFC-125 and HFC-227 as part of their fire suppression systems towards protect personal and valuable assets.

Undoubtedly, HFCs represent one of the best options as fire suppressants; however, these compounds have been associated with the promotion of combustion at certain conditions. Therefore, knowing the wide applicability of these substitutes, as well as their increasing demand, it became very important to understand the combustion properties to provide safe, optimal applications. The following section provides background related to the flame inhibition mechanism of halogenated compounds and highlights the need for further understanding.

5.2 Prior Studies Involving HFC Combustion Behavior

Halogenated compounds have shown to be good fire suppressants, especially when the flame is well established (after ignition). However, previous studies have demonstrated that they can also promote combustion at certain conditions [73, 87, 96, 105-107, 132-141]. Osorio et al. [141] and Suzuki et al.[105] observed reduction of the ignition delay time by the action of CF_3Br on methane mixtures, but the opposite effect was reported on systems containing ethane and propane. Hamins and Borthwick [107] observed that CF_3Br and CF_3I are very efficient ignition retardants of hydrocarbon/air mixtures on a heated nickel surface; while C_3HF_7 can sometimes lead to a small promoting effect on methane-air mixtures. On the other hand, Shebeko et al. [106] used a closed vessel to study the effect of different fluorinated compounds on H_2 and CH_4 flames in air. By examining flammability regions, maximum explosion pressure, and maximum rate of explosion pressure, they concluded that some of these agents can promote combustion, especially in lean mixtures. They attributed this effect to the exothermically conversion of the inhibitor. Gmurczyk and Grosshandlerg [139] focused on the effect of different halomethanes on C_2H_4-air mixtures under highly dynamic situations. Their results show that all the agents, except CHF_2Cl, can suppress turbulent flames and quasi detonations, then, they concluded that the chlorine contained in the CHF_2Cl molecule may behave as a combustion enhancer by acting as an oxidizer. They also suggested that despite the fact that bromine and iodine are good flame inhibitors, they can still be part of promoting and inhibition reactions; the final effect depends on the agent concentration. Among large-

scale experiments, Reinhardt [142] conducted aerosol can explosion tests involving C_2HF_5. Results showed that C_2HF_5 can increase the explosion overpressure if it is applied in concentrations below a critical value (inerting concentration).

To better understand such phenomena, many studies have focused on the development and analysis of chemical kinetics mechanisms. A fundamental work in this area has been done by Westbrook [94] who describes a detailed mechanism for CF_3Br on hydrocarbons flames. By numerical analysis, Westbrook shows that the flame inhibition properties of the halogenated compounds are mainly due to their ability to scavenge highly reactive radicals such as H atoms. Also, he demonstrates that CF_3Br is slightly more efficient than CH_3Br, and suggested that the fluorine contained in the CF_3Br molecule may be the cause of such an additional effect. This work has served as a basis for subsequent studies that focused on determining the role of specific fluorinated species on different scenarios. These include the study done by Westmoreland et al. [143] who analyzed different fluoro-methane systems. They found that CF_4 and CF_2O act as inert diluents; while CH_2F_2 and CH_3F behave as fuels by increasing both the adiabatic flame temperature and the flame speed. CHF_3 was found to help the chain-terminating reactions, but at the same time, this species can contribute to increasing the adiabatic flame temperature through exothermicity. Then, the final effect depends on the competition between the HF, (which contributes to chain termination reactions), and the production of H radicals from different oxidation mechanisms [143]. In general, the release of H radicals will be favored since the bond energy of C-F is higher than for C-

H. Nevertheless, this trend is not standard and will depend of the conditions and fuels involved.

Suzuki et al. [105] suggested that in CH_4 systems the decomposition of the agent is prevalent leading to a promoting effect, while in C_2H_6-CF_3Br systems, the ignition is controlled by the fuel oxidation. Babushok et al. [72, 96] concluded that the agent can decompose on different active species that either promote or inhibit active radical formation. Osorio et al. [141] conducted sensitivity analysis on ignition chemistry at high temperatures and found that fluorinated species play a significant role in ignition retardant processes through the reactions ($CH_3+CF_3 \rightleftarrows CH_2{:}CF_2+HF$) and ($H+CF_3Br \rightleftarrows CF_3+HBr$), but at the same time, CF_3 can promote the ignition of methane by activating the reaction $CF_3+O_2 \rightleftarrows CF_3O+O$. Linteris et al. [88] used detailed reaction kinetics and thermodynamic calculations, together with a perfectly stirred reactor model to examine the promotion effects of C_2HF_5 on aerosol can explosions (reported by Reinhardt [142]). From their analysis, it was concluded that an increment of the pressure can occur at certain concentrations of an agent only if a large amount of oxygen is consumed. In other words, these effects are dependent on the stoichiometric fuel-oxidizer-agent proportions.

Katta et al. [87] modeled the effects of CF_3H on cup burner flames and concluded that fluorinated species, such CF_3H, CF_3, CF_2, CF, and CF_2O, participate in termination reactions reducing radical concentrations in the flame and forming HF which is a

relatively more stable species. Nevertheless, in cup burner flames, CF_3H dilutes the oxidizer in the stream and also acts as a fuel requiring more oxygen. As a consequence, both the total heat released and the flame size become larger. Similar results were obtained from simulations conducted by Takahashi et al. [93], who found an increment of the heat released when C_2H_5F was added to microgravity cup-burner flames. These results are in agreement with Ural [140] and Babushok et al. [73], who indicated that halogenated agents possess their own heat release which can support the global combustion process.

Despite all the extensive research related to HFC effects on flame chemistry, basic understanding of the relevant chemical kinetics still remains elusive. Further progress in this area requires well validated chemical kinetics mechanisms that can provide fundamental insights, and therefore to better predict the behavior of HFC-125 and HFC-227 at different conditions. Such models represent powerful tools that need to be compared against acute measurements to address uncertainties in the mechanism. For this reason, experiments are particularly valuable.

Currently, there are scarce experimental data of HFCs that can be used for model validation, especially in terms of laminar flame speed and ignition delay time. Note that these parameters can be used as metrics for model validation but also as tools to examine combustion effects in the initiation and global processes. The present work remedies this deficiency by providing accurate measurements that can give insight to the effect of

HFCs on the ignition process in different fuels; it also serves as a metric for model validation when HFCs are compared directly with modeled data. The following section describes the modeling and experimental methodology used for this purpose.

5.3 Mechanism Used

Table 9 presents the assembled chemical kinetics mechanisms used in this study. They include the CF_3Br and HFC-125/HFC-227 mechanisms, provided by Luo et al. [34, 74-76], and Babushok et al. [73]; recently updated C_0-C_5 hydrocarbon chemistry [71]; and a set of OH* reactions [69, 70] that describes the rapid formation of OH* radicals. This last one is particularly important in the determination of ignition delay times since the rapid formation of the OH* radical is used as an indication of ignition. The two Br-HFC mechanisms used in this study were provided by different research groups. In essence, these two mechanisms have the same basis. However, they have some isolated modifications. The purpose of this numerical approach was to compare the mechanism against the experimental data, and then identify the most significant reactions that affect the ignition process. For this comparison, OH* A-factor sensitivity coefficients were calculated using SENKIN [80]. Note that OH* was used in sensibility analysis since its rapid formation is directly related to the ignition onset [141].

Table 9. Chemical kinetics mechanisms used in the examination of C_2HF_5, C_3HF_7, and CF_3Br.

	Sub-mechanisms	Ref.
Mechanism A	AramcoMech 1.0 (C_0-C_5) + OH* chemistry	[69-71]
Mechanism B	AramcoMech 1.0 (C_0-C_5) + OH* + Luos' Modified Br-HFC chemistry	[34, 74-76]
Mechanism C	AramcoMech 1.0 + OH*+ NIST Br-HFC chemistry	[73]

5.4 Results and Discussion

5.4.1 Ignition delay time

The effects of HFC-125 and HFC-227 on the fuel high-temperature chemistry were studied by adding 0.1% of the tested fire suppressants to the mixtures, and comparing them with the baselines (0% fire suppressants). Results were compared to those using CF_3Br which can be considered as the standard fire suppressant.

Table 10 shows the diluted mixtures of fuel (CH_4 or C_3H_8), oxygen (O_2), and Argon (Ar) that were analyzed using the shock-tube facility. The effects of HFC-125 and HFC-227 on the fuel high-temperature chemistry were studied by adding 0.1% of the tested fire suppressants to the mixtures and comparing them with the neat-fuel baselines (0% fire suppressants). The results were also compared to those using CF_3Br, which can be considered as the ideal fire suppressant. All the tests were performed at atmospheric

pressure since most of the fire protection applications are developed at these conditions. Experimental temperatures were in a range of 1350 K to 2200 K.

Table 10. Compositions of the mixtures used for measurements and predictions of ignition delay time.

Mixture	CF_3Br	C_2HF_5	C_3HF_7	CH_4	C_3H_8	O_2	Ar
1 (Baseline)	-	-	-	0.67	-	1.33	98.00
2	0.10	-	-	0.67	-	1.33	97.90
3	-	0.10	-	0.67	-	1.33	97.90
4	-	-	0.10	0.67	-	1.33	97.90
5 (Baseline)	-	-	-	-	0.33	1.67	98.00
6	0.10	-	-	-	0.33	1.67	97.90
7	-	0.10	-	-	0.33	1.67	97.90
8	-	-	0.10	-	0.33	1.67	97.90

Figure 24 shows the resulting experimental ignition delay times for the different methane and propane mixtures. Experiments show that all the tested fire suppressants tend to decrease the ignition delay time in methane mixtures (Figure 24a). Their promoting effect in CH_4 mixtures can be ranked as $CF_3Br < C_2HF_5 < C_3HF_7$. However, this trend is not general for all fuels. Propane measurements (Figure 24b) show that the ignition can be slighted promoted by C_2HF_5 but retarded by the action of CF_3Br. C_3HF_7 does not show a significant effect on propane mixtures in either direction. Note that the

range of practical application of the present experimental results remains strictly limited to the experimental conditions defined. It demonstrates the importance of numerical approaches since they allow one to predict the combustion properties of different systems and conditions that were not necessarily tested directly in an experiment. As discussed before, mechanisms should be validated using accurate measurements, which recall one of the main objectives of this work.

Figures 26-28 compare measured ignition delay times with model predictions when either CF_3Br, C_2HF_5, or C_3HF_7 are present. Both mechanisms behave very similarly, since they present the same basis, and both predict very well the effect of the tested fire suppressants. Nevertheless, improvements on the HFC-chemistry are suggested for better prediction, especially for those systems of CH_4/ C_2HF_5 and C_3H_8/ C_3HF_7 where the promoting effects are under predicted.

The following section describes the results obtained from a sensitivity analysis using the mechanisms; such comparisons serve as the basis for HFC-flame inhibition understanding but also as the basis for future mechanism improvements.

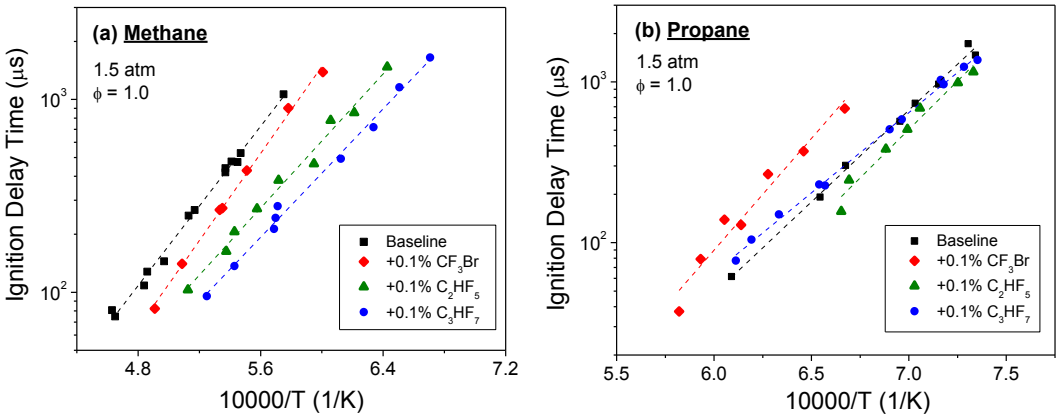

Figure 24. Experimental ignition delay times as a functions of the temperature of different mixtures with and without fire suppressants (CF_3Br, C_2HF_5, and C_3HF_7). (a) Methane, (b) Propane. Points represent the experiments, and dashed lines are the experimental trend.

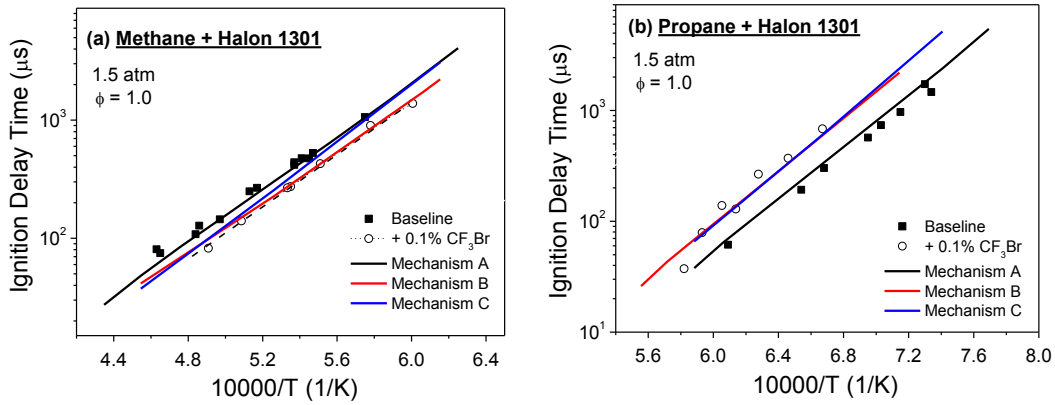

Figure 25. Comparison between experimental and modeled ignition delay times using the Mechanisms A, B and C for different (a) methane and (b) propane mixtures with 0.1% Halon 1301. The dashed line represents the best fit to the data containing the suppressant in each plot.

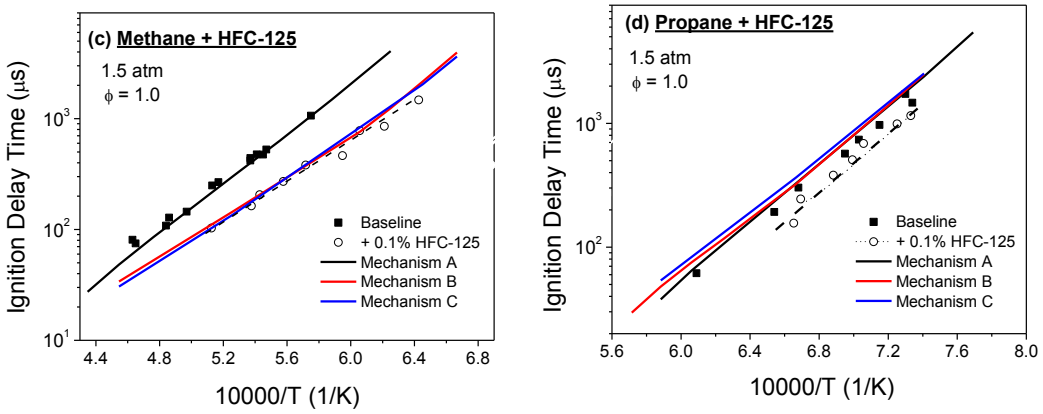

Figure 26. Comparison between experimental and modeled ignition delay times using the Mechanisms A, B and C for different (c) methane and (d) propane mixtures with 0.1% HFC-125. The dashed line represents the best fit to the data containing the suppressant in each plot.

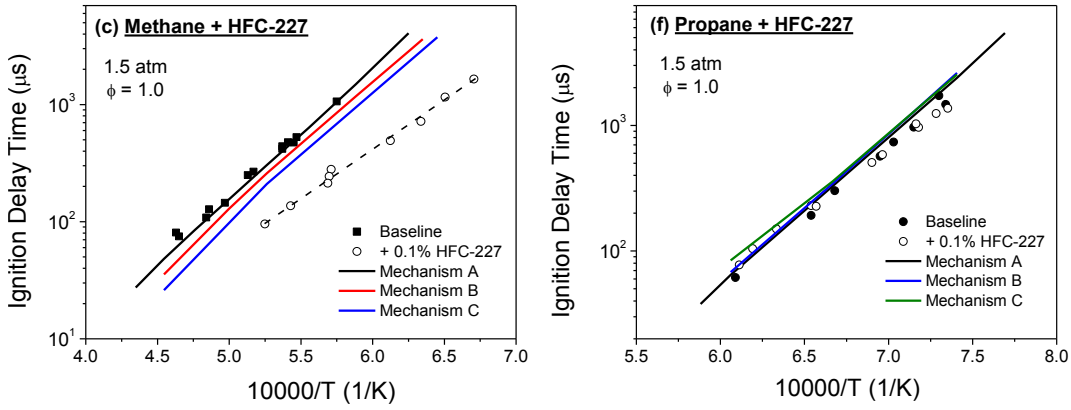

Figure 27. Comparison between experimental and modeled ignition delay times using the Mechanisms A, B and C for different methane and propane mixtures with 0.1% HFC-227. The dashed line represents the best fit to the data containing the suppressant in each plot.

5.4.2 Ignition sensitivity analysis

Sensitivity analyses were carried to find the key reactions responsible for the major effects of the tested agents on the two common alkane flames. For this analysis, SENKIN [82] was used through the CHEMKIN [80] interface. Figures 28 to 33 show the effect of the fire suppressants by comparing the sensitivity coefficients of the top reactions that most affect ignition on mixtures with and without fire suppressant. Positive and negative coefficients represent promotion and inhibition of the ignition, respectively. Sensitivity coefficients were normalized, using (R1) as the reference. For convenience, the reaction numbering in this section retains the same numbering used in the assembled, respective mechanism.

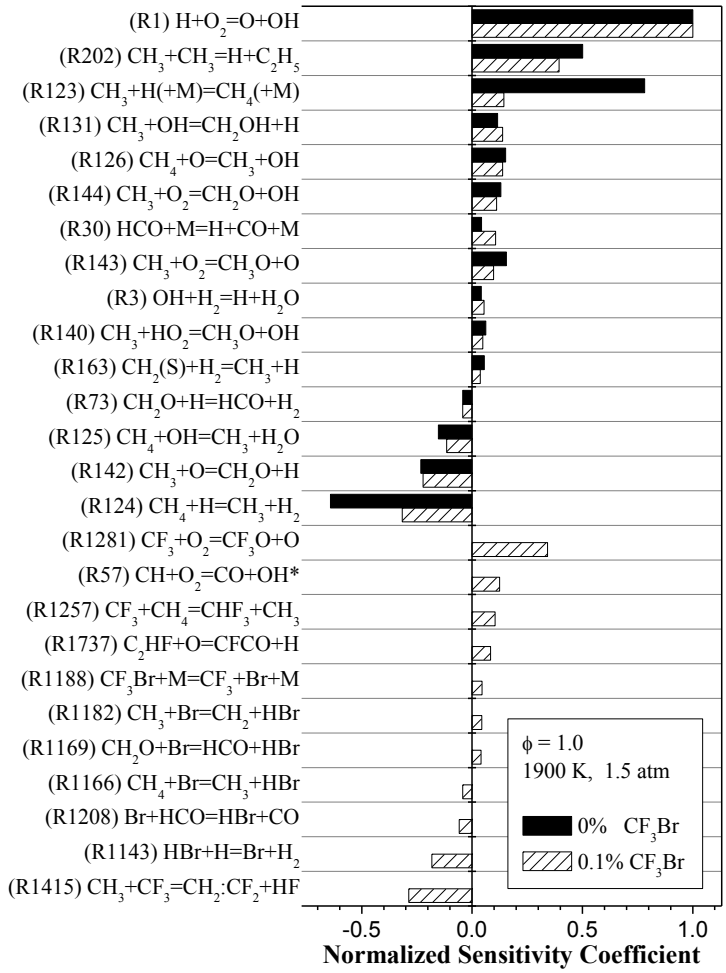

Figure 28. Comparison of the top coefficient sensitivities for stoichiometric mixtures of $CH_4/O_2/Ar$ with (dashed) and without (black) CF_3Br.

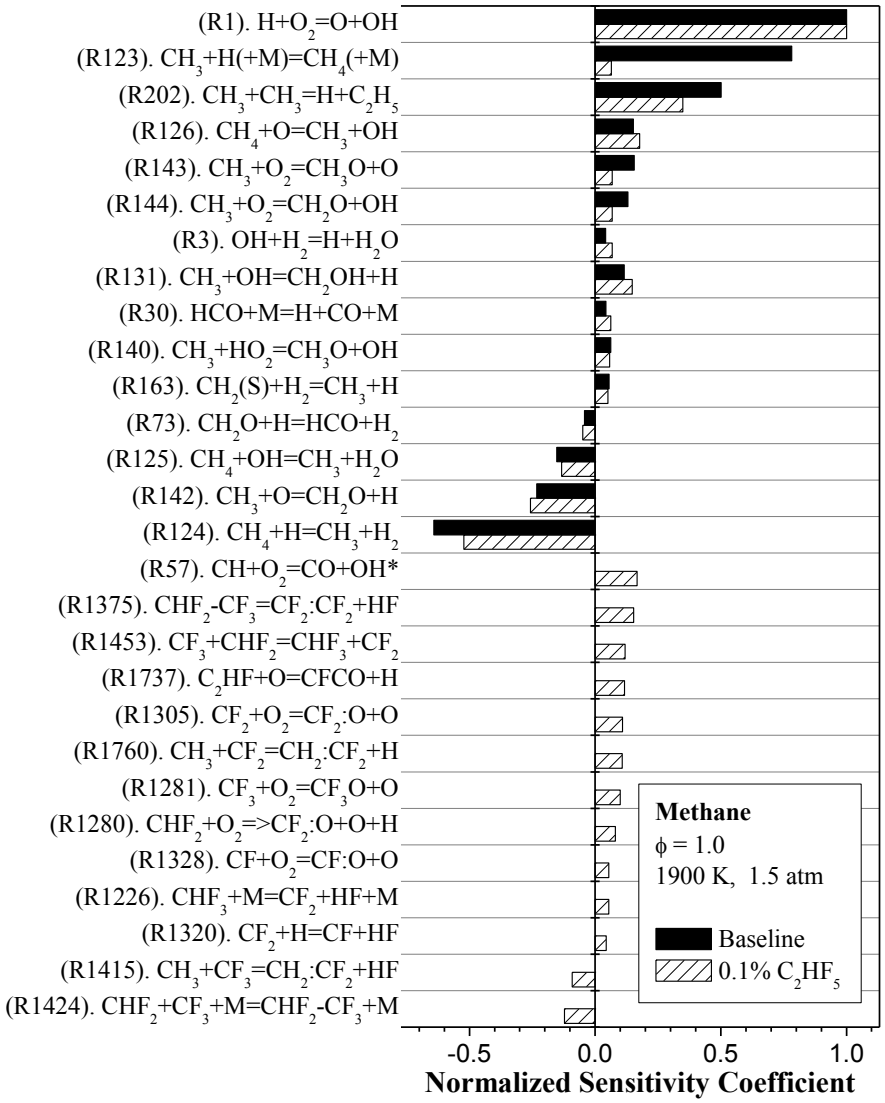

Figure 29. Comparison of the top reaction coefficient sensitivities for stoichiometric mixtures of $CH_4/O_2/Ar$ with (dashed) and without (black) C_2HF_5.

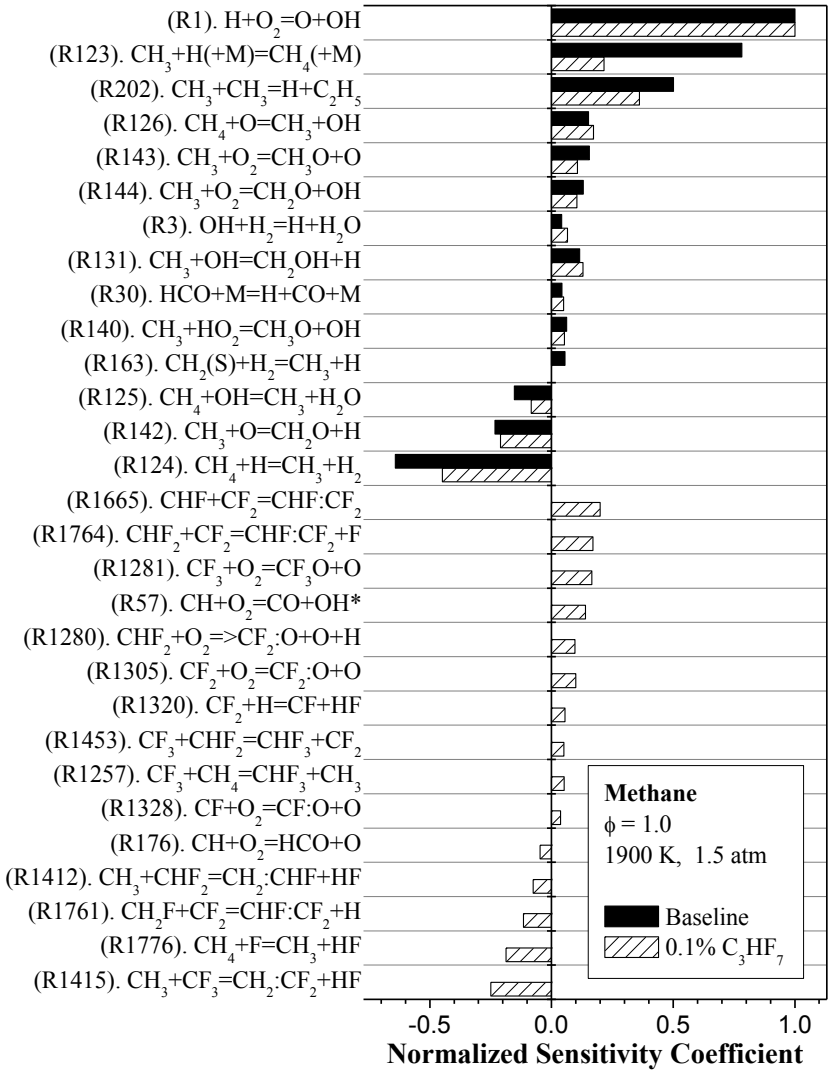

Figure 30. Comparison of the top reaction coefficient sensitivities for stoichiometric mixtures of $CH_4/O_2/Ar$ with (dashed) and without (black) C_3HF_7.

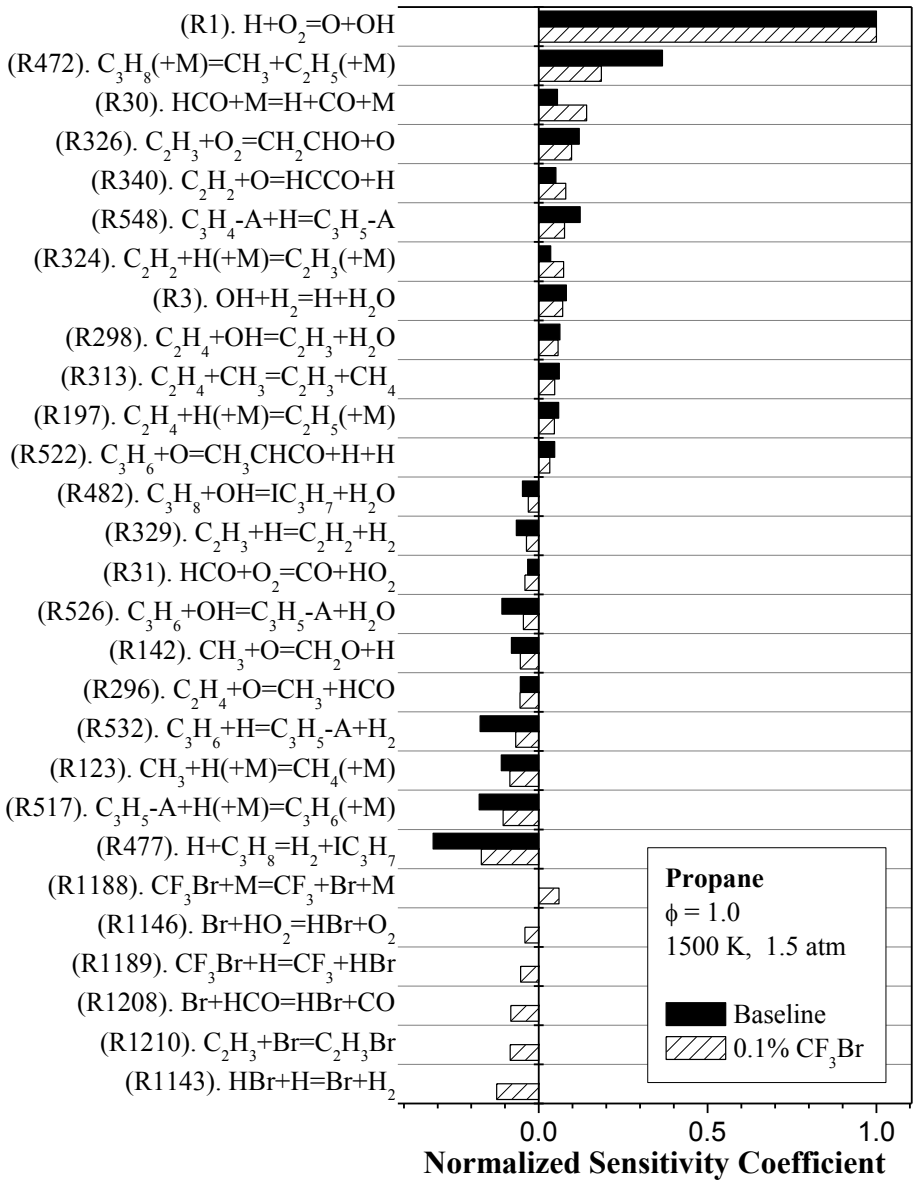

Figure 31. Comparison of the top reaction coefficient sensitivities for stoichiometric mixtures of $C_3H_8/O_2/Ar$ with (dashed) and without (black) CF_3Br.

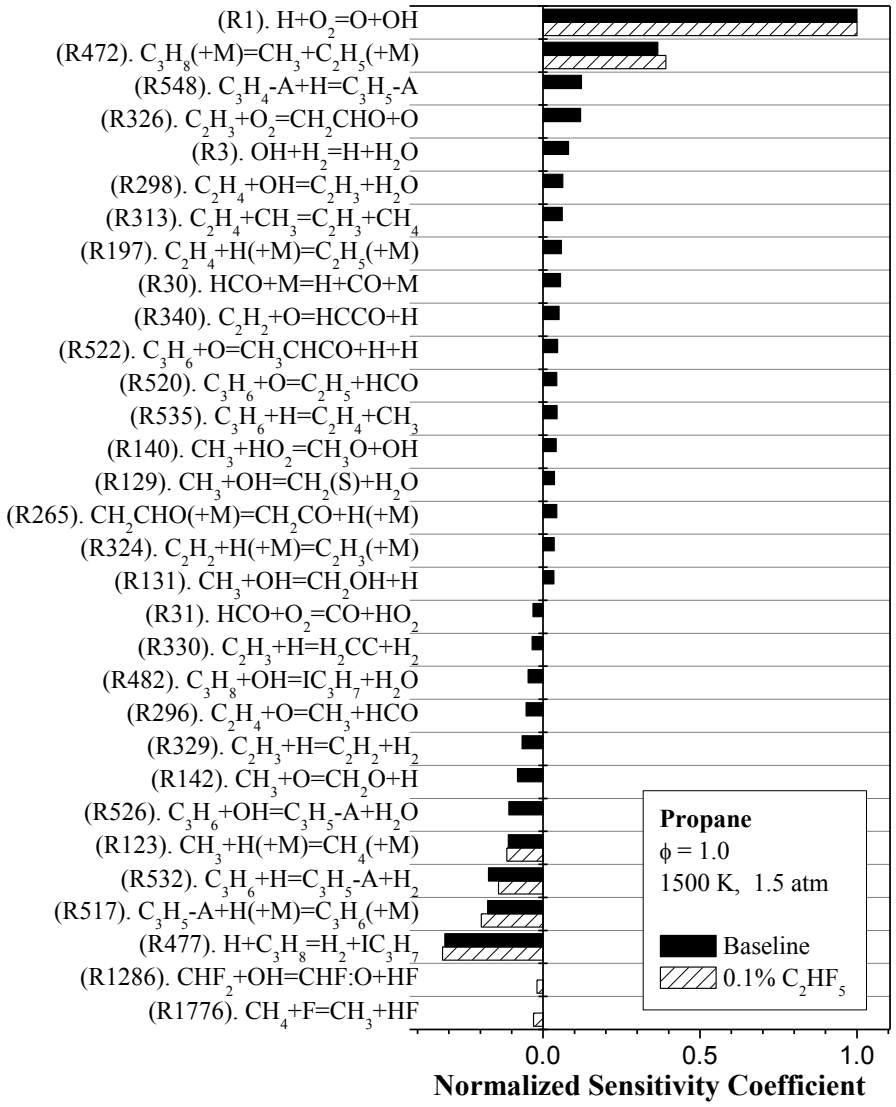

Figure 32. Comparison of the top reaction coefficient sensitivities for stoichiometric mixtures of $C_3H_8/O_2/Ar$ with (dashed) and without (black) C_2HF_5.

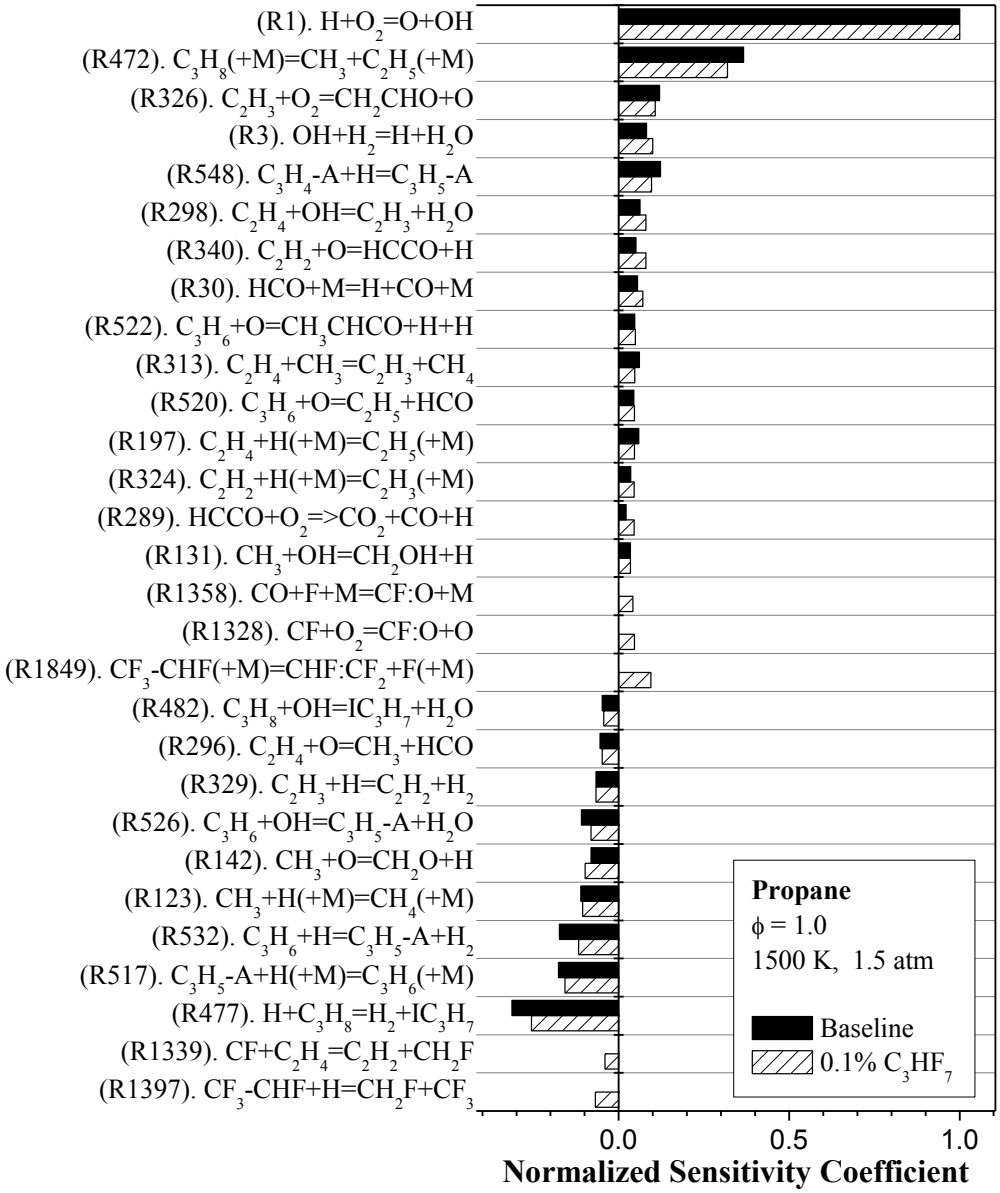

Figure 33. Comparison of the top reaction coefficient sensitivities for stoichiometric mixtures of $C_3H_8/O_2/Ar$ with (dashed) and without (black) C_3HF_7.

Ignition sensitivity analysis results, summarized in Table 11-13, show that halogenated species can participate in promoting and inhibiting reactions that compete to give a net effect. Fluorinated species may act as scavengers with lower radical removal efficiency, when compared with the catalytic mechanism where Br is present. However, it is surprising to see that most of the top reactions containing fluorine are classified as ignition promoters, while bromine-containing species mainly participate in strong inhibiting reactions. It is also worth noting that the promoting effect of the CF_3Br decomposition ($CF_3Br+M \rightleftarrows CF_3+ Br +M$) on ignition is very significant on CH_4-based systems compared with those with C_3H_8. This result confirms that CF_3Br decomposition controls the ignition process on CH_4-CF_3Br systems since C-Br bonds are much weaker than the C-H bonds presents in CH_4 decomposition. This trend however is not the case for C_3H_8 which, in comparison with CH_4, requires less energy to decompose, hence minimizing the effect of CF_3Br decomposition. On the other hand, it can be seen that reactions containing fluorinated compounds are more significant in CH_4 than in C_3H_8 systems. These results are in agreement with the discussion given in previous papers [105, 141] regarding CF_3Br, but current analysis allows better appreciation of such findings since higher concentrations have been used for such purposes. In general, the final effect of a specific fire suppressant does not depend of one single factor, and the kinetics mechanisms become more complex when larger molecules and more species are involved. The results of this sensitivity analysis can be used to improve the HFC-chemistry. Particular attention is required to those top reactions and their kinetic parameters that can provide better predictions.

Table 11. Summary of the OH* sensitive analysis results for mixtures with 0.1% CF_3Br.

Fuel	Net Effect	Partial Effect	Key Reactions
$CH_4/O_2/Ar$	Promotion	Promoting	1281. $CF_3+O_2=CF_3O+O$ 57. $CH+O_2=CO+OH^*$ 1257. $CF_3+CH_4=CHF_3+CH_3$ 1737. $C_2HF+O=CFCO+H$ 1188. $CF_3Br+M=CF_3+ Br +M$ 1182. $CH_3+BR=CH_2+HBR$ 1169. $CH_2O+Br=HCO+HBr$
		Inhibiting	1166. $CH_4+Br=CH_3+HBr$ 1208. $Br+HCO=HBR+CO$ 1143. $HBr+H=Br+H_2$
$C_3H_8/O_2/Ar$	Inhibition	Promoting	1188. $CF_3BR+M=CF_3+BR+M$
		Inhibiting	1146.$Br+HO_2=HBr+O_2$ 1189. $CF_3Br+H=CF_3+HBr$ 1208. $Br+HCO=HBr+CO$ 1210. $C_2H_3+Br=C_2H_3Br$ 1143. $HBr+H=Br+H_2$

Table 12. Summary of the OH* sensitive analysis results for mixtures with 0.1% C_2HF_5.

Fuel	Net effect	Partial effect	Key reactions
$CH_4/O_2/Ar$	Promotion	Promoting	57. $CH+O_2=CO+OH^*$ 1375. $CHF_2\text{-}CF_3=CF_2:CF_2+HF$ 1453. $CF_3+CHF_2=CHF_3+CF_2$ 1737. $C_2HF+O=CFCO+H$ 1305. $CF_2+O_2=CF_2:O+O$ 1760. $CH_3+CF_2=CH_2:CF_2+H$ 1281. $CF_3+O_2=CF_3O+O$ 1280. $CHF_2+O_2=>CF2:O+O+H$ 1328. $CF+O_2=CF:O+O$ 1226. $CHF_3+M=CF_2+HF+M$ 1320. $CF_2+H=CF+HF$
		Inhibiting	1415. $CH_3+CF_3=CH_2:CF_2+HF$ 1424. $CHF_2+CF_3+M=CHF_2\text{-}CF_3+M$
$C_3H_8/O_2/Ar$	Promotion	Promoting	-
		Inhibiting	1286. $CHF_2+OH=CHF:O+HF$ 1776. $CH_4+F=CH_3+HF$

Table 13. Summary of the OH* sensitive analysis results for mixtures with 0.1% C_3HF_7.

Fuel	Net effect	Partial effect	Key reactions
$CH_4/O_2/Ar$	Promotion	Promoting	1665. $CHF+CF_2=CHF:CF_2$ 1764. $CHF_2+CF_2=CHF:CF_2+F$ 1281. $CF_3+O_2=CF_3O+O$ 57. $CH+O_2=CO+OH^*$ 1280. $CHF_2+O_2=>CF_2:O+O+H$ 1305. $CF_2+O_2=CF_2:O+O$ 1375. $CHF_2-CF_3=CF_2:CF_2+HF$ 1453. $CF_3+CHF_2=CHF_3+CF_2$ 1737. $C_2HF+O=CFCO+H$ 1305. $CF_2+O_2=CF_2:O+O$ 1760. $CH_3+CF_2=CH_2:CF_2+H$ 1281. $CF_3+O_2=CF_3O+O$ 1280. $CHF_2+O_2=>CF_2:O+O+H$ 1305. $CF_2+O_2=CF_2:O+O$ 1320. $CF_2+H=CF+HF$ 1453. $CF_3+CHF_2=CHF_3+CF_2$ 1257. $CF_3+CH_4=CHF_3+CH_3$ 1328. $CF+O_2=CF:O+O$
		Inhibiting	176. $CH+O_2=HCO+O$ 1412. $CH_3+CHF_2=CH_2:CHF+HF$ 1761. $CH_2F+CF_2=CHF:CF_2+H$ 1776. $CH_4+F=CH_3+HF$ 1415. $CH_3+CF_3=CH_2:CF_2+HF$
$C_3H_8/O_2/Ar$	Promotion	Promoting	1358. $CO+F+M=CF:O+M$ 1328. $CF+O_2=CF:O+O$ R1849. $CF_3-CHF+M=CHF:CF_2+F+M$
		Inhibiting	1339. $CF+C_2H_4=>C_2H_2+CH_2F$ 1397. $CF_3-CHF+H=CH_2F+CF_3$

5.4.3 Flame speed analysis

Laminar flame speed measurements were carried out to evaluate the effect of C_2HF_5 and C_3HF_7 on CH_4 and C_3H_8 premixed flames. Evaluation of this parameter is very important since it represents an intrinsic property of the reacting system; then relevant information such the reactive and thermal effects of a specific fire suppressant can be extracted. Also, it can be used as an index for fire suppressant ranking. Figure 34 shows the laminar flame speed measurements of different premixed mixtures of methane/air and propane/air that were inhibited with 1% of HFC-125 and HFC-227, as a function of the equivalence ratio at ambient conditions. These results were compared with CF_3Br data obtained from a previously work [141]. As expected, all fire suppressants reduce the laminar flame speed in methane and propane mixtures, at all equivalence ratios. In general, fire suppressants can be ranked as $CF_3Br>C_3HF_7>C_2HF_5$ based on their effectiveness at reducing CH_4-air and C_3H_8-air flame speeds. However, it is noteworthy that the effect of CF_3Br is considerably larger than the two fluorocarbons tested. This greater tendency of the halon to reduce the flame speed is due to the participation of bromine species in catalytic cycles, where highly reactive radicals (i.e., H radicals) are removed from the flame reaction zone, as was suggested by Westbrook [94]. In terms of equivalence ratio, it can be seen that fire suppressants present stronger effects at fuel-rich conditions.

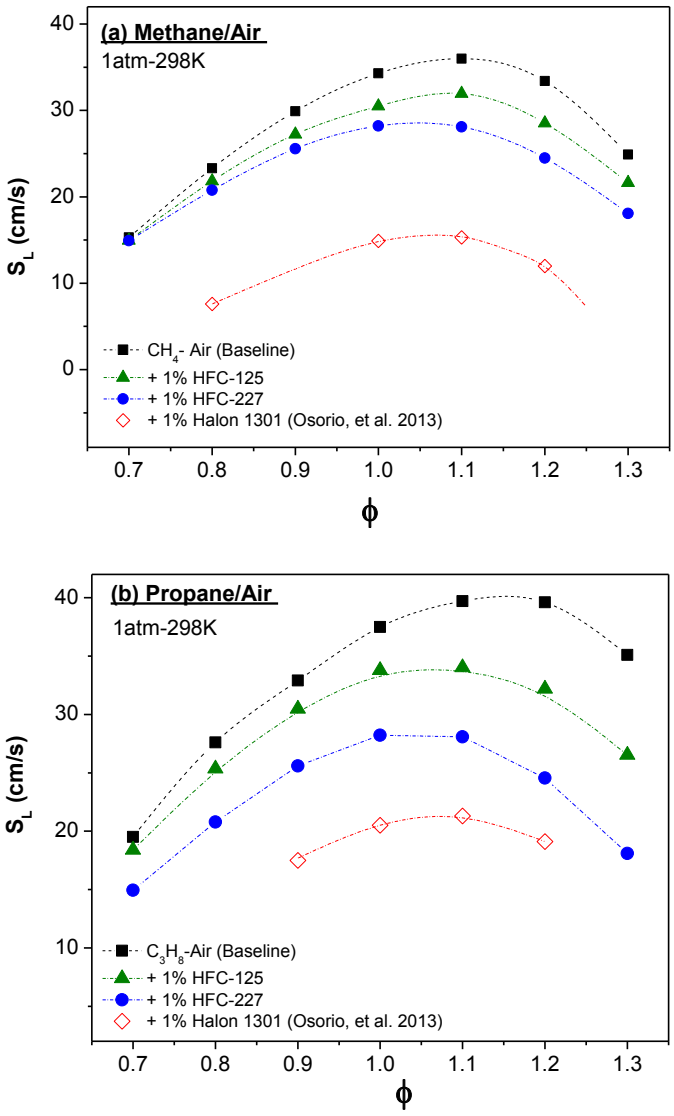

Figure 34. Experimental measurements from the present work of the effect of HFC-125, HFC-227, and Halon 1301 [141] on (a) Methane/Air (b) Propane/Air un-stretched Laminar Flame Speeds. Dashed lines represent curve fits to the data.

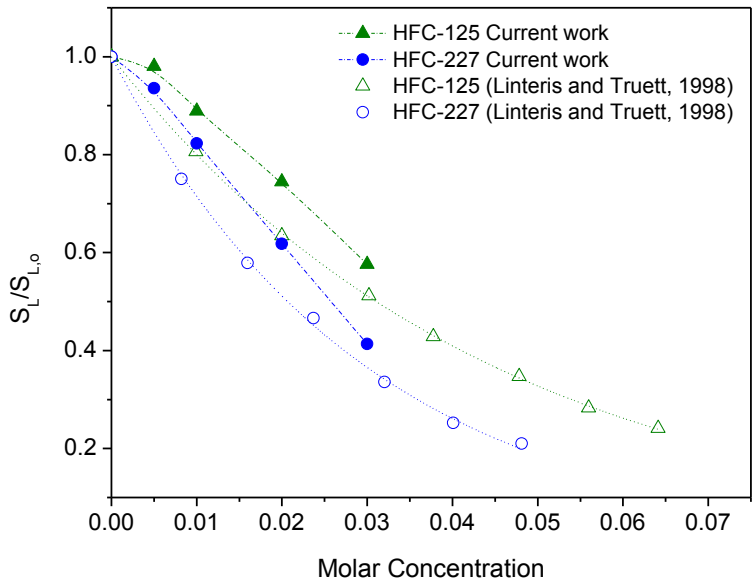

Figure 35. Reduction of the laminar flame speed by the effect of HFC-125, HFC-227, and Halon 1301 on (a) Methane/Air (b) Propane/Air flames [141, 144]. Dashed lines represent curve fits to the data.

To the best of the author's knowledge, only Linteris and Truett have provided experimental data on laminar flame speeds of methane-air with HFC-125 and HFC-227. Such measurements were obtained using a Mache-Hebra nozzle burner, giving higher values of laminar flames speeds when compared with the data from the present work (as detailed below). Also, Linteris and Trett presented larger efficiencies of HFC-125 and HFC-227 with respect to reducing the CH_4-air laminar flame speed when compared to the present work (Figure 35). These differences may be explained by the fact that the Mache-Hebra nozzle burner technique does not consider the compression effects and heat losses, and stretch effects present in the tested flame [145]. No data related to propane-air HFC systems were found in the literature.

5.5 Summary and Conclusions

This section discussed the importance of better understanding the fundamentals of chemical kinetics mechanisms of common fire suppressant alternatives, such as C_2HF_5 and C_3HF_7, to improve their performance and provide safer applications. Special attention was given to the dual behavior of C_2HF_5 and C_3HF_7, which can act as both promoters and inhibitors at certain combustion processes, including ignition. After providing a comprehensive summary of previous works in this area, this work focused on the need of accurate experimental data that can be used for model validation, and consequently for numerical analyses using modeling techniques.

To this end, accurate measurements of laminar flame speed and ignition delay time were provided as metrics for model validation. Experimental methodology included determination of ignition delay times using OH* emission from shock-tube measurements, and determination of un-stretched laminar flame speeds employing the spherical, freely propagating flame technique. Both methods involve optical diagnostic setups for accurate evaluation. Most of the experimental data provided in this work are the first measurements of their kind. Current results were also compared with CF_3Br performance, which is used as the point of reference.

Shock-tube measurements show that methane ignition is promoted, in all the cases, by the action of the tested fire suppressants. While in propane mixtures, only CF_3Br

presents an ignition-inhibiting effect. To better understand the dual effect of fire suppressants at this stage, sensitivity analyses were conducted. Then, the most significant reactions that contribute to the promotion or suppression of the ignition process were identified and summarized. The resulting effect of a fire suppressant can be thought of as a competition of individual reactions. This competition may depend on several factors, including agent-fuel chemical interaction, bonding energies, concentrations, ambient conditions, and equivalence ratios. It is surprising to see the number of fluorinated species that participate in ignition-promoting reactions, especially in CH_4 systems. These findings provide fundamental insight and can be used as the baseline for further research.

The present results suggest that the tested agents may not be good alternatives when used as ignition preventers; however, they still show inhibition properties as, in all the cases, they decrease the laminar flame speed. In fact, the capacity of reducing the laminar flame speed can be used as an index for flame inhibition performance. In these terms, CF_3Br has been shown to be considerably more effective than the HFC fire suppressants, with C_2HF_5 being slightly Less effective than C_3HF_7. Also, it has been shown that all fire suppressants are more effective at reducing flame speed at fuel-rich conditions.

Flame speed and shock-tube measurements were compared against modeled data. Modeling was carried out using an assembled kinetics mechanism that includes reactions

that describe the fuel (C_0-C_5 hydrocarbons), excited OH radicals (OH*), and Br-F chemistry. Results show that modeling behaves well in many cases; however, the HFC chemistry can be improved. Particular attention is required for the top reactions, and their Arrhenius kinetic parameters can be in need of better predictions. Current experimental data and modeling results, including sensitivity analyses, can be used as the basis for future HFC-chemical kinetics mechanism research.

6 SUMMARY, CONCLUSIONS AND FUTURE TRENDS

This study emphasizes the importance of combustion science and chemical kinetics modeling towards a search of suitable fire suppressants. In particular, the necessity to provide insight on the Halon 1301 flame inhibition mechanism, which serves as a benchmark for new fire suppressants, to guide the search of novel compounds with similar capabilities.

In this work, a systematic methodology has been proposed to analyze the flame inhibition mechanism of different fire suppressants, starting with CF_3Br, at a fundamental level. This methodology is based on both experimental and numerical approaches that help to identify whether a substance acts by chemical or thermal mechanisms, and if both, at which proportions.

This work provides accurate experimental results in terms of ignition delay time and laminar flame speed. These detailed data are much needed to fine tune chemical kinetics mechanisms over a wide range of conditions, particularly when interacting with hydrocarbon fuels (Class B fires). Most of these data are the first measurements of their kind for the compounds and mixtures explored in this thesis. Numerical analyses were performed to evaluate the flame inhibition performance of a single compound; however, a similar procedure can be applied to a fire suppressant blend performance analyses.

Analysis of two of the most currently used fire suppressants, C_2HF_5 (HFC-125) and C_3HF_7 (HFC-227), was presented as a case study. Results were compared with those obtained from CF_3Br which is considered as the point of reference. It gives an example that any gas phase chemical (or blend) can be analyzed following the mentioned methodology.

As expected, all the tested fire suppressants reduce the laminar flame speed in C_1-C_3 premixed mixtures, at all equivalence ratios. Based on their effectiveness at reducing the laminar flame speeds, the fire suppressants can be ranked as $CF_3Br > C_3HF_7 > C_2HF_5$, where the effect of CF_3Br is considerably larger than the two fluorocarbons tested. This greater tendency of the Halon 1301 may be explained by the fact that Halon 1301 acts mainly by chemical means (between 72% to 87%) through catalytic cycles, where highly reactive radicals are efficiently removed by the action of Br.

In terms of ignition delay times, our experiments show that all the tested fire suppressants tend to promote ignition in methane mixtures. Their promoting effect in methane mixtures can be ranked as $C_3HF_7 > C_2HF_5 > CF_3Br$. However, this trend is not general for all fuels. Propane measurements, for example, show that the ignition can be slighted promoted by C_2HF_5 but retarded by the action of CF_3Br. Note that the range of practical application of the present experimental results remains strictly limited to the experimental conditions defined.

It can be concluded that the combustion properties of halogenated compounds cannot be generalized and depends on different factors. From the current results, it could be seen that the fact that a chemical compound acts as a good flame suppressant does not imply it can be used to prevent ignition.

Sensitivity analyses were conducted in order to understand each fire suppressant's behavior by identifying the key elementary reactions that most affect the inhibition mechanism(s). Results show that halogenated species, coming from the fire suppressant decomposition, can participate in both promoting and inhibiting reactions which net effect in a competition between them. Several top reactions involving fluorine-containing species were classified as ignition promoters, while bromine-containing compounds participated mainly in inhibiting reactions. Results also show that fluorine-containing species that act as radical scavengers have lower efficiency than bromine-containing compounds. It may be explained by the fact that bromine species can actively participate in different catalytic cycles where free radicals are consumed to produce more stable molecules, and therefore breaking the chemical chain reaction that sustains the flame. These results serve as the basis for future fire suppressant mechanism improvements that can be used for better predictions at a wide range of conditions.

An important trend in the search of novel alternatives involves the design of fire suppressants composed of different substances present in one or more phases. These fire suppressants are known as hybrid fire suppressants. Some examples include the

commonly used flame extinguishers composed with a liquid or solid solute (e.g., Na_2CO_3 or Na_2CO) dissolved on a gas or liquid matrix (e.g., Ar, N_2, He, or H_2O). In most of the cases, the solute can act by chemical mechanisms, while the matrix can be a gas with high heat capacity. Therefore, the net effect can be attributed to an energetic effect that depends on the properties of the individual compounds and the potential combinations. Design of optimal hybrid fire suppressants may represent a tedious process since many combinations can be proposed. However, this design process can be supported with numerical analysis based on a validated chemical kinetics mechanism. Therefore, the methodology presented can be applied in the future for such purposes. Note that this application requires suitable equipment (or a modification of the current one) to test the properties of heterogeneous systems, as well as the kinetics mechanism that involves heterogeneous reactions as well.

REFERENCES

1. Purdue Research Foundation, Final Report on Fire Extinguishing for the Period of September 1, 1947 to June 30. Lafayette, IN, 1950.

2. M. J. Molina; F. S. Rowland, Nature 249 (1974) 810-812 10.1038/249810a0.

3. J. S. Daniel; S. Solomon; R. W. Portmann; R. R. Garcia, J. Geophys. Res. 104 (D19) (1999) 23871-23880 10.1029/1999jd900381.

4. G. M. Faeth; C. H. Kim; O. C. Kwon, Clean Air J. 4 (2) (2003) 115-186

5. J. M. Calm; D. J. Wuebbles; A. K. Jain, J. Climate Change 42 (1999) 439-474

6. J. C. Farman; B. G. Gardiner; J. D. Shanklin, Nature 315 (1985) 207-210 10.1038/315207a0.

7. S. Chubachi; R. Kajiwara, Geophys. Res. Lett. 13 (12) (1986) 1197-1198 10.1029/GL013i012p01197.

8. B. M. Mcelroy; R. J. Salawitch; S. C. Wofsy; J. A. Logan, Nature 321 (1986) 759-762 10.1038/321759a0.

9. R. S. Stolarski; A. J. Krueger; M. R. Schoeberl; R. D. Mcpeters; P. A. Newman; J. C. Alpert, Nature 322 (1986) 808-811

10. D. J. Hoffman; J. W. Harder; S. R. Rolf; J. M. Rosen, Nature 326 (1987) 59-62 10.1038/326059a0.

11. S. Solomon, Nature 347 (1990) 347-354 10.1038/347347a0.

12. Montreal Protocol on Substances that Deplete the Ozone Layer, Final Act, United Nations Environmental Program (UNEP), Montreal, Canada (1987)

13. Clean Air Act, Title VI - Stratosphereric Ozone Protection (CAA § 601-618; USC § 7671-7671q), 1990.

14. E. C. Weatherhead, Nature 441 (2006) 39-45 10.1038/nature04746.

15. D. Kaniaru (Ed.), The Montreal Protocol: Celebreting 20 years of Environmental Progress, Cameron May Ltd, 2007.

16. J. A. Mader; J. Staehelin; T. Peter; D. Brunner; H. E. Rieder; W. A. Stahel, Atmos. Chem. Phys. Discuss. (10) (2010) 12161–12171 10.5194/acp-10-12161-2010.

17. J. R. Ziemke; S. Chandra, Atmos. Chem. Phys. Discuss. 12 (2012) 3169–3211

18. J. Kuttippurath; F. Lefevre; J. P. Pommereau; H. K. Roscoe; F. Goutail; A. Pazmino; J. D. Shanklin, Atmos. Chem. Phys. Discuss. (12) (2012) 10775–10814 10.5194/acpd-12-10775-2012.

19. R. G. Gann, in: Advance Technology for Fire Suppression in Aircraft: Final Report of the Next Generation Fire Suppression Technology Program, R. G. Gann, (Ed.) National Insititute of Standard and Technology (NIST): 2007; pp 1-16.

20. G. T. Linteris, in: Fire Suppression in Aircraft: The Final Report if the Next Generation Fire Suppression Technology Program, R. G. Gann, (Ed.) National Institute of Standards and Technology (NIST): 2007.

21. G. T. Linteris; M. D. Rumminger; V. I. Babushok, Prog. Energy Combust. Sci. 34 (3) (2008) 288-329 10.1016/j.pecs.2007.08.002.

22. G. T. Linteris; V. D. Knyazev; V. I. Babushok, Combust. Flame 129 (3) (2002) 221-238 10.1016/s0010-2180(02)00346-2.

23. G. T. Linteris; V. I. Babushok, Proc. Combust. Inst. 32 (2) (2009) 2535-2542 10.1016/j.proci.2008.09.006.

24. M. D. Rumminger; D. Reinelt; V. I. Babushok; G. T. Linteris, Combust. Flame 116 (1-2) (1999) 207-219 10.1016/s0010-2180(98)00033-9.

25. M. D. Rumminger; G. T. Linteris, Combust. Flame 128 (1-2) (2002) 145-164 10.1016/s0010-2180(01)00341-8.

26. D. Reinelt; G. T. Linteris, Proc. Combust. Inst. 26 (1) (1996) 1421-1428 10.1016/s0082-0784(96)80362-6.

27. M. D. Rumminger; G. T. Linteris, Combust. Flame 120 (4) (2000) 451-464 10.1016/s0010-2180(99)00114-5.

28. M. D. Rumminger; G. T. Linteris, Combust. Flame 123 (1-2) (2000) 82-94 10.1016/s0010-2180(00)00153-x.

29. G. T. Linteris; M. D. Rumminger; V. I. Babushok, Combust. Flame 122 (1-2) (2000) 58-75 10.1016/s0010-2180(00)00103-6.

30. G. T. Linteris; M. D. Rumminger; V. I. Babushok; W. Tsang, Proc. Combust. Inst. 28 (2) (2000) 2965-2972 10.1016/s0082-0784(00)80722-5.

31. G. T. Linteris; V. R. Katta; F. Takahashi, Combust. Flame 138 (1-2) (2004) 78-96 10.1016/j.combustflame.2004.04.003.

32. G. T. Linteris; M. D. Rumminger; V. I. Babushok; W. Tsang, Proc. Combust. Inst. 28 (2) (2000) 2965-2972 10.1016/s0082-0784(00)80722-5.

33. R. E. Banks; E. K. Clarke; E. P. Johnson; P. N. Sharratt, Process Saf. Environ 76 (3) (1998) 229-238 10.1205/095758298529533.

34. C. Luo. Study on the Inhibition Mechanisms of $CBrF_3$, CF_3I and C_3F_7H in Methane Fuelled Premixed Flames. The University of Newcastle, Australia, 2010.

35. B. A. Williams; W. Fleming in: On the Suitability of CF_3Br as a Benchmarck For Replacement Fire Suppressants, Halon Options Technical Working Conference, Alburqueque, NM, 2001.

36. C. J. Aul. An Experimental Study into the Ignition of Methane and Ethane Blends in a New Shock Tube Facility. Texas A&M University, College Station, TX, 2009.

37. E. L. Petersen; M. J. A. Rickard; M. W. Crofton; E. D. Abbey; M. J. Traum; D. M. Kalitan, Meas. Sci. Technol. 16 (9) (2005) 14 10.1088/0957-0233/16/9/003.

38. B. Rotavera. Chemiluminescence and Ignition Delay Time Measurements of C_9H_2O Oxidation in O_2-Ar Behind Reflected Shock Waves. Texas A&M University, College Station, 2009.

39. E. L. Petersen, Combust. Sci. Technol. 181 (9) (2009) 1123-1144 10.1080/00102200902973323.

40. N. Donato. OH* Chemiluminescence: Pressure Dependency of O+H+M=OH*+M. Texas A&M University, College Station, TX, 2009.

41. O. Mathieu; A. Levacque; E. L. Petersen, Int. J. Hydrogen Energy 37 (20) (2012) 15393-15405 http://dx.doi.org/10.1016/j.ijhydene.2012.07.071

42. B. Rotavera; E. L. Petersen, Proc. Combust. Inst. 34 (1) (2013) 435-442 http://dx.doi.org/10.1016/j.proci.2012.06.042.

43. O. Mathieu; A. Levacque; E. L. Petersen, Proc. Combust. Inst. 34 (1) (2013) 633-640 http://dx.doi.org/10.1016/j.proci.2012.05.067.

44. O. Mathieu; M. M. Kopp; E. L. Petersen, Proc. Combust. Inst. 34 (2) (2013) 3211-3218 http://dx.doi.org/10.1016/j.proci.2012.05.008.

45. A. Kéromnès; W. K. Metcalfe; K. A. Heufer; N. Donohoe; A. K. Das; C.-J. Sung; J. Herzler; C. Naumann; P. Griebel; O. Mathieu; M. C. Krejci; E. L. Petersen; W. J. Pitz; H. J. Curran, Comb. Flame 160 (6) (2013) 995–1011 10.1016/j.combustflame.2013.01.001.

46. D. Healy; N. S. Donato; C. J. Aul; E. L. Petersen; C. M. Zinner; G. Bourque; H. J. Curran, Comb. Flame 157 (8) (2010) 1526-1539 http://dx.doi.org/10.1016/j.combustflame.2010.01.016.

47. J. de Vries; J. M. Hall; S. L. Simmons; M. J. A. Rickard; D. M. Kalitan; E. L. Petersen, Comb. Flame 150 (1–2) (2007) 137-150 http://dx.doi.org/10.1016/j.combustflame.2006.10.008.

48. J. M. Hall; M. J. A. Rickard; E. L. Petersen, Combust. Sci. Technol. 177 (3) (2005) 455-483 10.1080/00102200590909003.

49. K. S. Krishnan; R. Ravikumar, Combust. Sci. Technol. 24 (5-6) (1981) 239-245

50. E. L. Petersen; M. Röhrig; D. F. Davidson; R. K. Hanson; C. T. Bowman, Symp. (Int.) Combust. 26 (1) (1996) 799-806 10.1016/s0082-0784(96)80289-x.

51. J. de Vries; J. M. Hall; S. L. Simmons; M. J. A. Rickard; D. M. Kalitan; E. L. Petersen, Combust. Flame 150 (1–2) (2007) 137-150 10.1016/j.combustflame.2006.10.008.

52. N. Lamoureux; C. Paillard; V. Vaslier, Shock Waves (11) (2002) 14

53. W. J. M. Rankine, Philos. Trans. R. Soc. London, Ser. A, (1870) 277-288 10.2307/109061.

54. H. Hugoniot, Journal de l'Ecole Polytechnique 57 (1887)

55. I. Glassman; R. Yetter, Combustion, Academic Press, 2008, pp. 147-155.

56. S. R. Turns, An Introduction to Combustion: Concepts and Applications, McGraw Hill, Boston, 2000, pp. 253-283.

57. C. K. Wu; C. K. Law, Symp. (Int.) Combust. 20 (1) (1985) 1941-1949 http://dx.doi.org/10.1016/S0082-0784(85)80693-7.

58. C. K. Law, Combustion Physics, University Press, New York, 2006, pp. 144.

59. F. A. Williams, Combustion Theroy, Westview Press, Boulder, CO, 1985, pp.

60. K. K. Kuo, Principle of Combustion, John Wiley & Sons, Inc, Hoboken, NJ, 2002, pp.

61. J. de Vries. A Study on Spherical Expanding Flame Speeds of Methane, Ethane, and Methane/Ethane Mixtures at Elevated Pressures. Texas A&M University, College Station, 2009.

62. S. Kwon; L. K. Tseng; G. M. Faeth, Combust. Flame 90 (3-4) (1992) 230-246 10.1016/0010-2180(92)90085-4.

63. M. P. Burke; Z. Chen; Y. Ju; F. L. Dryer, Combust. Flame 156 (4) (2009) 771-779 10.1016/j.combustflame.2009.01.013.

64. J. de Vries; W. Lowry; Z. Serinyel; H. J. Curran; E. L. Petersen, Fuel 90 (1) (2011) 8 10.1016/j.fuel.2010.07.040.

65. R. J. Moffat, Exp. Thermal Fluid Sci. 1 (1) (1988) 3-17 10.1016/0894-1777(88)90043-x.

66. W. B. Lowry; Z. Serinyel; M. C. Krejci; H. J. Curran; G. Bourque; E. L. Petersen, Proc. Combust. Inst. 33 (1) (2011) 929-937 10.1016/j.proci.2010.05.042.

67. W. Lowry. Effect of Blending on High-Pressure Laminar Flame Speed Measurements, Markstein Lengths, and Flame Stability of Hydrocarbons. Texas A&M University, College Station, Texas, 2010.

68. NIST Chemical Kinetics Database.

69. D. Healy; M. M. Kopp; N. L. Polley; E. L. Petersen; G. Bourque; H. J. Curran, Energy Fuels 24 (3) (2010) 1617-1627 10.1021/ef901292j.

70. D. Healy; N. S. Donato; C. J. Aul; E. L. Petersen; C. M. Zinner; G. Bourque; H. J. Curran, Combust. Flame 157 (8) (2010) 1526-1539 10.1016/j.combustflame.2010.01.016.

71. N. S. Donato; C. J. Aul; E. L. Petersen; C. M. Zinner; H. J. Curran; G. Bourque, J. Eng. Gas Turbines Power 132 (5) (2010) 051502

72. V. I. Babushok; T. Noto; D. Burgess; A. Hamins; W. Tsang, Combust. Flame 107 (4) (1996) 17

73. V. I. Babushok; G. T. Linteris; O. C. Meier, Combust. Flame 159 (12) (2012) 3569-3575 10.1016/j.combustflame.2012.07.005.

74. C. Luo; B. Z. Dlugogorski; E. Kennedy, Fire Technol 44 (2008) 221-237.

75. E. M. Kennedy; B. Z. Dlugogorski; C. Luo, in: Proceedings of the Sixth Asia-Oceania Symposium on Fire Science and Technology, Daegu, South Korea, 2004.

76. C. Luo; B. Z. Dlugogorski; E. M. Kennedy; B. Moghtaderi, in: Suppression, Detection and Signaling Research and Applications: A Technical Working Conference (SUPDET 2010), Orlando, FL, 2010.

77. A. Burcat; R. Branko, in: Argonne National Laboratory Israel Institute of Technology: Argonne, IL, 2005.

78. T. Noto; V. I. Babushok; A. Hamins; W. Tsang, Combust. Flame 112 (1/2) (1998) 14.

79. Reaction Design Inc, CHEMKIN 4.1: A Software Package for the Analysis of Gas Phase Chemical and Plasma Kinetics; 2011.

80. A. E. Lutz; R. J. Kee; J. A. Miller; Reaction Design Inc, in: Livermore, CA, 1988.

81. R. J. Kee; M. D. Grcar; J. A. Smooke; J. A. Miller; E. Meeks; Reaction Design Inc, in: San Diego, CA, 1998.

82. R. J. Kee; F. M. Rupley; J. A. Miller; M. E. Coltrin; J. F. Grcar; E. Meeks; H. K. Moffat; A. E. Lutz; G. Dixon-Lewis; M. D. Smooke; J. Warnatz; G. H. Evans; R. S. Larson; R. E. Mitchell; L. R. Petzold; W. C. Reynolds; M. Caracotsios; W. E. Stewart; P. Glarborg; C. Wang; C. L. McLellan; O. Adigun; W. G. Houf; C. P. Chou; S. F. Miller; P. Ho; P. D. Young; D. J. Young; D. W. Hodgson; M. V. Petrova; K. V. Puduppakkam; Reaction Design Inc, in: San Diego, CA, 2007.

83. W. A. Rosser; H. Wise; J. Miller, Symp. (Int.) Combust.. 7 (1) (1958) 175-182 10.1016/s0082-0784(58)80039-9.

84. R. M. Fristrom; R. F. Sawyer, in: AGARD Conf. on Aircraft Fuels, Lubricants, and Fire Safety, The Hage, Netherlands, 1971; pp 71-84.

85. M. L. Robin, in: Halon Replacements: Technology and Science, A. W. Miziolek; W. Tsang, (Eds.) American Chemical Society: Washington, D.C., 1995; pp 85-98.

86. G. T. Linteris; F. Takahashi; V. R. Katta, Combust. Flame 149 (1–2) (2007) 91-103 10.1016/j.combustflame.2006.12.013.

87. V. R. Katta; F. Takahashi; G. T. Linteris, Combust. Flame 144 (4) (2006) 645-661 10.1016/j.combustflame.2005.09.006.

88. G. T. Linteris; D. R. Burgess; F. Takahashi; V. R. Katta; H. K. Chelliah; O. Meier, Combust. Flame 159 (3) (2012) 1016-1025 10.1016/j.combustflame.2011.09.011.

89. B. Andersson; P. Blomqvist, Fire Saf. J. 46 (3) (2011) 104-115 10.1016/j.firesaf.2010.11.004.

90. W. Han; E. M. Kennedy; J. C. Mackie; B. Z. Dlugogorski, J. Hazard. Mater. 180 (1–3) (2010) 181-187 10.1016/j.jhazmat.2010.04.011.

91. S. Zhang; M. B. Colket, Proc. Combust. Inst. 33 (2) (2011) 2497-2504 10.1016/j.proci.2010.05.070.

92. A. S. Nizovtsev; G. A. Bogdanchikov; A. V. Baklanov, Combust. Flame 157 (7) (2010) 1382-1389 10.1016/j.combustflame.2009.11.004.

93. F. Takahashi; V. R. Katta; G. T. Linteris; O. C. Meier, Proc. Combust. Inst. 34 (2) (2013) 2707-2717 10.1016/j.proci.2012.06.091.

94. C. K. Westbrook, Combust. Sci. Technol. 34 (1983) 201-225

95. T. Noto; V. I. Babushok; J. Burgess; A. Hamins; W. Tsang; A. W. Miziolek, Proc. Combust. Inst. 26 (1996) 1377-1383

96. V. I. Babushok; D. R. F. Burgess; W. Tsang; A. Miziolek, in: Halon Options Conf. Proc., Albuquerque, NM, 1994; pp 205-216.

97. C. R. Casias; J. Thomas McKinnon, Proc. Combust. Inst. 27 (2) (1998) 2731-2739 10.1016/s0082-0784(98)80129-x.

98. R. S. Sheinson; J. E. Penner-Hahn; D. Indritz, Fire Saf. J. 15 (6) (1989) 437-450 10.1016/0379-7112(89)90015-5.

99. R. N. Butlin; R. F. Simmons, Combust. Flame 12 (5) (1968) 447-456 10.1016/0010-2180(68)90057-6.

100. G. Dixon-Lewis; R. J. Simpson, Proc. Combust. Inst. 16 (1) (1977) 1111-1119 10.1016/s0082-0784(77)80400-1.

101. B. Walravens; F. Battin-Leclerc; G. M. Côme; F. Baronnet, Combust. Flame 103 (4) (1995) 339-342 10.1016/0010-2180(95)00204-9.

102. Y. Saso; Y. Ogawa; N. Saito; H. Wang, Combust. Flame 118 (3) (1999) 489-499 10.1016/s0010-2180(99)00012-7.

103. D. M. Tucker; D. D. Drysdale; D. J. Rasbash, Combust. Flame 41 (0) (1981) 293-300 10.1016/0010-2180(81)90063-8.

104. V. I. Babushok; W. Tsang, Combust. Flame 123 (4) (2000) 488-506 10.1016/s0010-2180(00)00168-1.

105. A. Suzuki; T. Inomata; H. Jinno; T. Moriwaki, Bull. Chem. Soc. Jpn. 64 (1991) 3345-3354

106. Y. N. Shebeko; V. V. Azatyan; I. A. Bolodian; V. Y. Navzenya; S. N. Kopylov; D. Y. Shebeko; E. D. Zamishevski, Combust. Flame 121 (3) (2000) 542-547 10.1016/s0010-2180(99)00168-6.

107. A. Hamins; P. Borthwick, Combust. Flame 112 (1–2) (1998) 161-170 10.1016/s0010-2180(97)81764-6.

108. C. H. Kim; O. C. Kwon; G. M. Faeth, J. Prop. Power 18 (5) (2002) 9

109. D. Healy; N. S. Donato; C. J. Aul; E. L. Petersen; C. M. Zinner; G. Bourque; H. J. Curran, Combust. Flame 157 (8) (2010) 1540-1551 10.1016/j.combustflame.2010.01.011.

110. D. Healy; H. J. Curran; J. M. Simmie; D. M. Kalitan; C. M. Zinner; A. B. Barrett; E. L. Petersen; G. Bourque, Combust. Flame 155 (3) (2008) 441-448 10.1016/j.combustflame.2008.07.003.

111. J. M. Hall; E. L. Petersen, Int. J. Chem. Kinet. 38 (12) (2006) 714-724

112. M. Brower; E. L. Petersen, (In Prep.) Combust. Sci. Technol. (2012)

113. J. M. Hall; J. A. Richard; E. L. Petersen, Combust. Sci. Technol. 177 (3) (2005) 455-483

114. K. J. Bosschaart; L. P. H. De Goey, Combust. Flame 136 (3) (2004) 261-269

115. C. M. Vagelopoulos; F. N. Egolfopoulos, Symp. (Int.) Combust. 27 (1) (1998) 513-519

116. O. Park; P. S. Veloo; N. Liu; F. N. Egolfopoulos, Proc. Combust. Inst. 33 (1) (2011) 887-894 10.1016/j.proci.2010.06.116.

117. F. N. Egolfopoulos; D. L. Zhu; C. K. Law, Symp. (Int.) Combust. 23 (1) (1990) 8

118. M. I. Hassan; K. T. Aung; O. C. Kwon; G. M. Faeth, J. Propul.Power 14 (4) (1998) 479-488 10.2514/2.5304.

119. G. Jomaas; X. L. Zheng; D. L. Zhu; C. K. Law, Proc. Combust. Inst. 30 (2005) 193-200

120. G. Rozenchan; D. L. Zhu; C. K. Law; S. D. Tse, Proc. Combust. Inst. 29 (2002) 1461-1469

121. X. J. Gu; M. Z. Haq; M. Lawes; R. Woolley, Combust. Flame 121 (1-2) (2000) 41-58

122. F. Halter; T. Tahtouh; C. Mounaïm-Rousselle, Combust. Flame 157 (10) (2010) 1825-1832

123. O. Sanogo; J. L. Delfau; R. Akrich; C. Vovelle, J. Chim. Phys. 93 (11-12) (1996) 1939-1957

124. D. J. Parks, Fire Saf. J. 2 (4) (1980) 237

125. W. Lowry; J. de Vries; M. Krejci; E. Petersen; Z. Serinyel; W. Metcalfe; H. Curran; G. Bourque, J. Eng. Gas Turbines Power 133 (9) (2011) 091501-9

126. J. A. Manion; R. E. Huie; R. D. Levin; D. R. Burgess Jr; V. L. Orkin; W. Tsang; W. S. McGivern; J. W. Hudgens; V. D. Knyazev; D. B. Atkinson; E. Chai; A. M. Tereza; C.-Y. Lin; T. C. Allison; W. G. Mallard; F. Westley; J. T. Herron; R. F. Hampson; D. H. Frizzell, in: National Institute of Standards and Technology: 2011.

127. G. Poulet; G. Laverdet; G. LeBras, J. Chem. Phys. 80 (1984)

128. M. L. Robin, in: International Fire Protection 2012; p 4.

129. A. G. Shmakov; O. P. Korobeinichev; V. M. Shvartsberg; S. A. Yakimov; A. N. Baratov; S. N. Kopylov; D. B. Zhiganov, Combust. Explos. Shock Waves 44 (3) (2008) 266-272 10.1007/s10573-008-0034-9.

130. U. S. Environmental Protection Agency, Protection of Stratospheric Ozone: Listing of Substitutes for Ozone-Depleting Substances-Fire Suppression and Explosion Protection (40 CFR 82, 77 FR 74381), December, 2012.

131. R. G. Gann (Ed). Advance Technology for Fire Suppression in Aircraft, NIST Special Publication 1069, 2007, pp. 3-5.

132. H. Ohtani, J. Loss Prev. Process Ind. 17 (5) (2004) 377-379 10.1016/j.jlp.2004.06.001.

133. V. V. Azatyan; Y. N. Shebeko; A. Y. Shebeko; V. Y. Navzenya, J. Loss Prev. Process Ind. 20 (4–6) (2007) 486-493 10.1016/j.jlp.2007.03.017.

134. Y. Saso; D. L. Zhu; H. Wang; C. K. Law; N. Saito, Combust. Flame 114 (3–4) (1998) 457-468 10.1016/s0010-2180(97)00319-2.

135. G. T. Linteris; L. Truett, Combust. Flame 105 (1-2) (1996) 15-27 Doi: 10.1016/0010-2180(95)00152-2.

136. R. G. Hynes; J. C. Mackie; A. R. Masri, Combust. Flame 113 (4) (1998) 554-565 10.1016/s0010-2180(97)00267-8.

137. B. Skinner Gordon, in: Halogenated Fire Suppressants, J. Am. Chem. Soc. Society: 1975; Vol. 16, pp 295-317.

138. S. Kondo; K. Takizawa; A. Takahashi; K. Tokuhashi; A. Sekiya, Fire Saf. J. 44 (2) (2009) 192-197 10.1016/j.firesaf.2008.06.001.

139. G. Gmurczyk; W. Grosshandler, Symp. (Int.) Combust. 25 (1) (1994) 1497-1503 10.1016/s0082-0784(06)80794-0.

140. E. A. Ural, Process Saf. Prog. 22 (1) (2003) 65-73 10.1002/prs.680220109.

141. C. H. Osorio; A. J. Vissotski; E. L. Petersen; M. S. Mannan, Combust. Flame 160 (6) (2013) 1044-1059 http://dx.doi.org/10.1016/j.combustflame.2013.01.025.

142. J. W. Reinhardt, in: Federal Aviation Administration: Washington, DC, 2004; p 26.

143. P. R. Westmoreland; D. R. F. Burgess Jr; M. R. Zachariah; W. Tsang, Symp. (Int.) Combust. 25 (1) (1994) 1505-1511 10.1016/s0082-0784(06)80795-2.

144. G. T. Linteris; L. Truett, in: International Conference on Fire Research and Engineering, Orlando, FL, 1995; p 7.

145. R. A. Strehlow; L. D. Savage, Comb. Flame 31 (0) (1978) 209-211 http://dx.doi.org/10.1016/0010-2180(78)90130-X.

APPENDIX A: TABULATION OF SHOCK-TUBE MEASUREMENTS FROM CF_3BR ANALYSIS

Table A1. Summary of the mixtures (highly diluted in Argon) analyzed using the High Pressure Shock Tube.

Fuel	ϕ	Mixture	CF_3Br/Fuel	CF_3Br (%)	Fuel (%)	O_2 (%)	Ar (%)
Methane	0.50	1	-	0.00	0.40	1.60	98.00
		2	1/10	0.04	0.40	1.60	97.96
	1.00	3	-	0.00	0.67	1.33	98.00
		4	1/50	0.01	0.67	1.33	97.99
		5	1/20	0.03	0.67	1.33	97.97
		6	1/10	0.07	0.67	1.33	97.93
	2.00	7	-	0.00	1.00	1.00	98.00
		8	1/10	0.10	1.00	1.00	97.90
Ethane	0.50	9	-	0.00	0.25	1.75	98.00
		10	1/10	0.02	0.25	1.75	97.98
	1.00	11	-	0.00	0.44	1.56	98.00
		12	1/20	0.02	0.44	1.56	97.98
		13	1/10	0.04	0.44	1.56	97.96
	2.00	14	-	0.00	0.73	1.27	98.00
		15	1/10	0.07	0.73	1.27	97.93
Propane	0.50	16	-	0.00	0.18	1.82	98.00
		17	1/10	0.02	0.18	1.82	97.98
	1.00	18	-	0.00	0.33	1.67	98.00
		19	1/10	0.03	0.33	1.67	97.97
	2.00	20	-	0.00	0.57	1.43	98.00
		21	1/10	0.06	0.57	1.43	97.94

Table A2. Experimental ignition delay times of $CH_4/O_2/Ar$ mixtures (Φ=0.5) with 0% CF_3Br (Mixture 1) and 0.04% CF_3Br (Mixture 2).

	T_5 (K)	$10^4/T_5$ (K^{-1})	P5 (atm)	τ_{ign} (μs)	τ_{adj} * (μs)
Mixture 1	2112	4.73	1.40	81	70
	2100	4.76	1.48	88	80
	2052	4.87	1.49	102	93
	2022	4.95	1.52	131	121
	2002	5.00	1.55	152	142
	1912	5.23	1.73	196	198
	1915	5.22	1.51	237	218
	1898	5.27	1.58	277	263
	1840	5.43	1.71	404	405
	1779	5.62	1.66	617	606
Mixture 2	1917	5.22	1.75	110	112
	1883	5.31	1.81	134	140
	1854	5.39	1.72	154	155
	1858	5.38	1.62	171	165
	1851	5.40	1.86	176	188
	1805	5.54	1.81	222	232
	1795	5.57	1.75	248	253
	1817	5.50	1.72	256	258
	1751	5.71	1.70	347	347
	1740	5.75	1.73	429	434
	1730	5.78	1.74	447	454
	1703	5.87	1.75	526	536

*Ignition delay time adjusted to the pressure average = 1.7 atm

Table A3. Experimental ignition delay times of $CH_4/O_2/Ar$ mixtures (Φ=1.0) with 0% CF_3Br (Mixture 3), 0.01% CF_3Br (Mixture 4), 0.03% CF_3Br (Mixture 5), and 0.07% CF_3Br (Mixture 6).

1.3 atm	T_5 (K)	$10^4/T_5$ (K^{-1})	P_5 (atm)	τ_{ing}(μs)	τ_{adj} * (μs)
Mixture 3	2158	4.63	1.33	88	90
	2152	4.65	1.18	89	83
	2068	4.84	1.19	128	120
	2056	4.86	1.20	150	141
	2012	4.97	1.23	167	160
	1951	5.13	1.29	278	276
	1934	5.17	1.27	301	296
	1863	5.37	1.25	477	463
	1861	5.37	1.26	499	488
	1849	5.41	1.30	528	528
	1834	5.45	1.25	540	524
	1827	5.47	1.16	634	582
	1739	5.75	1.32	1165	1180
Mixture 4	2163	4.62	1.20	59	56
	2070	4.83	1.19	98	92
	2018	4.96	1.21	129	122
	1944	5.14	1.25	181	176
	1960	5.10	1.21	188	179
	1893	5.28	1.26	331	324
	1832	5.46	1.25	422	410
	1818	5.50	1.29	465	463
	1799	5.56	1.33	554	562
	1756	5.69	1.33	621	630
	1694	5.90	1.33	1063	1078
Mixture 5	2139	4.68	1.18	56	52
	2096	4.77	1.21	70	66
	2028	4.93	1.21	108	103
	2030	4.93	1.22	122	117
	1973	5.07	1.23	144	138
	1956	5.11	1.27	157	154
	1919	5.21	1.29	183	182
	1938	5.16	1.27	215	211
	1865	5.36	1.29	305	304
	1857	5.39	1.28	322	319
	1853	5.40	1.31	346	348

	1849	5.41	1.28	367	363
	1802	5.55	1.32	413	417
	1820	5.49	1.30	457	456
	1751	5.71	1.33	622	633
	1775	5.63	1.30	639	640
	1757	5.69	1.36	702	724
	1751	5.71	1.31	717	721
	1731	5.78	1.28	921	910
	1711	5.84	1.33	956	973
Mixture 6	2174	4.60	1.15	38	35
	2123	4.71	1.18	57	53
	2064	4.84	1.26	69	68
	2051	4.88	1.19	85	80
	1973	5.07	1.24	132	128
	1911	5.23	1.24	183	177
	1875	5.33	1.25	274	267
	1832	5.46	1.26	386	378
	1795	5.57	1.27	434	427
	1771	5.65	1.29	613	611
	1739	5.75	1.29	765	761
	1731	5.78	1.32	771	780
	1691	5.91	1.35	1224	1258

*Ignition delay time adjusted to the pressure average = 1.3 atm

Table A4. Experimental ignition delay times of $CH_4/O_2/Ar$ mixtures (Φ=2.0) with 0% CF_3Br (Mixture 7) and 0.10% CF_3Br (Mixture 8).

1.2 atm	T_5 (K)	$10^4/T_5$ (K^{-1})	P_5 (atm)	τ_{ing}(μs)	τ_{adj}* (μs)
Mixture 7	2140	4.67	1.13	110	105
	2098	4.77	1.14	138	133
	2055	4.87	1.17	162	159
	2044	4.89	1.25	167	172
	2051	4.88	1.21	199	200
	1975	5.06	1.23	306	311
	1908	5.24	1.19	510	508
	1907	5.24	1.28	588	615
	1865	5.36	1.34	711	768
	1865	5.36	1.29	779	822
	1815	5.51	1.30	1017	1077
	1804	5.54	1.28	1083	1137
	1768	5.66	1.28	1325	1386
Mixture 8	2139	4.68	1.13	70	67
	2022	4.95	1.15	189	183
	1978	5.06	1.18	274	271
	1980	5.05	1.22	278	281
	1889	5.29	1.25	479	493
	1850	5.41	1.27	755	786
	1809	5.53	1.30	948	1002
	1789	5.59	1.26	966	999

*Ignition delay time adjusted to the pressure average = 1.2 atm

Table A5. Experimental ignition delay times of $C_2H_6/O_2/Ar$ mixtures (Φ=0.5) with 0% CF_3Br (Mixture 9) and 0.02% CF_3Br (Mixture 10).

1.4 atm	T_5 (K)	$10^4/T_5$ (K^{-1})	P_5 (atm)	τ_{ing}(μs)	τ_{adj} * (μs)
Mixture 9	1485	6.73	1.37	109	107
	1417	7.06	1.42	184	186
	1407	7.11	1.36	184	180
	1360	7.35	1.34	294	283
	1346	7.43	1.34	307	295
	1334	7.50	1.36	354	345
	1313	7.62	1.39	509	507
	1313	7.62	1.41	536	539
	1299	7.70	1.44	666	680
	1257	7.96	1.44	1038	1065
Mixture 10	1477	6.77	1.35	192	187
	1455	6.87	1.40	251	250
	1394	7.17	1.34	487	468
	1378	7.26	1.35	583	564
	1384	7.23	1.38	604	598
	1320	7.58	1.35	954	923
	1306	7.66	1.37	1521	1496

*Ignition delay time adjusted to the pressure average = 1.4 atm

Table A6. Experimental ignition delay times of C_2H_6/O_2/Ar mixtures (Φ=1.0) with 0% CF_3Br (Mixture 11), 0.02% CF_3Br (Mixture 12), and 0.04% CF_3Br (Mixture 13).

1.4 atm	T_5 (K)	$10^4/T_5$ (K^{-1})	P_5 (atm)	τ_{ing}(μs)	τ_{adj} * (μs)
Mixture 11	1578	6.34	1.43	106	108
	1526	6.55	1.42	146	148
	1440	6.94	1.36	292	284
	1400	7.14	1.40	328	328
	1366	7.32	1.49	609	642
	1359	7.36	1.44	643	657
	1289	7.76	1.40	1035	1037
	1288	7.76	1.54	1387	1503
Mixture 12	1583	6.32	1.33	126	120
	1550	6.45	1.41	175	176
	1493	6.70	1.40	301	302
	1454	6.88	1.43	442	450
	1385	7.22	1.39	927	920
	1360	7.35	1.42	1289	1308
	1349	7.41	1.47	1497	1556
Mixture 13	1632	6.13	1.34	101	97
	1552	6.44	1.37	193	189
	1541	6.49	1.42	231	234
	1505	6.64	1.43	335	340
	1444	6.93	1.43	579	589
	1434	6.97	1.37	804	790
	1395	7.17	1.41	1256	1260
	1391	7.19	1.47	1404	1461

*Ignition delay time adjusted to the pressure average = 1.4 atm

Table A7 Experimental ignition delay times of $C_2H_6/O_2/Ar$ mixtures (Φ=2.0) with 0% CF_3Br (Mixture 14) and 0.07% CF_3Br (Mixture 15).

1.3 atm	T_5 (K)	$10^4/T_5$ (K^{-1})	P_5 (atm)	τ_{ing}(μs)	τ_{adj}* (μs)
Mixture 14	1508	6.63	1.34	278	284
	1492	6.70	1.38	313	328
	1493	6.70	1.42	320	345
	1451	6.89	1.40	385	409
	1421	7.04	1.43	574	621
	1402	7.13	1.36	612	635
	1375	7.27	1.39	760	805
	1355	7.38	1.43	996	1076
Mixture 15	1584	6.31	1.30	348	348
	1584	6.31	1.27	445	437
	1488	6.72	1.25	855	828
	1483	6.74	1.30	926	926
	1470	6.80	1.27	1145	1126
	1464	6.83	1.30	1310	1307
	1436	6.96	1.31	1671	1683

*Ignition delay time adjusted to the pressure average = 1.3 atm

Table A8. Experimental ignition delay times of $C_3H_8/O_2/Ar$ mixtures (Φ=0.5) with 0% CF_3Br (Mixture 16) and 0.02% CF_3Br (Mixture 17).

1.5 atm	T_5 (K)	$10^4/T_5$ (K^{-1})	P_5 (atm)	τ_{ing}(μs)	τ_{adj} * (μs)
Mixture 16	1614	6.20	1.51	28	28
	1542	6.49	1.45	80	79
	1535	6.51	1.50	94	94
	1496	6.68	1.54	150	152
	1437	6.96	1.53	321	324
	1396	7.16	1.56	524	533
	1354	7.39	1.56	882	897
	1332	7.51	1.56	1365	1388
Mixture 17	1641	6.09	1.47	33	33
	1588	6.30	1.48	59	59
	1500	6.67	1.47	200	198
	1452	6.89	1.48	382	380
	1419	7.05	1.53	499	503
	1385	7.22	1.57	1153	1178
	1369	7.30	1.51	1193	1198
	1353	7.39	1.55	1749	1774

*Ignition delay time adjusted to the pressure average = 1.5 atm

Table A9. Experimental ignition delay times of $C_3H_8/O_2/Ar$ mixtures (Φ=1.0) with 0% CF_3Br (Mixture 18) and 0.03% CF_3Br (Mixture 19).

1.5 atm	T_5 (K)	$10^4/T_5$ (K^{-1})	P_5 (atm)	τ_{ing}(μs)	τ_{adj} * (μs)
Mixture 18	1642	6.09	1.42	63	62
	1528	6.54	1.42	197	192
	1498	6.68	1.49	303	302
	1438	6.95	1.47	574	569
	1422	7.03	1.50	737	736
	1398	7.15	1.50	969	969
	1362	7.34	1.51	1463	1469
	1369	7.30	1.56	1696	1726
Mixture 19	1671	5.98	1.40	70	68
	1645	6.08	1.45	104	102
	1609	6.22	1.47	158	156
	1535	6.51	1.43	338	331
	1539	6.50	1.44	374	367
	1456	6.87	1.50	1152	1153
	1421	7.04	1.50	1439	1437

*Ignition delay time adjusted to the pressure average = 1.5 atm

Table A10. Experimental ignition delay times of $C_3H_8/O_2/Ar$ mixtures (Φ=2.0) with 0% CF_3Br (Mixture 20) and 0.06% CF_3Br (Mixture 21).

1.4 atm	T_5 (K)	$10^4/T_5$ (K^{-1})	P_5 (atm)	τ_{ing}(μs)	τ_{adj}* (μs)
Mixture 20	1736	5.76	1.48	59	59
	1639	6.10	1.40	139	135
	1566	6.39	1.42	283	276
	1516	6.60	1.45	445	438
	1456	6.87	1.46	927	915
	1435	6.97	1.56	1153	1172
	1436	6.96	1.50	1326	1325
	1424	7.02	1.48	1356	1346
	1386	7.22	1.54	1882	1903
Mixture 21	1780	5.62	1.37	80	77
	1751	5.71	1.43	138	135
	1710	5.85	1.42	174	170
	1644	6.08	1.36	318	305
	1644	6.08	1.39	472	456
	1552	6.44	1.36	907	866
	1532	6.53	1.42	1347	1312
	1530	6.54	1.45	1545	1523

*Ignition delay time adjusted to the pressure average = 1.4 atm

Table A11. Experimental peak OH* and Full With at Half Maximum (FWHM) of CH_4/O_2/Ar mixtures (Φ=0.5) with 0% CF_3Br (Mixture 1) and 0.04% CF_3Br (Mixture 2).

	T_5 (K)	FWHM (μs)	Peak OH*
Mixture 1	2112	31.0	1.00
	2100	31.5	1.01
	2052	33.9	0.86
	2022	39.1	0.77
	2002	35.2	0.89
	1912	48.4	0.58
	1915	48.9	0.59
	1898	56.3	0.53
	1840	55.1	0.46
	1779	64.4	0.43
Mixture 2	1917	23.8	0.55
	1883	20.6	0.59
	1854	24.7	0.50
	1858	23.3	0.49
	1851	26.5	0.49
	1805	30.3	0.37
	1795	26.3	0.38
	1817	28.6	0.39
	1751	45.5	0.28
	1740	65.5	0.32
	1730	61.7	0.35
	1703	95.3	0.25

• Peaks are normalized taking 2261K and 1.4 atm as reference

Table A12. Experimental peak OH* and Full With at Half Maximum (FWHM) of CH_4/O_2/Ar mixtures (Φ=1.0) with 0% CF_3Br (Mixture 3), and 0.07% CF_3Br (Mixture 6).

	T_5 (K)	FWHM (μs)	Peak OH*
Mixture 3	2140	41.3	1.00
	2004	70.3	0.58
	1951	61.8	0.61
	1837	124.1	0.29
	1739	167.1	0.20
Mixture 6	2136	39.6	1.01
	2043	47.4	0.75
	1933	72.3	0.45
	1826	93.6	0.29
	1766	118.5	0.23

• Peaks are normalized taking 2140K and 1.14 atm as reference

Table A13. Experimental peak OH* and Full With at Half Maximum (FWHM) of CH_4/O_2/Ar mixtures (Φ=2.0) with 0% CF_3Br (Mixture 7) and 0.10% CF_3Br (Mixture 8).

	T_5 (K)	FWHM (μs)	Peak OH*
Mixture 7	2140	65.9	1.00
	2098	73.7	0.82
	2055	84.8	0.70
	2044	81.2	0.69
	2051	89.5	0.61
	1975	116.0	0.46
	1908	162.8	0.31
	1907	172.4	0.29
	1865	176.4	0.25
	1865	190.8	0.22
	1815	212.1	0.19
	1804	253.7	0.19
	1768	307.1	0.14
Mixture 8	2139	77.9	0.68
	2022	116.7	0.34
	1978	134.2	0.29
	1980	159.1	0.22
	1889	233.8	0.14
	1850	277.0	0.10
	1809	277.9	0.09
	1789	338.6	0.07

• Peaks are normalized taking 2140K and 1.13 atm as reference

Table A14. Experimental peak OH* and Full With at Half Maximum (FWHM) of $C_2H_6/O_2/Ar$ mixtures (Φ=0.5) with 0% CF_3Br (Mixture 9) and 0.02% CF_3Br (Mixture 10).

Table A 12

	T_5 (K)	FWHM (μs)	Peak OH*
Mixture 9	1485	73.3	1.00
	1417	86.8	0.68
	1407	91.1	0.66
	1360	115.4	0.48
	1346	120.3	0.42
	1334	116.9	0.38
	1313	141.7	0.30
	1313	154.0	0.26
	1299	158.2	0.25
	1257	224.2	0.17
Mixture 10	1477	99.8	0.42
	1455	123.2	0.31
	1394	112.8	0.29
	1378	207.3	0.16
	1384	299.0	0.11
	1320	395.3	0.07
	1306	366.1	0.06

• Peaks are normalized taking 1485K and 1.37 atm as reference

Table A15. Experimental peak OH* and Full With at Half Maximum (FWHM) of $C_2H_6/O_2/Ar$ mixtures (Φ=1.0) with 0% CF_3Br (Mixture 11), 0.02% CF_3Br (Mixture 12), and 0.04% CF_3Br (Mixture 13).

	T_5 (K)	FWHM (μs)	Peak OH*
Mixture 11	1578	54.2	1.00
	1526	63.6	0.86
	1440	106.8	0.46
	1400	115.3	0.42
	1366	160.4	0.25
	1359	116.5	0.32
	1289	220.9	0.16
Mixture 12	1583	66.8	1.01
	1550	66.8	0.68
	1493	84.0	0.47
	1454	86.8	0.41
	1471	136.5	0.37
	1385	163.1	0.20
	1360	184.0	0.16
	1349	224.6	0.14
Mixture 13	1632	51.8	0.94
	1552	87.7	0.56
	1541	71.3	0.59
	1505	92.0	0.42
	1444	192.9	0.21
	1434	141.7	0.26
	1395	169.7	0.18
	1391	288.0	0.11

• Peaks are normalized taking 1578K and 1.43 atm as reference

Table A16. Experimental peak OH* and Full With at Half Maximum (FWHM) of $C_2H_6/O_2/Ar$ mixtures (Φ=2.0) with 0% CF_3Br (Mixture 14) and 0.07% CF_3Br (Mixture 15).

	T_5 (K)	FWHM (μs)	Peak OH*
Mixture 14	1508	342.8	1.00
	1492	314.9	1.10
	1493	334.0	1.03
	1451	430.0	0.73
	1421	479.0	0.57
	1402	540.0	0.50
	1375	832.0	0.32
	1355	638.0	0.34
Mixture 15	1584	493.0	0.53
	1584	352.0	0.70
	1592	390.8	0.59
	1562	462.1	0.46
	1488	744.0	0.26
	1483	939.0	0.15
	1528	469.4	0.36
	1470	747.7	0.17
	1464	851.0	0.10

• Peaks are normalized taking 1508K and 1.34 atm as reference

Table A17. Experimental peak OH* and Full With at Half Maximum (FWHM) of $C_3H_8/O_2/Ar$ mixtures (Φ=0.5) with 0% CF_3Br (Mixture 16) and 0.02% CF_3Br (Mixture 17).

	T_5 (K)	FWHM (μs)	Peak OH*
Mixture 16	1614	45.7	1.00
	1542	52.6	0.76
	1535	53.0	0.73
	1496	62.9	0.59
	1437	98.1	0.35
	1354	235.9	0.14
	1332	267.2	0.12
Mixture 17	1641	55.5	0.69
	1588	64.0	0.59
	1500	70.2	0.42
	1452	122.9	0.24
	1419	288.0	0.10
	1385	346.6	0.09
	1369	284.7	0.10
	1353	429.3	0.06

• Peaks are normalized taking 1614K and 1.5 atm as reference

Table A18. Experimental peak OH* and Full With at Half Maximum (FWHM) of $C_3H_8/O_2/Ar$ mixtures (Φ=1.0) with 0% CF_3Br (Mixture 18) and 0.03% CF_3Br (Mixture 19).

	T_5 (K)	FWHM (μs)	Peak OH*
Mixture 18	1642	44.2	1.00
	1528	76.2	0.65
	1498	100.4	0.43
	1422	129.7	0.27
	1369	217.7	0.17
Mixture 19	1671	49.6	0.80
	1645	52.7	0.71
	1609	77.2	0.49
	1535	109.0	0.33
	1539	95.5	0.40
	1456	109.0	0.33
	1421	450.2	0.09

• Peaks are normalized taking 1642K and 1.4 atm as reference

Table A19. Experimental peak OH* and Full With at Half Maximum (FWHM) of $C_3H_8/O_2/Ar$ mixtures (Φ=2.0) with 0% CF_3Br (Mixture 20) and 0.06% CF_3Br (Mixture 21).

	T_5 (K)	FWHM (μs)	Peak OH*
Mixture 20	1736	85.9	1.00
	1639	152.5	0.48
	1566	193.4	0.32
	1516	321.8	0.18
	1456	493.6	0.10
	1435	432.2	0.11
	1436	429.3	0.10
	1424	380.2	0.12
	1386	540.2	0.04
Mixture 21	1780	88.7	0.96
	1751	126.1	0.66
	1710	118.1	0.64
	1644	159.8	0.42
	1644	184.4	0.35
	1552	232.3	0.23
	1532	296.9	0.16
	1530	324.0	0.13

• Peaks are normalized taking 1736K and 1.5 atm as reference

APPENDIX B: TABULATION OF LAMINAR FLAME SPEED MEASUREMENTS

Table B1. Experimental laminar flame speed data for fuel-air mixtures with CF3Br at 298K and 1 atm

ϕ	S_L (cm/s)								
	CH_4			C_2H_6			C_3H_8		
	0%	0.5%	1.0%	0%	0.5%	1.0%	0%	0.5%	1.0%
0.7	15.3	-	-	21.5	-	-	19.5	-	-
0.8	23.3	12.9	7.6	28.3	19.6	13.5	27.6	17.9	-
0.9	29.9	18.8	-	35.2	25.9	19.0	32.9	24.8	17.5
1.0	34.3	22.7	14.9	38.8	29.5	22.6	37.5	28.3	20.5
1.1	36.0	23.3	15.3	39.8	30.8	23.1	39.7	29.3	21.3
1.2	33.4	19.9	12.0	38.9	29.1	21.0	39.6	27.0	19.1
1.3	24.9	-	-	34.3	-	-	35.1	-	-

Table B2. Comparison of current data with previous studies

	Ref.	Technique	S_{Lo} (cm/s) (0% CF_3Br)	S_L (cm/s) (1% CF_3Br)	S_L/S_{Lo}
CH_4/Air	Parks. et al [124]	acoustically tuned flame tube	34	14	0.41
	Westbrook [94]	Numerical	36	19	0.53
	Noto, et al [95]	Numerical	42.5	22.5	0.53
	Current work	Numerical	36.2	19.8	0.55
		Windowed Vessel	35.3	14.9	0.42
C_2H_6/Air	Noto, et al [95]	Numerical	46.1	31.5	0.68
	Current work	Numerical	41.2	27.4	0.66
		Windowed Vessel	36.8	22.6	0.61
C_3H_8/Air	Parks. et al [124]	acoustically tuned flame tube	40	20	0.50
	Current work	Numerical	40.3	27.2	0.68
		Windowed Vessel	37.5	20.5	0.55

APPENDIX C: LOCAL SENSITIVITY ANALYSIS WITH RESPECT TO OH*: CF_3BR ANALYSIS

Local sensitivity analysis with respect to OH* was carried out for the different systems represented in Table C1, including baselines (0% CF_3Br) and those containing CF_3Br. Methane and Ethane systems were evaluated at 1900K and 1400K respectively, all at 1.4 atm. This analysis is used to identify the key reactions responsible for the formation of OH*. Taking into account the direct relation between the formation of OH* and ignition delay time, it is possible to express these findings as the effect of CF_3Br on the key reactions that most affect the ignition behavior.

Table C1. Mixtures highly diluted in Argon that are considered for the sensitivity analysis.

System	τ_{ign} (μs)	% CF_3Br	% Fuel	% O_2	Φ	Fuel	Temp	P
A	348	-	0.67	1.33	1.0	Methane	1900 K	1.4 atm
B	266	0.067						
C	281	-	0.40	1.60	0.5			
D	175	0.040						
E	437	-	1.00	1.00	2.0			
F	368	0.1						
G	258	-	0.44	1.56	1.0	Ethane	1400 K	
H	363	0.044						
I	156	-	0.25	1.75	0.5			
J	168	0.025						
K	484	-	0.73	1.27	2.0			
L	940	0.073						
M	222	-	0.00333	0.01667	1.0	Propane	1500 K	
N	262	0.00033						
O	101	-	0.00182	0.01818	0.5			
P	158	0.00018						
Q	477	-	0.00572	0.01428	2.0			
R	615	0.00057						

Sensitivity coefficients were calculated using the SENKIN code from CHEMKIN released 4.1. All calculations were made using absolute tolerance (ATOL) and relative tolerance (RTOL) values of 1E-20 and 1E-8, respectively, considering these as indicators of the of the accuracy desired in the physical solution.

Figures C1-C12 show the results obtained for each of the systems and the ranking of the most significant reactions observed at their ignition delay times (as indicated by the dished vertical line).

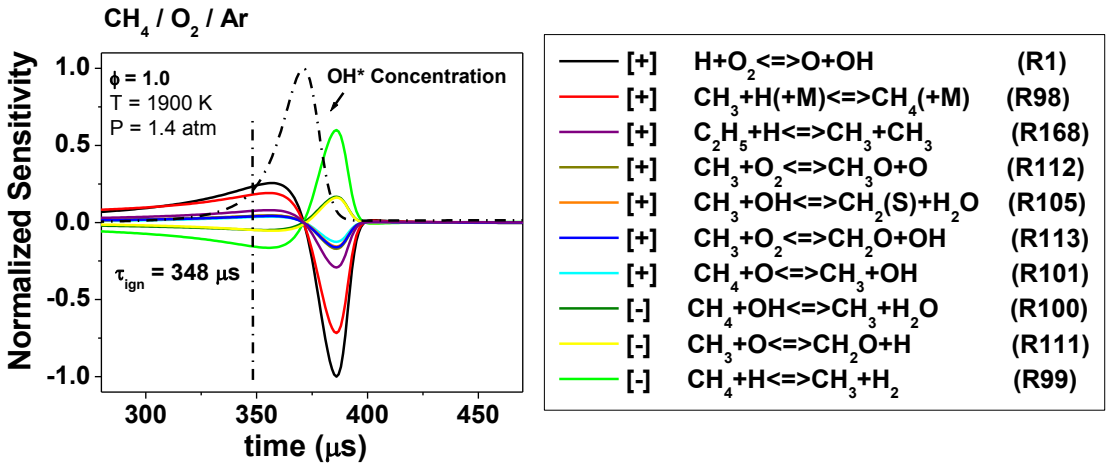

Figure C1. Local sensitivity analysis for System A with respect to OH*, and ranking of the most significant reactions observed at the ignition time.

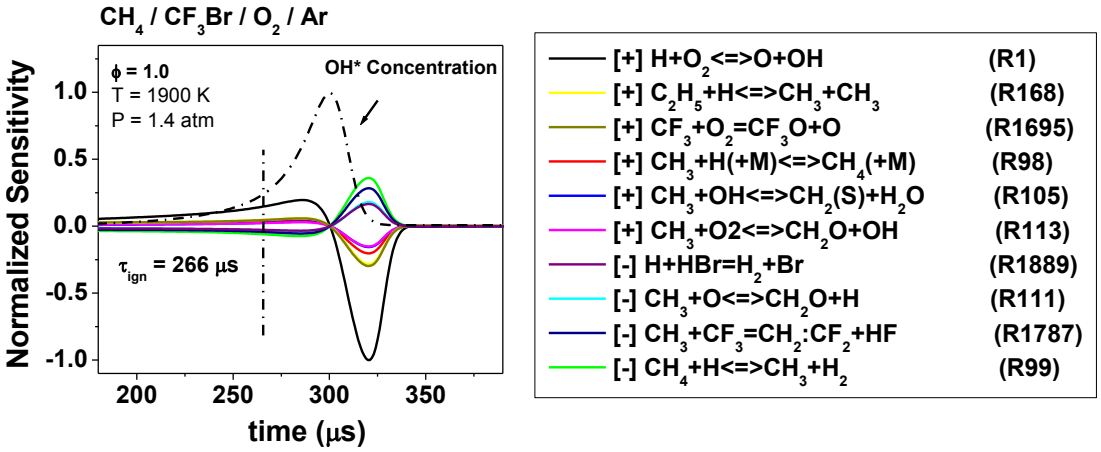

Figure C2. Local sensitivity analysis for System B with respect to OH*, and ranking of the most significant reactions observed at the ignition time.

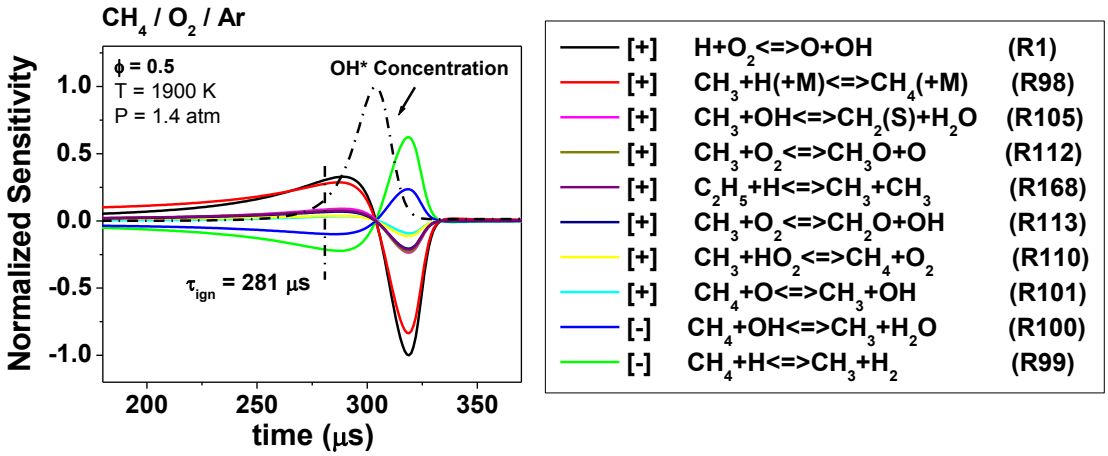

Figure C3. Local sensitivity analysis for System C with respect to OH*, and ranking of the most significant reactions observed at the ignition time.

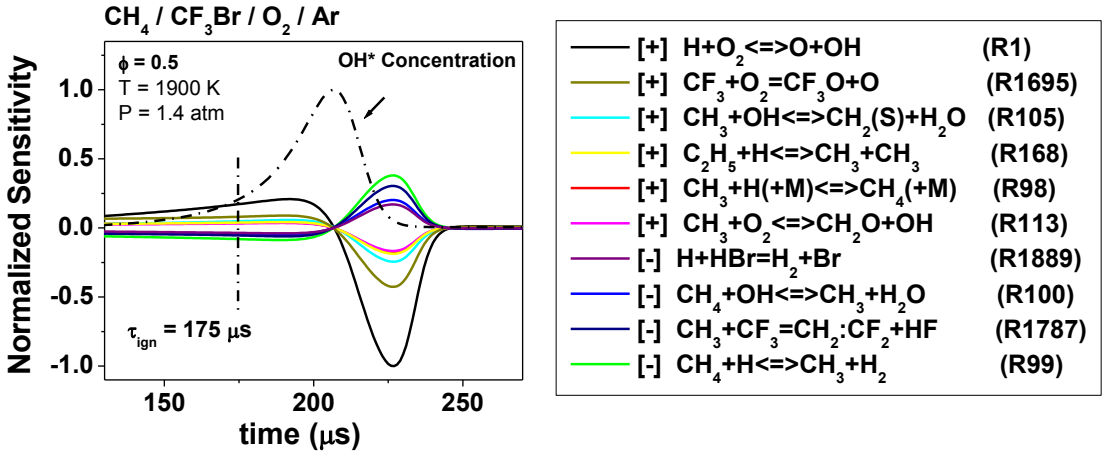

Figure C4. Local sensitivity analysis for System D with respect to OH*, and ranking of the most significant reactions observed at the ignition time.

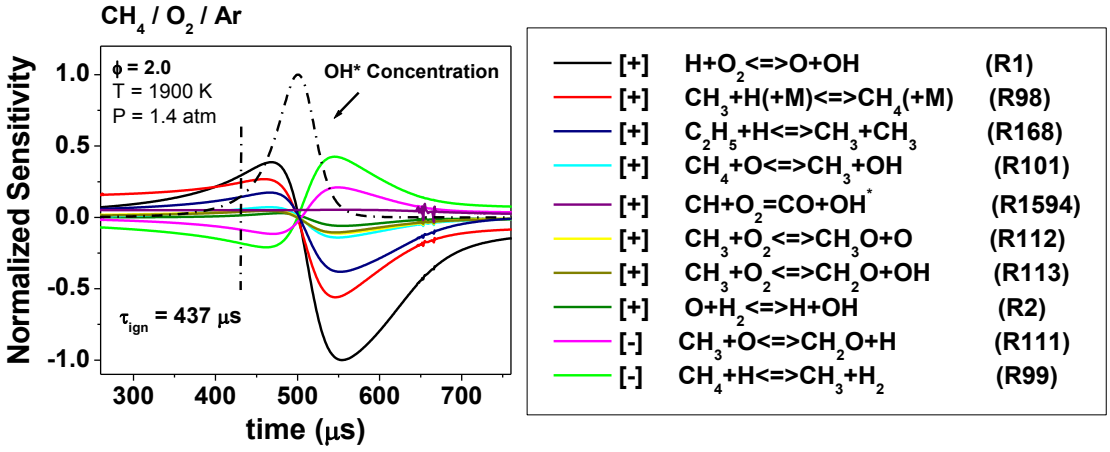

Figure C5. Local sensitivity analysis for System E with respect to OH*, and ranking of the most significant reactions observed at the ignition time.

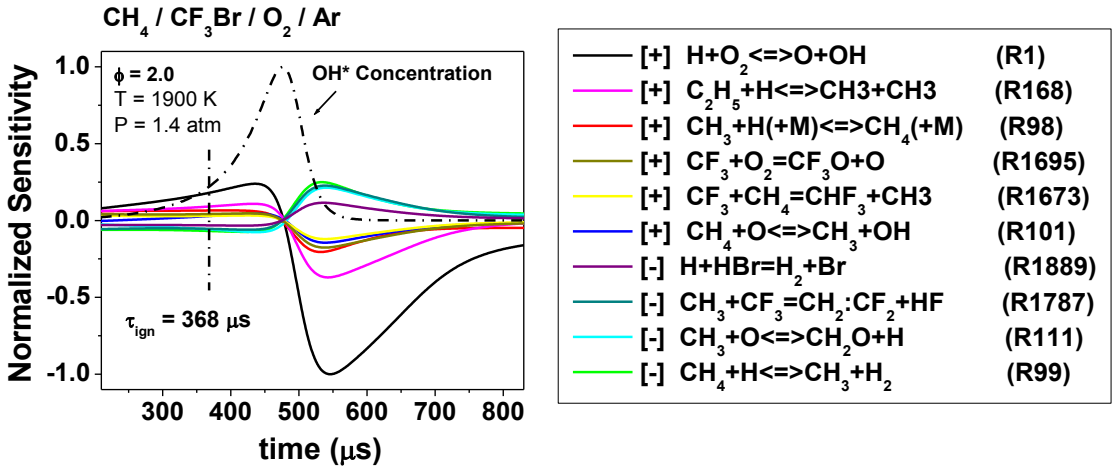

Figure C6. Local sensitivity analysis for System F with respect to OH*, and ranking of the most significant reactions observed at the ignition time.

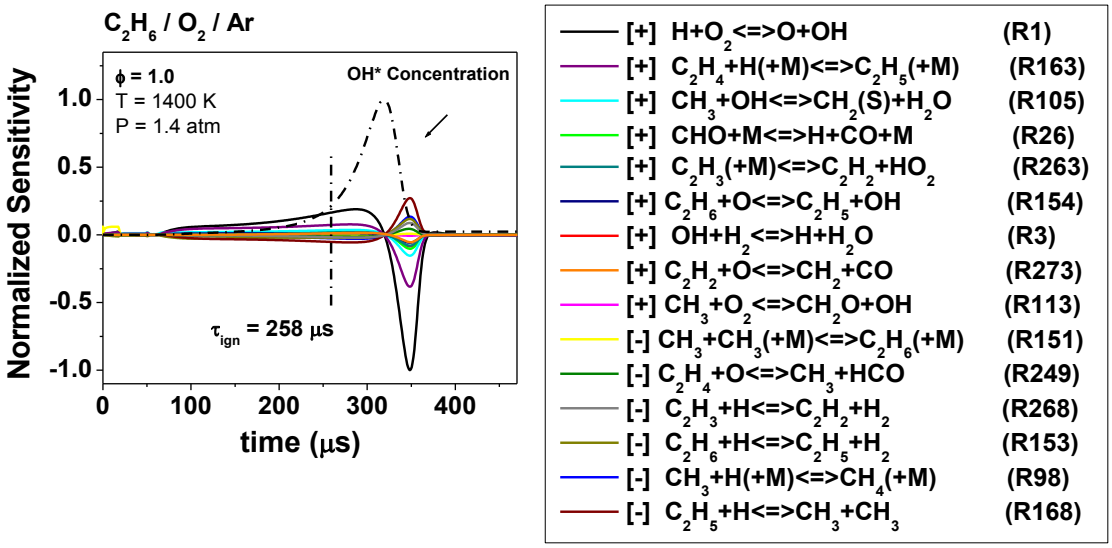

Figure C7. Local sensitivity analysis for System G with respect to OH*, and ranking of the most significant reactions observed at the ignition time.

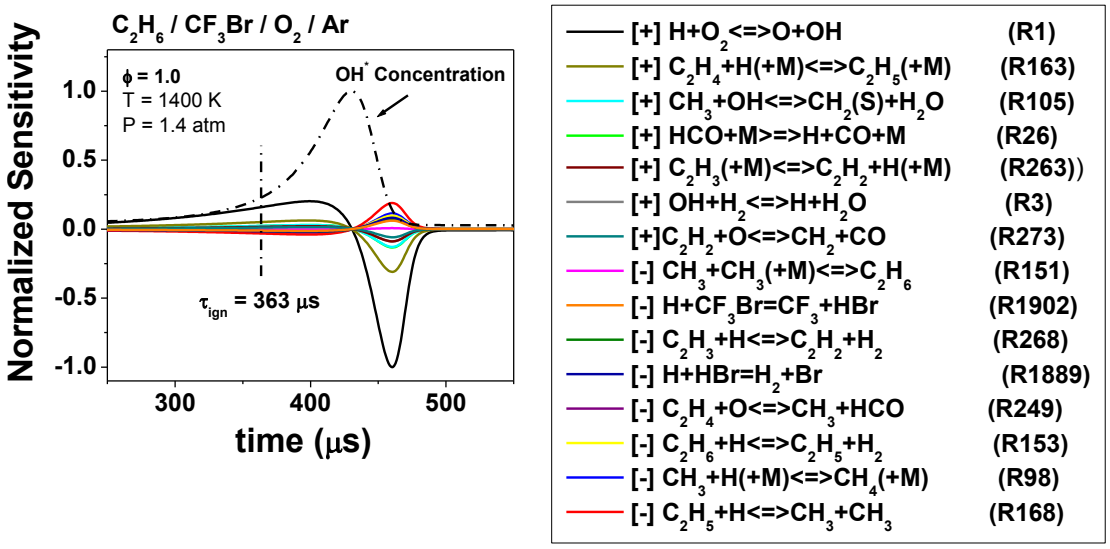

Figure C8. Local sensitivity analysis for System H with respect to OH*, and ranking of the most significant reactions observed at the ignition time.

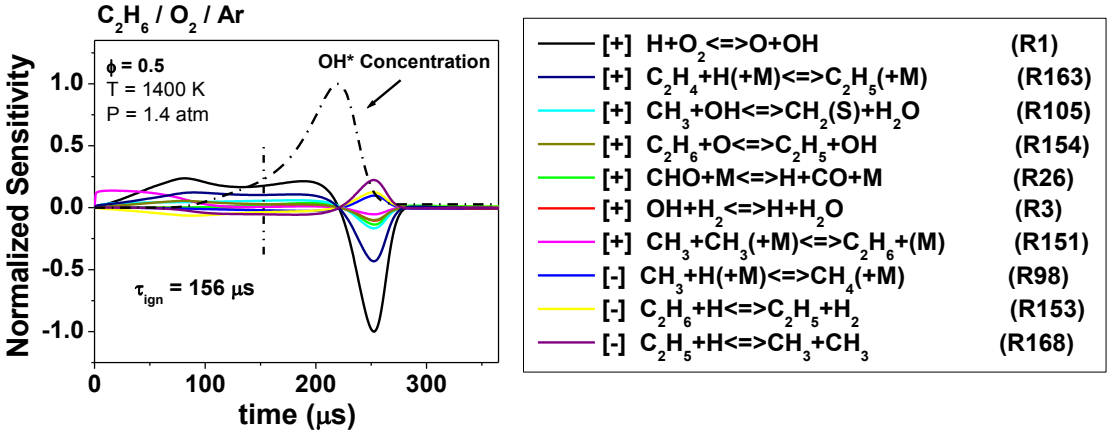

Figure C9. Local sensitivity analysis for System I with respect to OH*, and ranking of the most significant reactions observed at the ignition time.

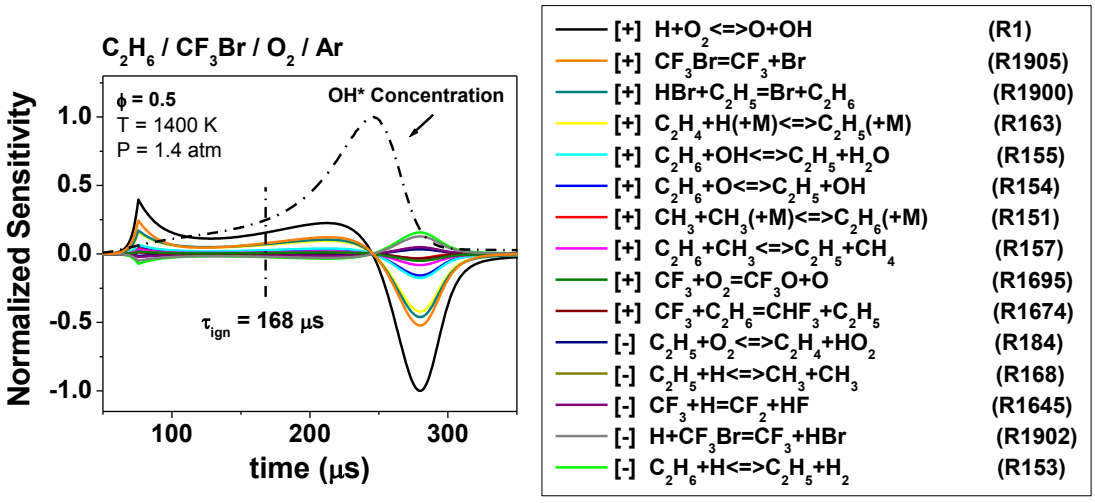

Figure C10. Local sensitivity analysis for System J with respect to OH*, and ranking of the most significant reactions observed at the ignition time.

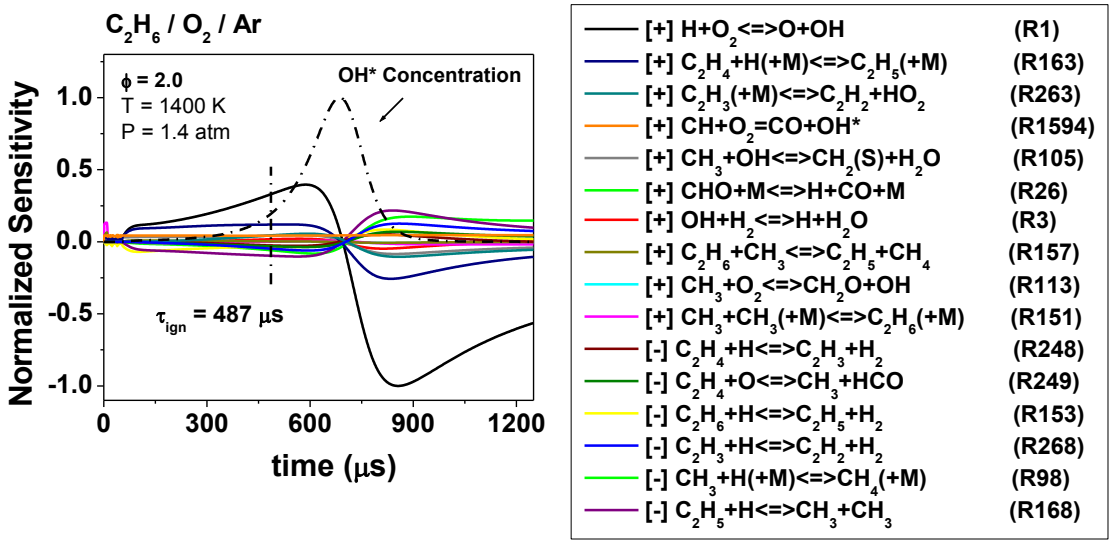

Figure C11. Local sensitivity analysis for System K with respect to OH*, and ranking of the most significant reactions observed at the ignition time.

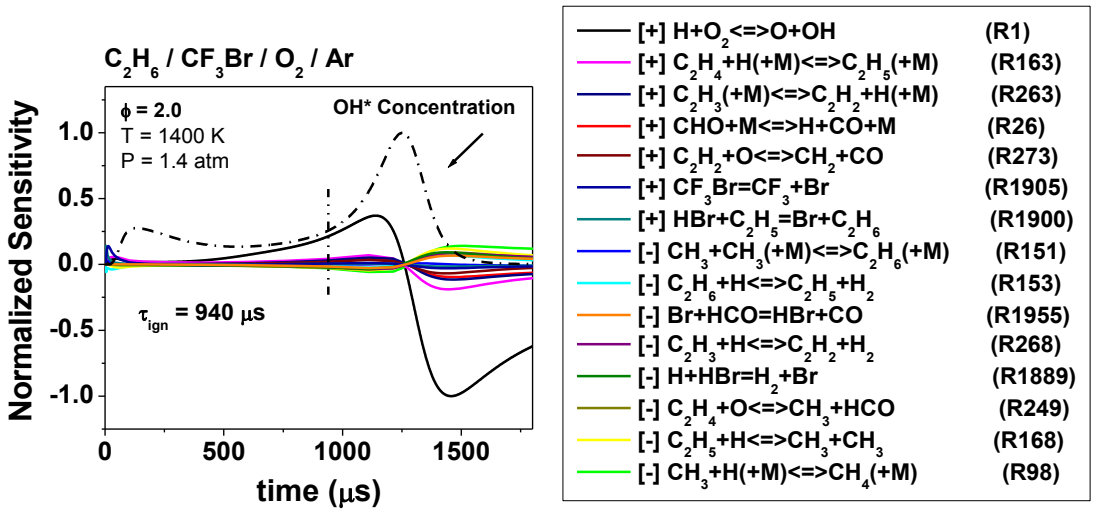

Figure 12. Local sensitivity analysis for System L with respect to OH*, and ranking of the most significant reactions observed at the ignition time.

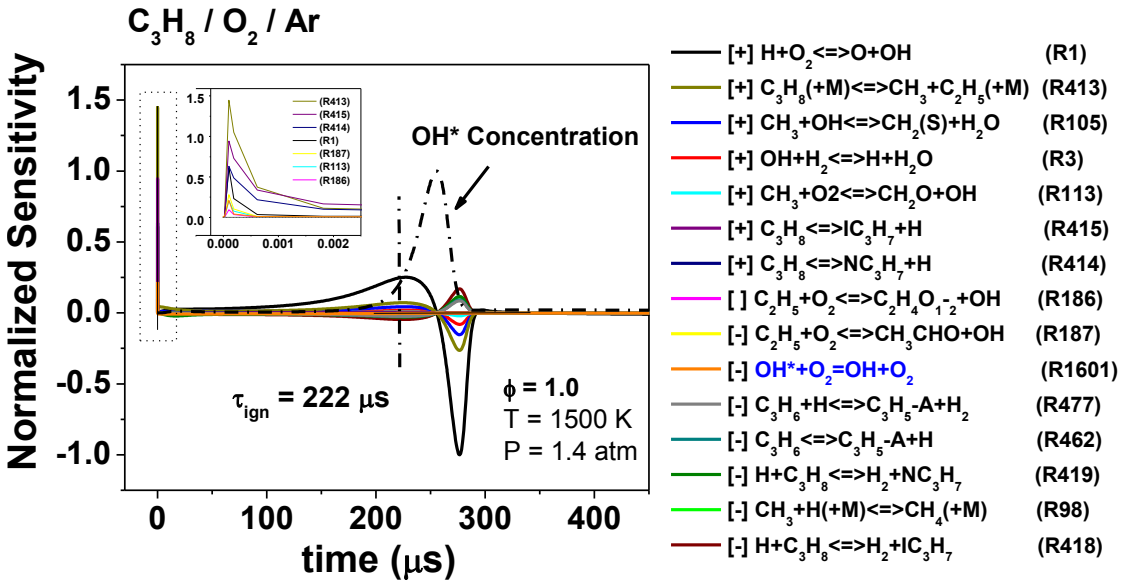

Figure 13. Local sensitivity analysis for System M with respect to OH*, and ranking of the most significant reactions observed at the ignition time.

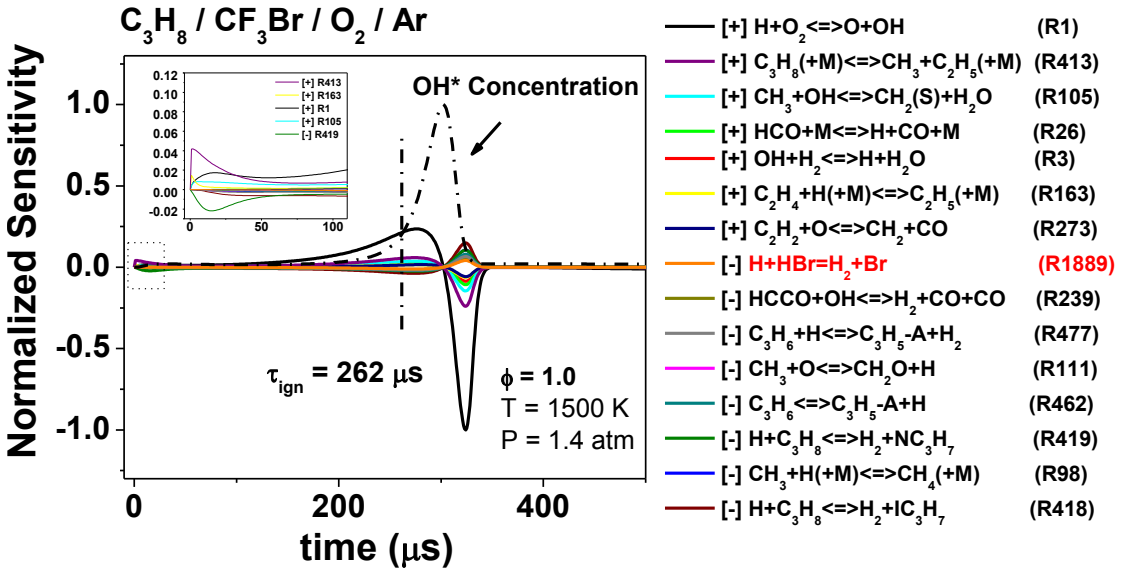

Figure 14. Local sensitivity analysis for System N with respect to OH*, and ranking of the most significant reactions observed at the ignition time.

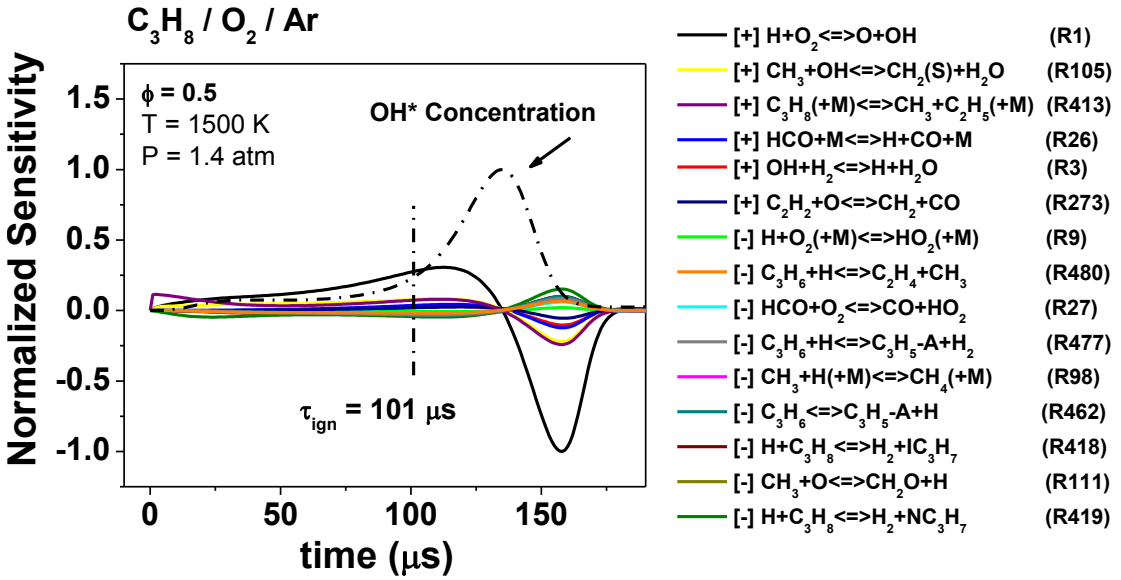

Figure 15. Local sensitivity analysis for System O with respect to OH*, and ranking of the most significant reactions observed at the ignition time.

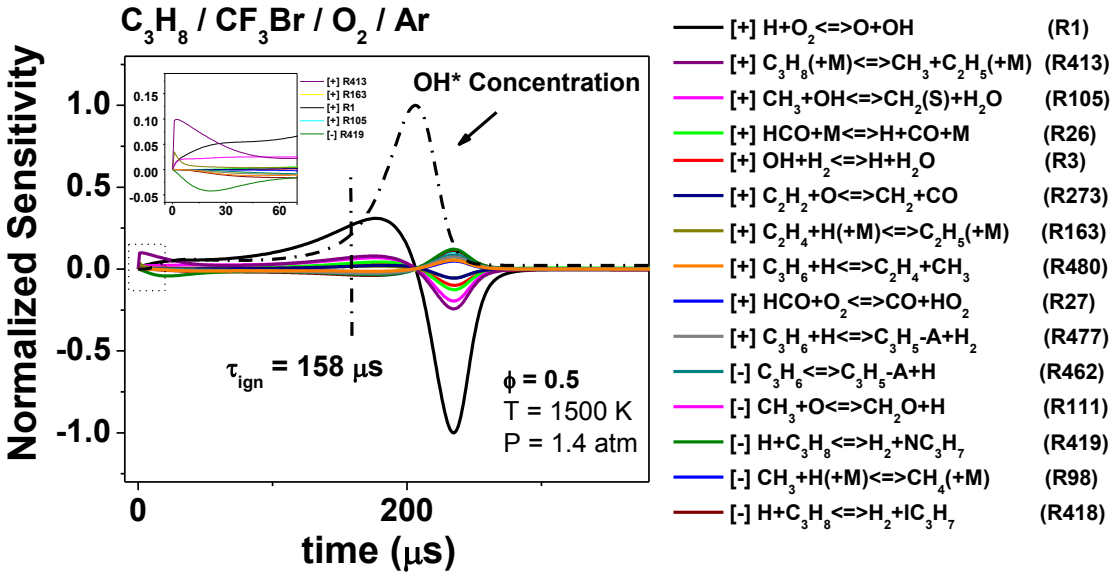

Figure 16. Local sensitivity analysis for System P with respect to OH*, and ranking of the most significant reactions observed at the ignition time.

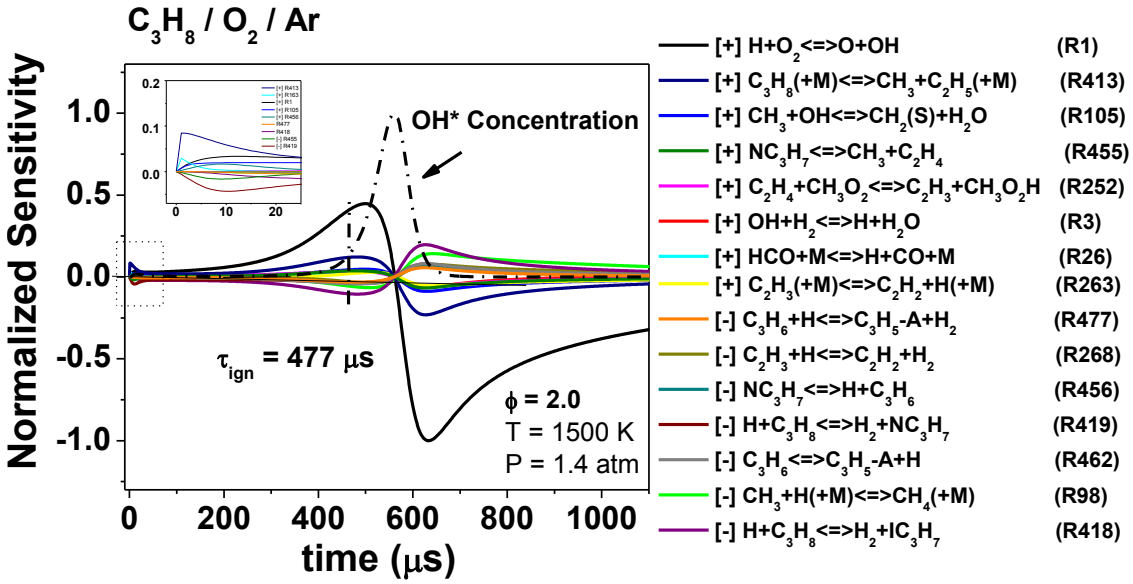

Figure 17. Local sensitivity analysis for System Q with respect to OH*, and ranking of the most significant reactions observed at the ignition time.

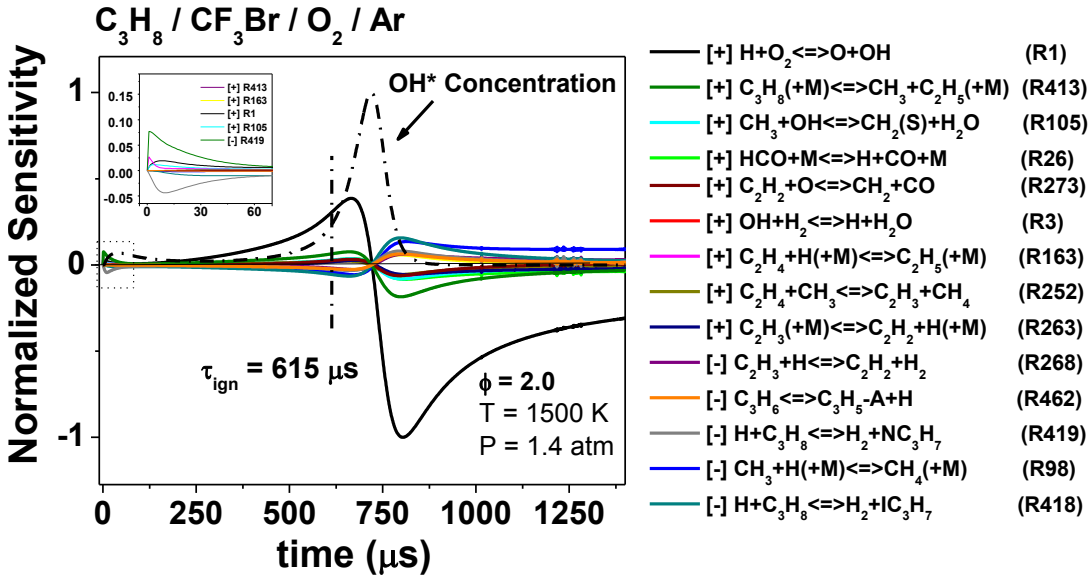

Figure 18. Local sensitivity analysis for System R with respect to OH*, and ranking of the most significant reactions observed at the ignition time.